Digitising sheave wheel profiles for condition monitoring

P Steyn

24182648

Dissertation submitted in fulfilment of the requirements for the degree *Magister* in Mechanical Engineering at the Potchefstroom Campus of the North-West University

Supervisor: Prof. L. Liebenberg

May 2015

For my two beautiful girls Lezaan and Zoe-Jane
for understanding far more than you should
ever have had to.

ABSTRACT

Title: Digitising sheave wheel profiles for condition monitoring

Author: Paul Steyn

Supervisor: Prof. Leon Liebenberg

Keywords: condition monitoring, sheave wheel, sheave profile, rope groove, light sectioning

In both open-cast and underground mining operations, sheave wheels are an integral part of the conveyance system. Sheave wheels are usually made of ductile cast iron which assists with lubrication of the rope as it passes over the sheave. This in turn subjects the sheave to considerable (although usually not rapid) wear during its normal operation. When a sheave is misaligned or incorrectly machined, it can experience rapid deterioration.

Although a worn sheave wheel could lead to failure of the sidewall, a more concerning aspect is its effect on the rope: a worn sheave will damage a rope significantly in a short time. Ropes are critical for the safety of miners in an underground mine and for production on both open-cast and underground mines.

As far as the deterioration of sheave wheels go, catastrophic failure is unlikely. Failure is indicated well in advance and thus the situation lends itself to a condition based maintenance strategy. Bi-annual inspection of sheaves is therefore mandated by legislation and several different methods exist for the recording of sheave profiles.

A survey was done to determine the current state of the art. It was noticed that the methods that are used in the industry at the moment have several drawbacks and none of the manufacturers provided information as to the accuracy or repeatability of these measuring instruments and techniques. This was concerning since the measurements serve as the input for critical engineering decisions that may have costly (or fatal) consequences. The study was aimed at the development of a new method for the profiling of sheave wheels. It was further aimed at determining the repeatability and accuracy of the methods currently employed in the industry and to then provide an objective comparison between the current state-of-the-art and the newly developed profiler.

An α-prototype profiler was developed using structured light photogrammetry together with a low cost webcam and the MATLAB® Image Processing Toolbox®. An analytical verification of the profiler was conducted to ensure that it will meet the requirements as determined in the document.

To validate the results, the profiler was subjected to the same experiments that the profilers/methods from the current state of the art were subjected to. It was then compared to the analytical solution. There were technical challenges with the hardware that was developed and accurate conclusions could not be drawn for the developed prototype profiler. The study does however conclude with a critical evaluation of the areas that could be investigated and with recommended areas of further research as well as other areas of application of the same technology to determine profiles of other wear components.

Acknowledgements

I would like to firstly thank my Creator for giving me the necessary abilities to have completed this work and for providing me with the opportunities to utilise my capabilities. I was humbled by the realisation that research cannot happen in a vacuum. The progress made, if any, is the result of serious sacrifices, not only by me, but also by many others. My gratitude cannot really be expressed in a simple paragraph, but I will try:

My lovely wife Lezaan, I cannot begin to describe my appreciation for the sacrifices you have made to support me on this project. I honestly don't know how you did it, but I am really glad that you did. I am so grateful for what you have done for me. You have, without fail, celebrated with me for every small success and helped me up after every failure. You really are my hero.

To my mother Esti, you are the one who started my academic career and you have been cheering for me constantly during good and bad times and for always staying positive and making a plan. I am very grateful for everything you have done. To my father Paul, thank you for instilling insatiable curiosity in me and for teaching me to work really, really hard and to never stop asking questions (and also daily pep talks). I would not be where I am without the two of you.

Thank you to all my friends and family members who have supported me throughout this project. To my brothers Ben, Stephen and my father Paul: thank you for assistance with proofreading and editing of the document. Your critique and advice has proved invaluable and you have made a significant contribution to my work.

Sometimes asking the right question is much more important than providing the correct answer (to paraphrase Douglas Adams). Three years ago Gert van der Walt asked the right question: "Is there not a better way to take sheave wheel profiles?" The quest to answer that simple question was what sparked my research in this area. Gert also spent several days assisting me with the experimental work, supplying samples for the experiments and providing me with invaluable advice on the work done in industry. I am very grateful for that.

Thanks to Chris Els for providing me with a Pantograph, a sheave wheel sample and mountains of valuable advice. Thanks to Deon Botma, Johan Schoeman, Alan Stirk, Jaime Goncalves and Roland Verreet for endless discussions and advice about sheave wheels and profiles. Thank you to every person who took the time to fill in the survey. To Greg Lewis and Lezaan: thank you for assisting me with the data capturing. This was not a job to be taken lightly - it involved performing agonisingly monotonous tasks for hours on end and at very strange hours of the night. It can best be likened to the Chinese water torture techniques of old. I am grateful for your assistance.

I would like to thank my examiners in advance for taking their valuable time to evaluate my work. I look forward to learning from your assessments. Thanks to Prof. Eddie Mathews and Dr. Johann van Rensburg and the team at CRCED for accepting me as a student and a special thanks to Liza Lotter for ensuring that the administrative side of the project ran smoothly and for always answering my (sometimes pedantic) questions eagerly and promptly. This work was funded in full by myself.

Lastly but by no means least Prof. Leon Liebenberg: Never have I come across someone who is able to wear the hat of an astute and rigorous academic mentor as well as that of a super-enthusiastic cheerleader at the same time. You have the ability of leaving me to my own devices for just long enough to come up with creative solutions but not long enough to get stuck in the belly of the beast. I could not have asked for a better supervisor. You have been a true inspiration for me. This project would certainly not have been possible without you.

PAUL STEYN

CONTENTS

LIST OF FIGURES

LIST OF TABLES

LIST OF SYMBOLS

Symbol	Definition	Unit
T	Thickness of rope	mm
R	Rope groove radius	mm
FOV	Field of view	°
FOV_{active}	Active field of view (of CCD)	°
d	Distance between sensor and obstruction source.	mm
β	Angle between sensor and camera plane	°
a	Vertical distance between camera plane and shadow plane.	mm
P_{vert}	Vertical pixels in sensor	pixels
W_0	Working area start point	mm
W	Length of working area	mm
γ	Angle between camera and ray line	°
A	Fleet angle of sheave wheel	°
R	Rope groove radius of sheave wheel	mm
H	Height of sheave wheel groove	mm
W_1	Sheave wheel web thickness	mm
W_2	Sheave wheel web thickness	mm

NOMENCLATURE

KSE	: Known sample experiment
SWE	: Sheave wheel experiment
HSV	: hue, saturation and value (colour image representation)
RGB	: red, green and blue (colour image representation)
NDT	: Non-destructive testing
CMM	: Coordinate Measuring Machine
ROI	: Region of interest
FOV	: Field of view
CCD	: Charge coupled device
CMOS	: Complementary metal-oxide semiconductor
OEM	: Original Equipment Manufacturer

GLOSSARY

α-prototype	: A first level, functional prototype. This is a proof of concept type prototype.
Conveyance	: The vertical transport vehicle (the cage)
Intrinsic parameters	: In the context of image processing this refers to the internal parameters of the camera itself.
Extrinsic parameters	: In the context of image processing this refers to the external parameters of the camera set-up. In this dissertation it shall refer to the relative set-up of the three cameras and the combined environment they are found in.
Rope	: In this context, a "rope" is a steel wire rope. This should not be used interchangeably with a "cable" which typically implies that it is something that carries electric charge.
Point cloud	: A set of data points. They are typically stored as a text file with three columns, each representing the x, y and z coordinates of a point.
Sheave wheel	: Sheave wheels are defined formally in the dissertation, but it should be noted that sheave wheel and sheave are used interchangeably throughout the document.
Profile	: Refers to the profile of the sheave wheel rim. This is also referred to as a "scan" when mentioning the digital methodologies.

CHAPTER 1: INTRODUCTION

"If I had eight hours to cut down a tree, I would use the first six to sharpen my axe"

Abraham Lincoln

1.1. BACKGROUND

A sheave wheel is a large pulley that supports a rope in various hoisting applications. It works by rotating freely as the rope passes over it. It is typically located at the top of a headgear or at various strategic places on a dragline.

Sheave wheels are made of a soft, ductile cast iron which, by design, allows it to degrade slowly as the rope runs over it. This assists with the lubrication of the rope (since the carbon from the cast iron comes out as the wheel degrades) and ensures that the sheave acts sacrificially to increase the usable life of the rope. During normal operation, the sheave will wear out fairly slowly and as long as it is monitored this is a controlled degradation. The sheave will degrade uncontrollably under three conditions:

i) Incorrect set-up of the sheave wheel assembly

ii) Incorrect rim profile cut into the sheave wheel

iii) New rope on an old sheave

The third condition occurs when a new rope is added to an old sheave wheel. When a rope and a sheave work together, the rope tends to "seat" into the sheave groove. This is acceptable since the amount of wear on the rope is negligible and the sheave tends to wear in such a way as to accommodate the rope which will have by then elongated and thus will have a smaller diameter than when it was initially installed. When an old rope is replaced by a new rope without adjusting the rim profile, the new rope would immediately be forced into the groove worn in by the old rope. Since the new rope would not yet have experienced the elongation that was present in the old rope, it will still have a larger diameter. It will therefore be subject to rapid deterioration and the risk of failure of the rope and sheave increases dramatically. All three the conditions that are listed above are entirely preventable through proper condition monitoring regimes implemented for sheave wheels.

Sheave wheels are monitored and their inspection intervals are mandated by legislation. There appears to be a lack of information on the methods available for the monitoring of sheaves and on the efficacy of the methods used. This makes it difficult for the mine managers to make educated decisions on the proper maintenance to be done on their sheaves.

1.2 Motivation for the study

Strangely, although sheave wheels are a critical component relating to safety and operational integrity, their maintenance seems to be neglected with an "out of sight, out of mind" mentality. One may sometimes even get the impression that the production manager would think, "If the wheel is still turning, it must be okay". In all fairness: sheave profiling is a grudge buy. It costs time and money and the benefits of not having an accident are not always obvious or quantifiable.

The author proposes that, were it cheaper, faster and simpler to take the sheave profiles, the mines would in all likelihood take the profiles more regularly. It is further proposed that if profiles were available in digital format, it would be easier for the Department of Minerals and Energy to monitor mines and ensure that sheave profiles are up to date. It would also be easier for mines to keep track of the wear on wheels.

At a later stage, it may even become possible to trend the wear rates of sheave wheels to such an extent that maintenance can be optimised on a per-wheel basis, instead of the inefficient blanket cover approach that scheduled/ time-based maintenance suggests at the moment. The first step on the road to reaching this goal would therefore be to develop a method to easily, digitally measure the profile of a sheave wheel.

1.3 Objectives of the study

Aim of the project:

"To develop a method of digitally measuring the profile of a sheave wheel and to verify and validate the accuracy of this method while critically evaluating it against the current state of the art."

Objectives:

I. Clarify the problem of what exactly needs to be scanned and the implications of such a scan using available literature and a survey of the people performing the scans.

II. Investigate the theory behind possible solutions to check for feasibility

III. Use the information acquired in (I-II) to develop a clear set of design specifications.

IV. Use the design specifications to design and manufacture an α-prototype sheave wheel profiler.

V. Verify that the designed profiler would be able to meet the design specifications (in theory).

VI. Validate that the manufactured profiler is able to meet the design specifications (in practice).

VII. Compare the scan data from the sample to other scans from other methods.

1.4 Layout of the dissertation

Chapter 2 provides an **overview of condition monitoring of sheave wheels**. It starts out by placing sheave wheels in context of their application and looks at their expected and unexpected wear. This is followed by an investigation of the requirements for the inspection of sheave wheels. The final (and most important) section of the chapter focuses on the methods currently employed to record sheave profiles. They are critically evaluated by the author and discussed in detail. They will later be compared to each other and to the newly developed profiler.

The information for the former sections was obtained through a review of literature and legislation while the information of the latter section was found through a survey that was done on technicians in the field actually taking the profiles on a regular basis.

Chapter 3 is an **introduction to digitisers and image acquisition**, this is not knowledge that pertains directly to the problem, but will be relevant to the solution.

At this stage, all the prerequisite knowledge has been discussed and the author moves on to **Chapter 4** which is the **design of the prototype profiler**. Here, the steps starting out with user requirements and technical requirements are combined with a functional analysis to determine a set of final design specifications. These are used in a detailed mechanical design which is presented. The process of algorithm development for the profiler's software is discussed and shown graphically.

The **design** is then verified in **Chapter 5**. The design requirements are listed, and each of them individually verified.

Chapter 6 describes the **experimental investigation** that was done to validate the profiler as per the design objectives. The experiments include the measurement of a known sample to determine the accuracy of the designed profiler. The other profilers listed as the current state of the art from Chapter 2 are also tested for accuracy with this experiment. The second set of experiments conducted, was done on a sample of an actual sheave wheel to test for functionality in a real-life environment for each of the methods.

The experimental results are discussed in **Chapter 7**. A critical evaluation of the newly developed profiler is done. Methods comprising the current state of the art were then critically compared to each other and to the newly proposed method.

In **Chapter 8**, conclusions were drawn from the experimental results and the theoretical results. Proposals were made for **future work.** In the appendices, all excessive text, that is merely supplied for the reader's information, is listed. **Appendix 1** is a **discussion of the references** that were used. In Appendix 2 an experimental uncertainty analysis was done. In Appendix 3 the survey results are presented with specification sheets and calibration documents shown in Appendix 4.

Chapter 2: Survey of the state-of-the-art in condition monitoring of sheave wheels

2.1. Introduction

In countries with abundant natural resources, mining activities make an important contribution to the GDP. In South Africa, the mining sector contributed R2.1 trillion to the GDP between 2002 and 2012 and is responsible for an 8.3% contribution to the GDP in 2012 (Chamber of Mines of South Africa, 2012). This includes only the actual mining operations and not the knock-on contributions that result from industries that exist to serve mines and processing plants. By 2012 there were 524 632 South Africans employed by the various types of mines (Chamber of Mines of South Africa, 2012). Many of the employees on these mines make direct use of the conveyances to get to their workplaces on underground mines. The conveyance consists of several components including the cage (or skip for material transport), the drive system and hoist drum, the sheave wheel and the rope. The premise here is that the safe operation of the sheave wheel and rope is critical for the safety of mine workers not to mention the GDP of South Africa or any other country that derives their income from exploiting their mining resources.

2.2. Sheave wheels

The goal of this chapter is to investigate condition monitoring as it applies to sheave wheels. It is first necessary to get a clear idea of what a sheave wheel is.

On heavy duty industrial hoisting equipment (mine shafts, dragline booms etc.) the sheave wheel is the large pulley where the steel wire rope crosses over between the hoist drum and the payload (see Figure 1 below). The sheave wheel rotates freely and only facilitates a change in direction of the rope from the hoist drum to the payload.

Figure 1: Sheave wheels in headgears in underground mines.

2.2.1. Anatomy of a sheave wheel

The anatomy of a sheave wheel can best be described in relation to the images below. It should however be noted, that there is not one single design for a sheave wheel. They can have several different kinds of spokes, rim profiles and depths depending on the application. They also range in diameters from under 1m to around 7m. Sheave wheels are made of cast iron which possesses good inherent toughness characteristics and provides good lubrication due to the high carbon content of the metal.

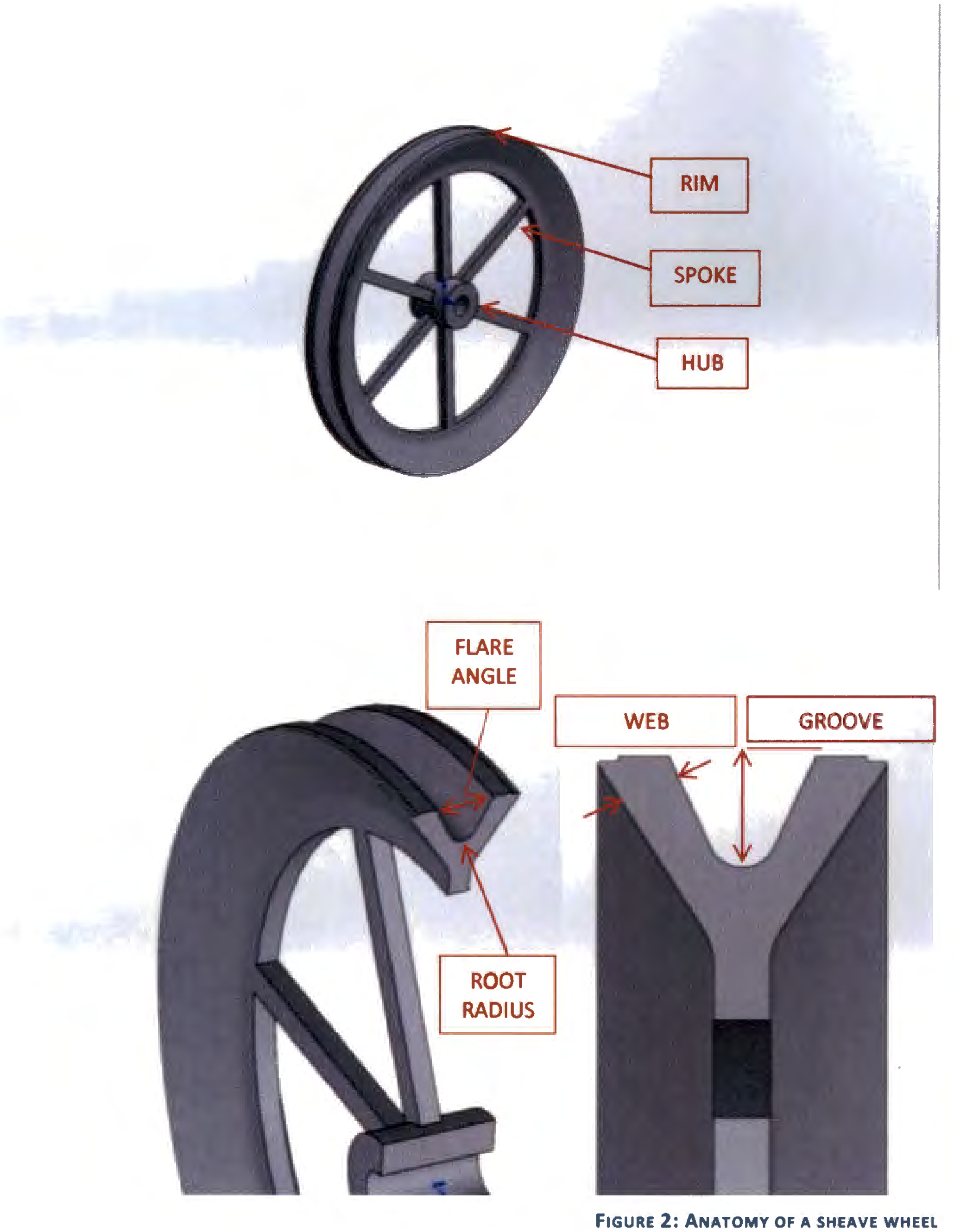

Figure 2: Anatomy of a sheave wheel

2.2.2. Where are sheave wheels used?

Sheave wheels are used in most heavy duty hoisting applications. While they are most widely used in the mining sector, there are also several other applications which will be shown later.

Mines: underground

Sheave wheels (also known as headgear pulleys) are used extensively in underground mining operations. A typical cross section of an underground mine can be seen in the image below. In this case, the steel wire rope runs from the hoist house through the head-frame (where the sheave wheel is located) to the cage holding the payload (people or ore).

On mines where the ore is located deep under the surface of the earth, the mine uses a multiple independent hoist system. This means that there is another sheave wheel underground at the start of the secondary shaft.

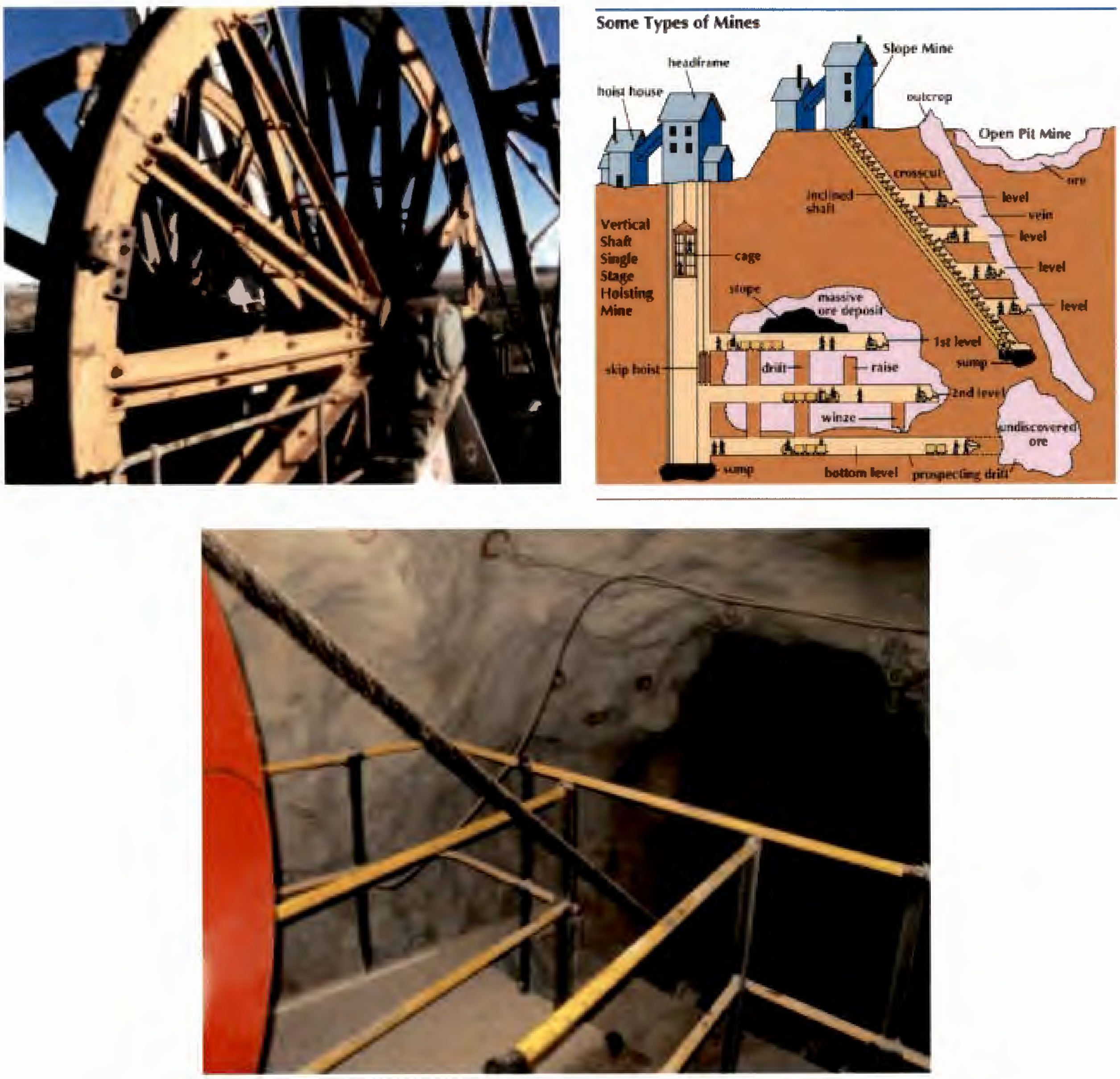

Figure 3: Sheave Wheels in underground mining applications

Mines: open cast

A dragline is used in open cast mining operations. As can be seen from Figure 4 below, it is a large bucket-scoop machine that is able to scoop the ore from an open pit mine and deliver it to trucks that can take it away for processing. Sheave wheels are used every time that the rope changes direction or the bucket lifts or lowers.

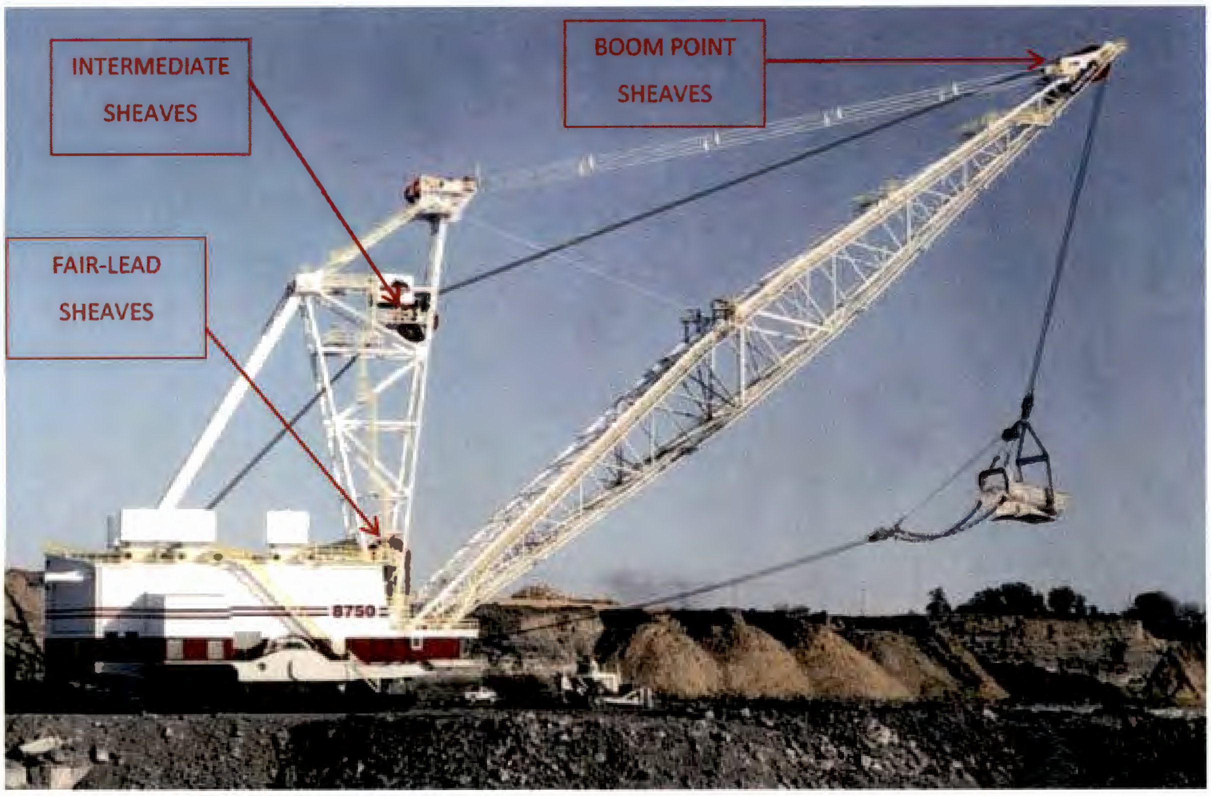

FIGURE 4: SHEAVE WHEELS USED ON DRAGLINES FOR OPEN CAST MINING OPERATIONS

Other hoisting equipment

There are several other places where sheave wheels are used for hoisting operations (as can be seen in Figure 5 below). From theme park rides to the (now defunct) cable way between Barberton and Swaziland. Sheave wheels can even be found anywhere from the Eiffel Tower to the elevators in buildings.

FIGURE 5: SHEAVE WHEELS IN VARIOUS APPLICATIONS

2.3. Wear in a sheave wheel

2.3.1. Causes, critical areas and effects of wear

As mentioned earlier in the discussion of wear, sheave wheels experience two types of wear namely **Natural Wear** and **Accelerated Wear.** Since the sheave wheel is made of relatively soft cast iron and the ropes are made from much harder steel, a certain degree of wear is to be expected. This type of wear is in fact part of the design of the system, since the carbon that is set free from the wear process acts as an added lubricant between the rope and sheave wheel.

The more concerning type of wear is accelerated wear. This is often caused by an erroneous setup of the rope system. It can cause damage to both the sheave wheel and the rope. The known causes of accelerated wear in sheaves are:

Misalignment between sheave and hoist drum (fleet angle)

If the fleet angle is more than 2°, the rope will touch the sidewall of the sheave wheel and cause premature wear to the web while causing irreparable damage to the rope.

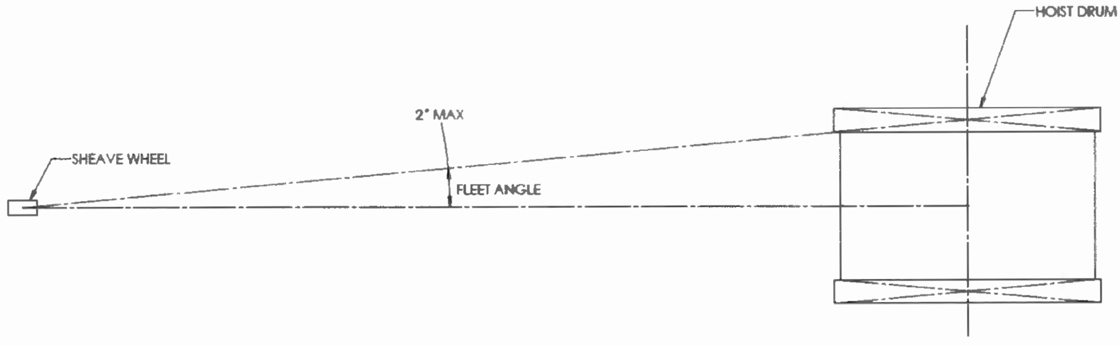

Figure 6: Fleet angle

Incorrect rope groove root radius

An incorrect rope groove root radius may be generally attributed to one of two causes: Firstly, if it was not machined to the correct size or not re-machined when it was due. The second possibility is that the sheave has worn to such an extent that the rope now runs in the new groove caused by wearing rather than the initial, machined groove.

When looking at incorrect machining practices, two problematic situations can be present namely oversize grooves and undersize grooves. When a sheave wheel has an oversized rope groove, the area of the rope that is in contact with the sheave wheel is small, meaning that the localised forces are larger than those designed for (Wirerope Works Inc., 2008). This has a tendency to cause flat spots on the rope (Bridon Mining, 2011). Due to the fact that the rope is comprised of twisted strands of steel wires, the rope has a tendency to veer from side to side as it rolls over the sheave. If the groove is oversized, the lack of support on the sidewalls may allow the rope to accumulate enough momentum to roll out of the sheave (Verreet, 2011). This is known as "jumping the sheave".

A sheave wheel can also have an **undersized rope groove**. This happens when either the groove was not machined to the correct size to start off with, or when the rope has worn the sheave down to the point that it has created a new rope groove. The latter case is of little concern when the initial rope that wore out the groove is still used, since it would have slowly worn out a groove that is roughly suitable for its size. However, when a new rope is fitted over a worn out groove, it would lead to rapid deterioration of the new rope as the worn groove will not have a sufficient diameter to accommodate the new rope, which at that point has not yet stretched to a reduced diameter.

Operating a rope with an undersized groove for as little as one or two weeks can cause irreparable damage to the ropes by leading to a phenomenon known as a "popped core". (SCAW Metals Group, 2006)

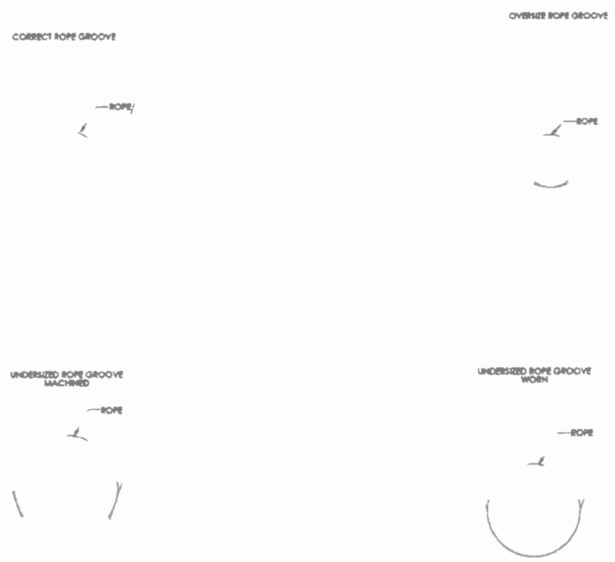

FIGURE 7: A) A CORRECTLY SIZED GROOVE B) AN OVERSIZED GROOVE, C) AN UNDERSIZED GROOVE DUE TO INCORRECT MACHINING AND D) AN UNDERSIZED GROOVE DUE TO EXCESSIVE WEAR

Figure 7 above indicates the various ways in which a rope groove can be incorrectly sized. Figure 7(a) represents a correctly sized rope groove. Figure 7(b) shows a rope groove that has been machined too large. Figure 7(c) shows an undersized rope grove that was cause by incorrect machining and Figure 7(d) shows an undersized rope groove due to excessive wear in the sheave wheel. Notice in this image how large the area of the rope is that is physically in contact with the sheave wheel. The friction component changes through the cross section of the rope which in turn leads to excessive wear of the rope. Figure 8 below shows results of ropes that have been subjected to incorrect rope grooves.

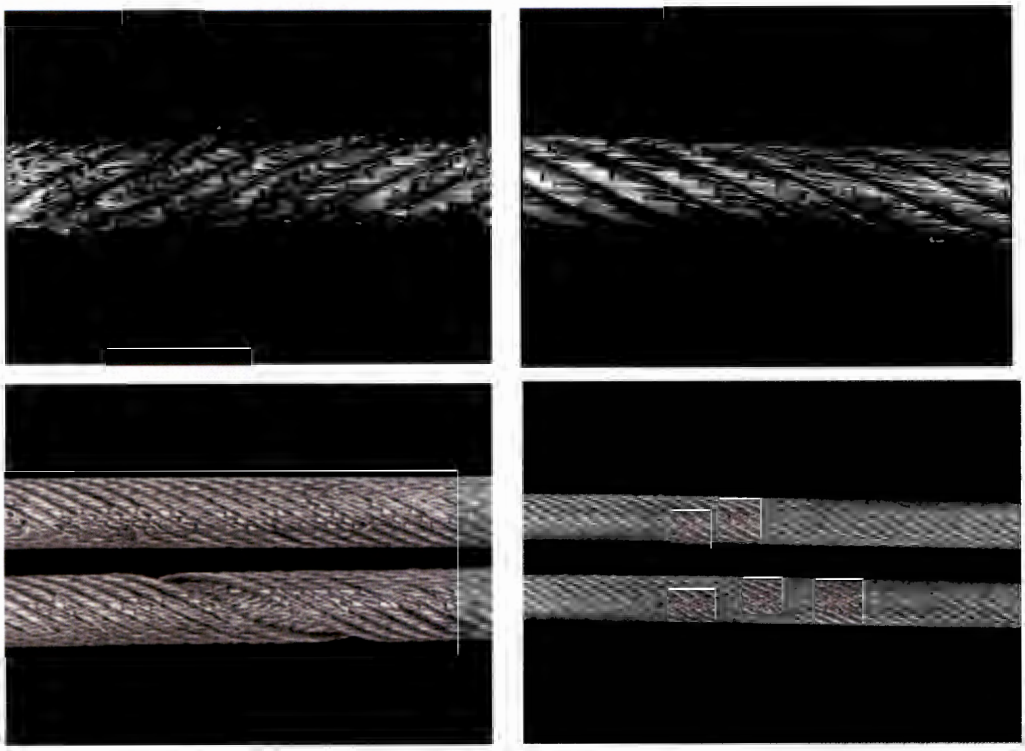

FIGURE 8: ROPE DAMAGE DUE TO INCORRECT ROPE GROOVES (IMAGE COURTESY OF ROLAND VERREET)

When one considers that the length of the ropes used in mining sometimes exceeds 2500m[1] for a single rope, it becomes apparent that a change in diameter from the top to the bottom of the rope is inevitable due to the strain in the rope. On very deep winds in these mines, the difference in diameter between the bottom and the top ends of the rope can be so large that the sheave groove is worn to a size less than the actual rope diameter at the top end of the rope. In this case, the groove must be machined to 2% greater than the maximum measured diameter. (SCAW Metals Group, 2010)

A rope that has been subjected to an incorrect rope groove may develop flat spots due to excessive contact pressure applied to the rope. A flat spot in the rope may cause a "whip" in the line, which will travel to one of the ends of the rope. When the "whip" reaches the end, it tends to cause severe kinks in the rope or to induce vibration along the rope. (Wire Rope Technical Board, 1993).

[1] South Deep Shaft in Carletonville, Gauteng is the deepest single shaft mine in the world at 2995m deep (Mining-Technology, 2014).

Incorrect flare angle

According to South African standards, the flare angle must be larger than 38° and ideally around 45° (SANS 10294, 2000) while other standards (ISO 4308-1, 2003) state that it should be between 30° and 60° depending on the fleet angle.

A large flare angle can cause the rope to jump the sheave at large fleet angles which is one of the most common modes of catastrophic failure of wire ropes. (Verreet, 2011). A rope that has jumped the sheave will get tangled in the machinery and get cut, curled and wires in the strands will get burred (Wire Rope Technical Board, 1993).

Figure 9 below demonstrates what is meant by a large and small flare angle (these are exaggerated for display purposes)

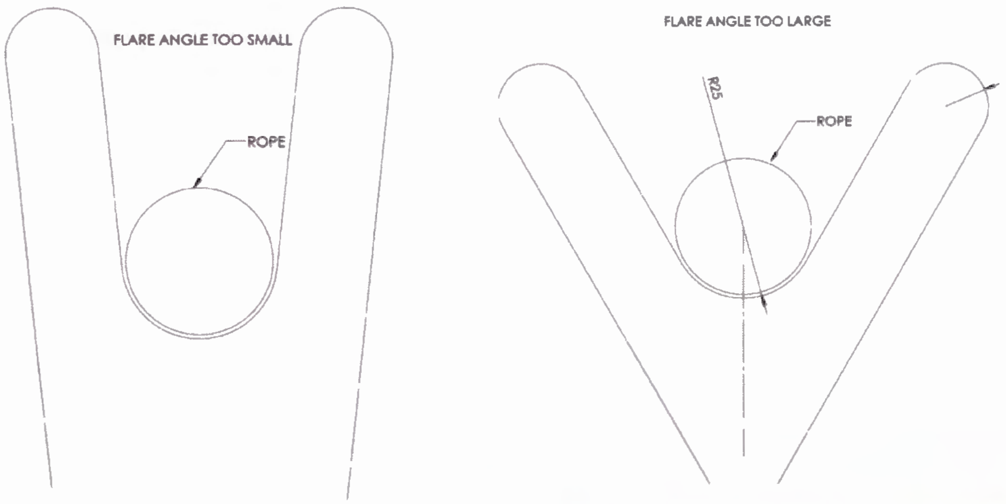

FIGURE 9: (A) FLARE ANGLE TOO SMALL, (B) FLARE ANGLE TOO LARGE

When the flare angle is too small, the rope will contact the sidewall as the rope hits the extreme ends of the drum winding (when the fleet angle is at its highest). This will degrade the sheave web as well as damage the rope. Figure 10 shows the damage to the sidewall of an underground sheave wheel at a mine in Welkom. This was likely due to an incorrect flare angle. Incidentally, the author was informed that there was a failure on this rope about four months after this photograph was taken.

FIGURE 10: WEB WEAR LIKELY DUE TO AN INCORRECT FLARE ANGLE

Sheave web

Under normal expected wear conditions, there should be virtually no wear in the sidewall of a sheave. When a sheave and hoist drum are not set up exactly right, there will be wear on the sidewalls of the sheave. Sheaves have limitations on the allowable web wear due to structural constraints of the wheel. Each manufacturer will specify tolerances for wear on their sheaves (SANS 10294, 2000). According to KEW (a manufacturer of sheaves based in Kimberly, South Africa) the minimum typical sidewall thickness is around 22mm and depending on the sheave diameter, wear of between 30mm and 38mm is allowed on the tread diameter. (Goncalves, 2009)

FIGURE 11: A) WEAR IN THE SIDEWALL DUE TO MISALIGNMENT, (B) WEAR IN SIDEWALL AT ROOT DUE TO MISALIGNMENT

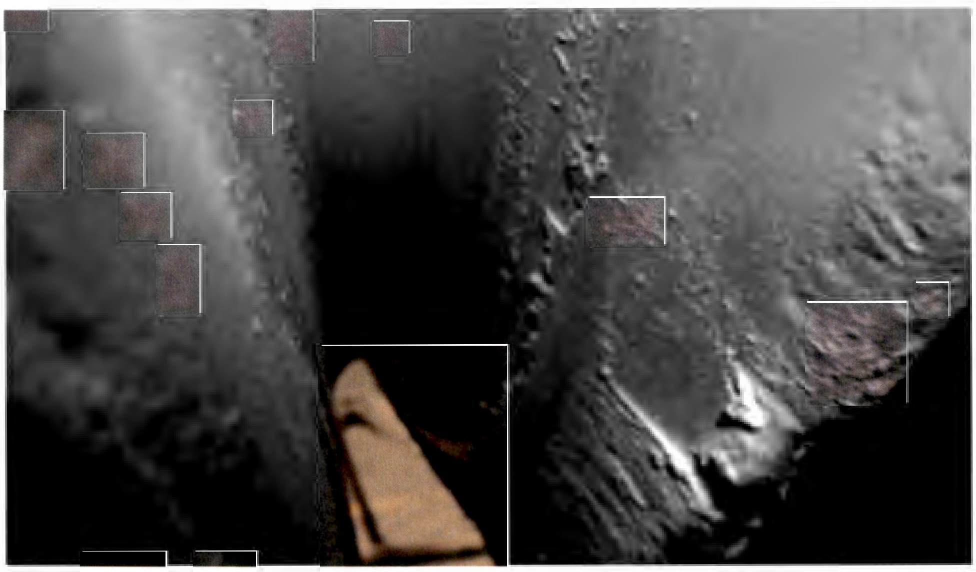

FIGURE 12: WEAR IN SHEAVE WHEEL WEB

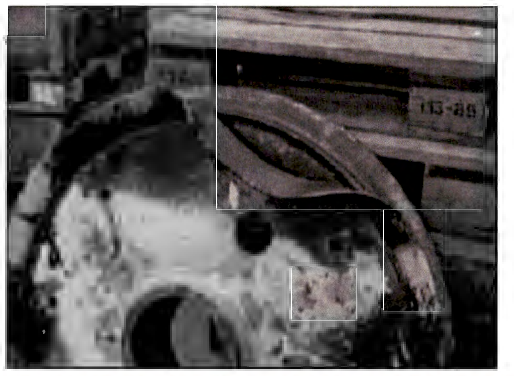

FIGURE 13: THE RESULT OF EXCESSIVE WEB WEAR IN A SHEAVE (IMAGE COURTESY OF ROLAND VERREET)

Height of the groove

The height of the groove has to do with the way the sheave has been machined for a particular rope. If the groove is too shallow, there is the risk of the rope jumping the sheave.

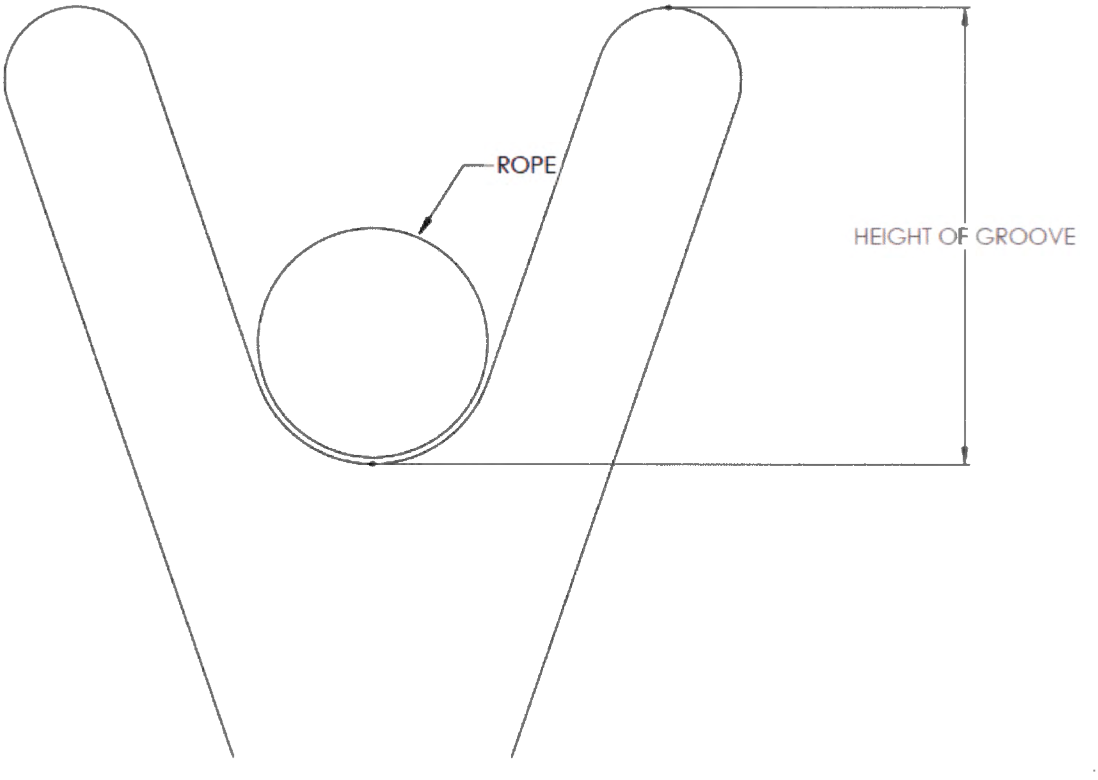

FIGURE 14: HEIGHT OF ROPE GROOVE

In summary, there are four critical areas to consider when looking at sheave wheels:

- Rope groove radius
- Web thickness (both sides)
- Height of groove
- Flare angle

2.3.2. What is being done to combat wear in sheave wheels?

Fleet angle checks

The fleet angle is checked at certain mandatory intervals. The legislation is strict about the parameters within which the fleet angle must fall. Technicians use laser alignment to confirm that the fleet angle is within limits.

Wear inserts

Some mines choose to use wear inserts in the root of the sheave. These are plastic inserts that are designed to wear down much faster than the rope. The plastic is also designed to be a lubricant for the rope as it passes over the sheave. While some mines do implement this technique, it has shown little promise. The technique holds implicit risks in the placement of the inserts. If the inserts come out during operation, the rope wears directly onto a critical, incorrectly shaped root, causing rapid wear on the rope and the sheave, which may lead to critical failure

Cutting of sheaves

If wear on a sheave wheel can be detected while it is still below the limits set out in the standards, it is possible to fix the wear relatively cheaply by cutting the rim to the correct profile. Cutting of sheaves is also mandated whenever new ropes are installed.

A disc-type cutting bit is used together with an x-y-controllable tool post. The sheave wheel is rotated and the desired rim profile is machined. This technique is however only viable if there is sufficient material left on the sheave. As this is a highly specialised technique it is becoming an increasingly rare skill.

Re-rimming of sheave wheels

One sheave wheel manufacturer claims that they are able to recondition sheave wheels by removing the entire rim, while saving the spoke and hub. They state that, irrespective of rim wear, it is possible to get a good-as-new sheave wheel for approximately 60% of the cost of a new wheel and with a reduced lead time (Goncalves, 2009).

2.4. Condition monitoring of sheaves

Although the steps mentioned above can be successful and are usually a more viable option than replacing the sheave wheel completely, the age old maxim still prevails: prevention is better than cure. Sheave wheels are designed to fulfil a certain function and if one operates it within the design limits, a suitable lifespan should be obtained.

Since operational perfection is not readily achieved, the second best option is to keep a watchful eye for symptoms of problems which may cause a shortened lifespan. This can only be done with inspections. If sheave wheels are regularly monitored, early indications of wear can be detected and acted on before it is necessary to do much remedial work. This, although vital, is not new. Legislation and OEMs require operators of hoisting equipment to inspect their sheave wheels periodically.

According to (SANS 10294, 2000) the rope grooves should be inspected every three months and these values should be recorded. It further indicated (as can be seen in Figure 15 below), the relevant critical areas and provides minimum required values for each area.

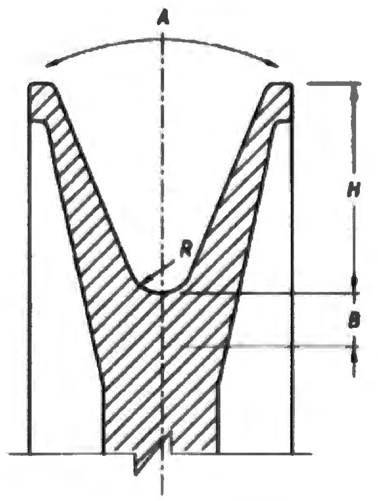

Legend
A is the angle of flare not less than 38 recommended 45
R is the root radius of the groove (0,525 *d* to 0,55 *d*)
H is the minimum height of the groove (2,5 *d*)
B is the maximum allowable groove wear
d is the nominal rope diameter

FIGURE 15: SHEAVE PROFILE WITH CRITICAL AREAS

According to an OEM of steel wire ropes (SCAW Metals Group, 2006), whenever a new rope is installed, a sheave must be checked to ensure that it is the correct size.

There is no information in the standards nor any legislation that determines the interval of inspection of the flare angle, but according to one OEM of sheave wheels (Goncalves, 2009), it is recommended that the entire rim profile be checked at least annually.

In summary, a good rule of thumb (according to legislation) would be to inspect the rope grooves every three months and the rim profile annually or whenever a new rope is installed. The author believes that this is a dubious suggestion since it was asserted earlier that as little as two weeks' operation with an incorrect rope groove is enough to damage a rope. Again, if it were simple, quick and cost effective to measure sheave wheel profiles, it could be done much more often, ensuring a safer, more productive environment.

2.5. What is being done to measure wear on sheaves?

The legislation and OEM requirements state that the sheave profiles should be checked and also provide required parameters for the various critical areas. What none of these entities seem to be specific about is the method by which these profiles should be checked and the kind of accuracy required in these measurements. This begs the question: What is the current state of the art?

It was noticed that since neither legislation nor OEMs provide guidelines of the sheave profiling methods required, yet state that profiles must be taken and saved for several years, there has been a scurry amongst affected parties to develop or find suitable profilers to comply with legislation.

The people mentioned above are production oriented and have thus not published any documents (as far as the author could tell) pertaining to the methods they use to record sheave profiles. Since it was necessary to determine the current state of the art, it was decided that the most suitable way to make this determination, was through survey. The scope of the survey spanned to include the full scope of affected parties:

- Employees of open-cast mines
- Employees of underground mines.
- Employees of 3rd party contractors that provide sheave profiling service to mines.
- Employees of OEMs that manufacture/import ropes.

The actual survey was conducted online, with each person having been located and telephonically contacted beforehand to verify their identity. A more comprehensive summary of the survey result can be found in Appendix 3. In the interest of brevity, the raw data has been left out of this document, but can be made available on request. Figure 16 sets out the results of the survey conducted.

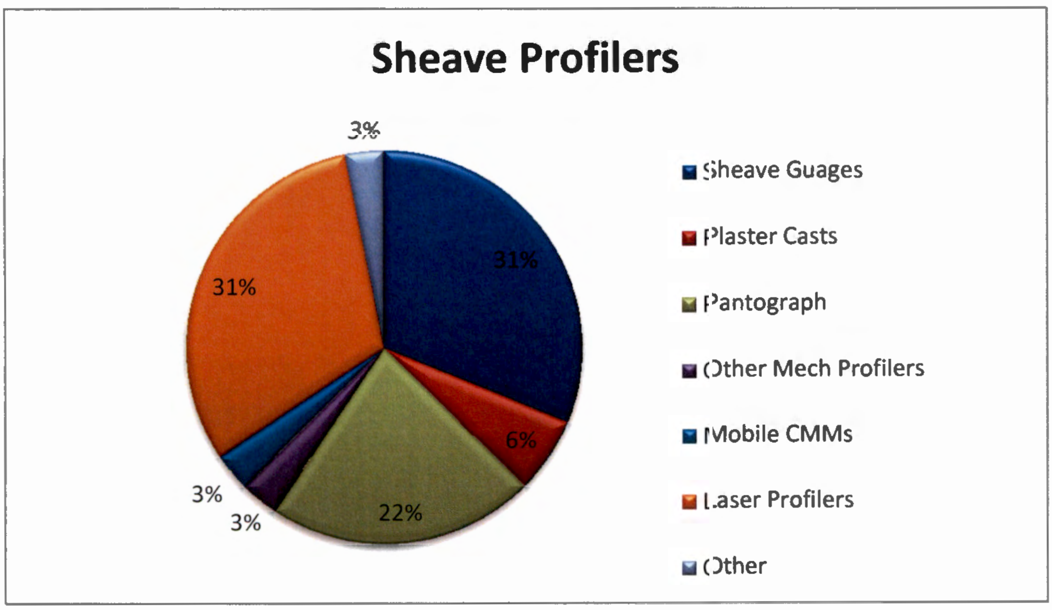

Figure 16: Sheave profilers used in industry - survey results

In the following section, each of the methods determined from the survey will be briefly discussed.

2.5.1. Sheave gauges

Sheave gauges (such as those in Figure 17) are a very handy and inexpensive tool to check the rope groove of a sheave wheel. They consist of a stack of plates with various radii at their tips. These are then pressed into the rope groove until the best fit is found.

Figure 17: Sheave gauges for measuring the rope groove profile

One drawback of using sheave gauges is that they can only measure the groove profile to the nearest size available. This limits the potential to detect small amounts of wear and is thus more suited to a go/no-go type of test as opposed to rigorous wear rate trending. Another concern is that they are only able to measure the rope groove itself, so another method still needs to be employed to measure the rim profile and web thickness.

2.5.2. Plaster casts

According to one of the manufacturers of steel wire ropes (SCAW Metals Group, 2006) , the process to follow to determine a sheave profile by plaster cast is as follows:

i. Clean section of sheave that is to be measured
ii. Grease or oil the section very lightly
iii. Immerse a plaster of paris bandage briefly in water
iv. Drain it for about 10 seconds
v. Force it into the groove
vi. Hold firmly for 1 minute
vii. Leave to set for 5-10 minutes in position

viii. Remove it by tapping lightly with a hammer

ix. Send to Haggie Technical Services Department for comments

Experienced technicians would often replace the last step by tracing the profile onto paper and measuring the required values with a ruler (Els, 2012). A brief overview of the plaster casting process can be seen in Figure 18 below.

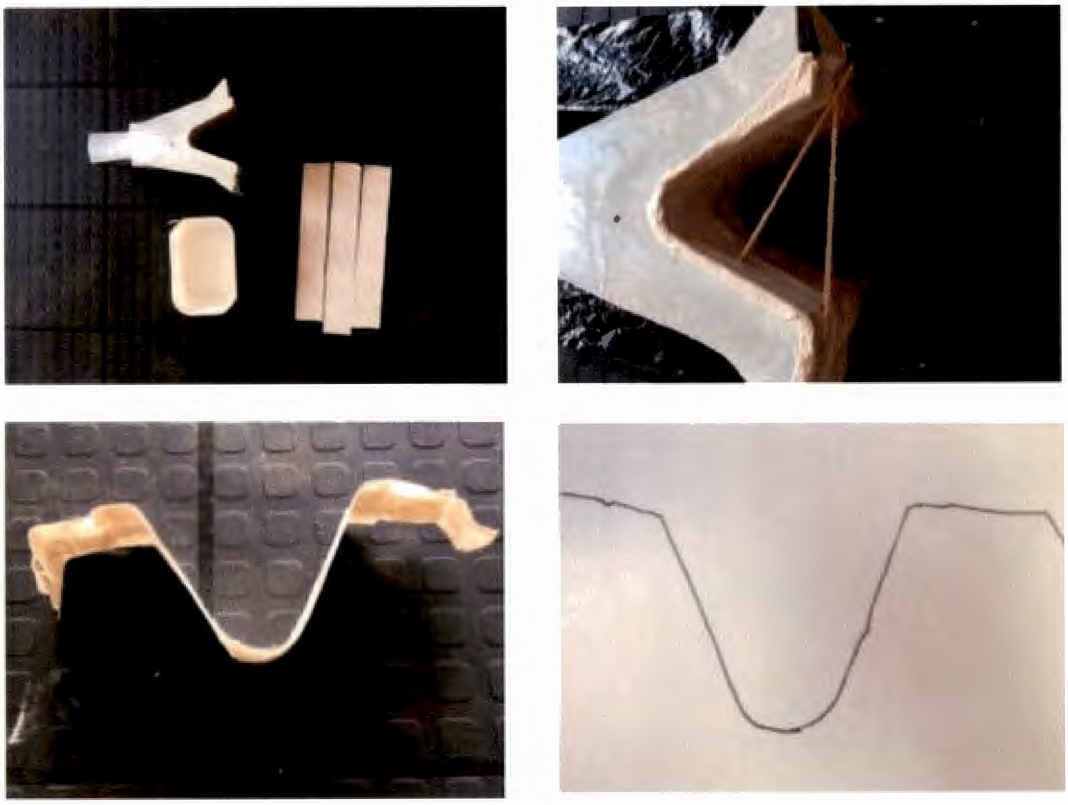

FIGURE 18: SHEAVE PROFILES TAKEN BY PLASTER CAST

Plaster casts were very widely used several years ago, but have become obsolete due to a several drawbacks:

- The set-up time to produce a plaster cast is roughly 15 minutes (judging by the experiment that was done above).
- The accuracy of the profile is limited by the thickness of the line drawn when the profile is copied onto the piece of paper.
- It becomes laborious to redo a profile if it was not perfectly taken the first time.
- Sheaves are almost always inspected *in-situ* and it is usually not practical to take a plaster cast.

- The plaster cast can measure the flare angle, root radius and the groove depth, but it is not able to measure the web thickness since it does not wrap around the sheave.[2]

2.5.3. Pantograph

The pantograph (as can be seen in Figure 19) is a very widely used mechanical profiler. It works by tracing a scribe against the surface of the sheave wheel rim (as shown in Figure 20 below). The scribe is rigidly connected to a pencil through a set of levers, which traces the profile drawn by the scribe at a 1:1 ratio. In practice, some technicians use graphing paper to allow them to measure the critical areas.

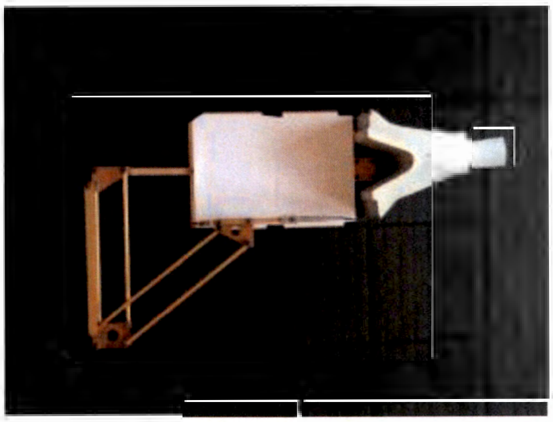

Figure 19: Pantograph

The system, although fairly simple to use, has been noted to have several drawbacks.

- The system does not provide a means of comparing the latest profile with previous profiles.
- Surface contact method – scan time and set-up time is fairly long.
- Accuracy is limited by the thickness of the pencil line as well as the deflection in the tracing arms. This was claimed to be around 5-10mm judging on the repeatability (Els, 2012) this will be determined experimentally.
- The fairly large structure makes it difficult to take profiles in some situations where the sheave wheel is not at a convenient angle.

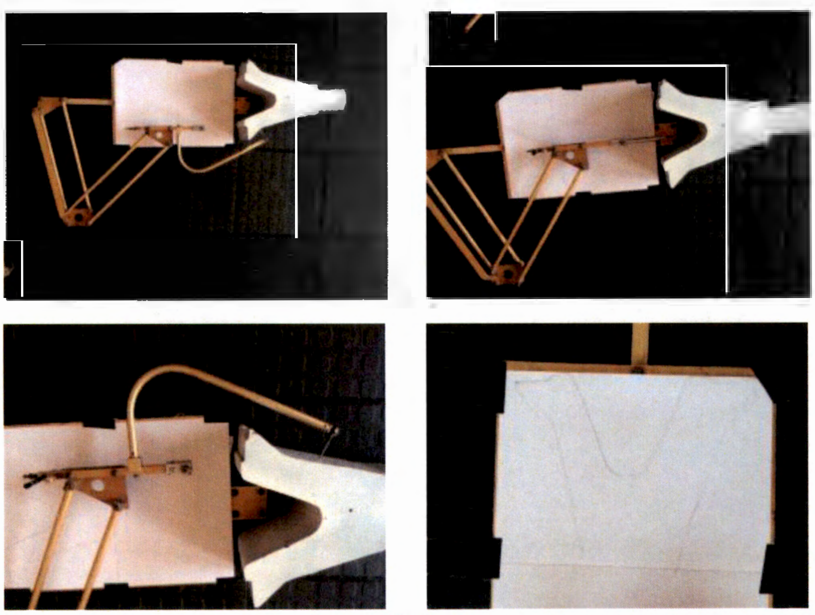

Figure 20: Process of taking profiles with a pantograph

---

[2] There were experiments done with wrapping the plaster around the sheave, but cast was not rigid enough to provide and accurate value of the web thickness (van der Walt, 2014)

2.5.4. Other mechanical tracing mechanisms

Figure 21 below shows a South African made sheave wheel profiler. It is a system that uses gears to create a 1:1 image on a sheet of paper. The system is reasonably priced, but has a few drawbacks.

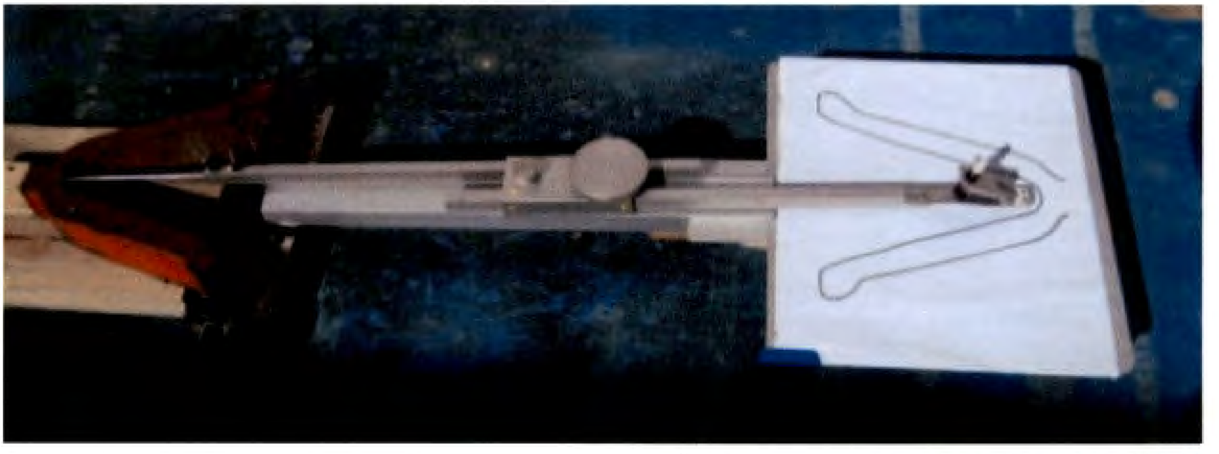

Figure 21: South African made sheave wheel profiler

- The use of a pen/pencil to draw the profile adds the width of the line to the experimental uncertainty of the system.
- The use of gears means that the inherent backlash in the system is unavoidable. This will negatively impact the accuracy and repeatability of the results.
- As with the other methods described so far, the system does not provide a means of comparing the latest profile with previous profiles.

2.5.5. Digital tracing mechanisms – Microscribe®

The Microscribe®, as illustrated in Figure 22 below, is a type of portable CMM (Coordinate Measuring Machine) used in several reverse engineering applications. At roughly five times the price of the system shown above, it is a high precision instrument 0.38mm for the G2 (Microscribe, 2014).

Figure 22: Microscribe coordinate measuring machine

Interestingly enough, it was not designed for use with sheave profiles but was an initial attempt by staff of Anglo Technical Services to digitise sheave profiles (Els, 2012). This is illustrated by the fact that it measures coordinates in three dimensions while sheave profiles are only required to be in two dimensions.

Due to the specialised nature of this instrument, it uses an advanced CAD package to operate which puts a high training burden as well as an added setup cost to institutions wanting to take sheave profiles digitally (Els, 2012). Another drawback of the system is that due to its high precision, combined with its multi degree of freedom measurements, it is susceptible to environmental influences (like vibration) when a profile is being taken (Els, 2012).

2.5.6. Laser profiler

Figure 23: The laser based sheave wheel profiler

A triangulation laser-based system, shown in Figure 23, was developed by a South African company in an attempt to address the shortcomings of all the systems above. The result was interesting. The system improved scan time significantly and had a simple user interface which allowed for digitisation of profiles. It also allowed for comparison of successive scans and digital measurement of various critical areas. At first glance it seemed to address most of the shortcomings of the other systems, even though it came out at roughly the same price as the Microscribe® mentioned above. Figure 24 shows the results from the laser profiler.

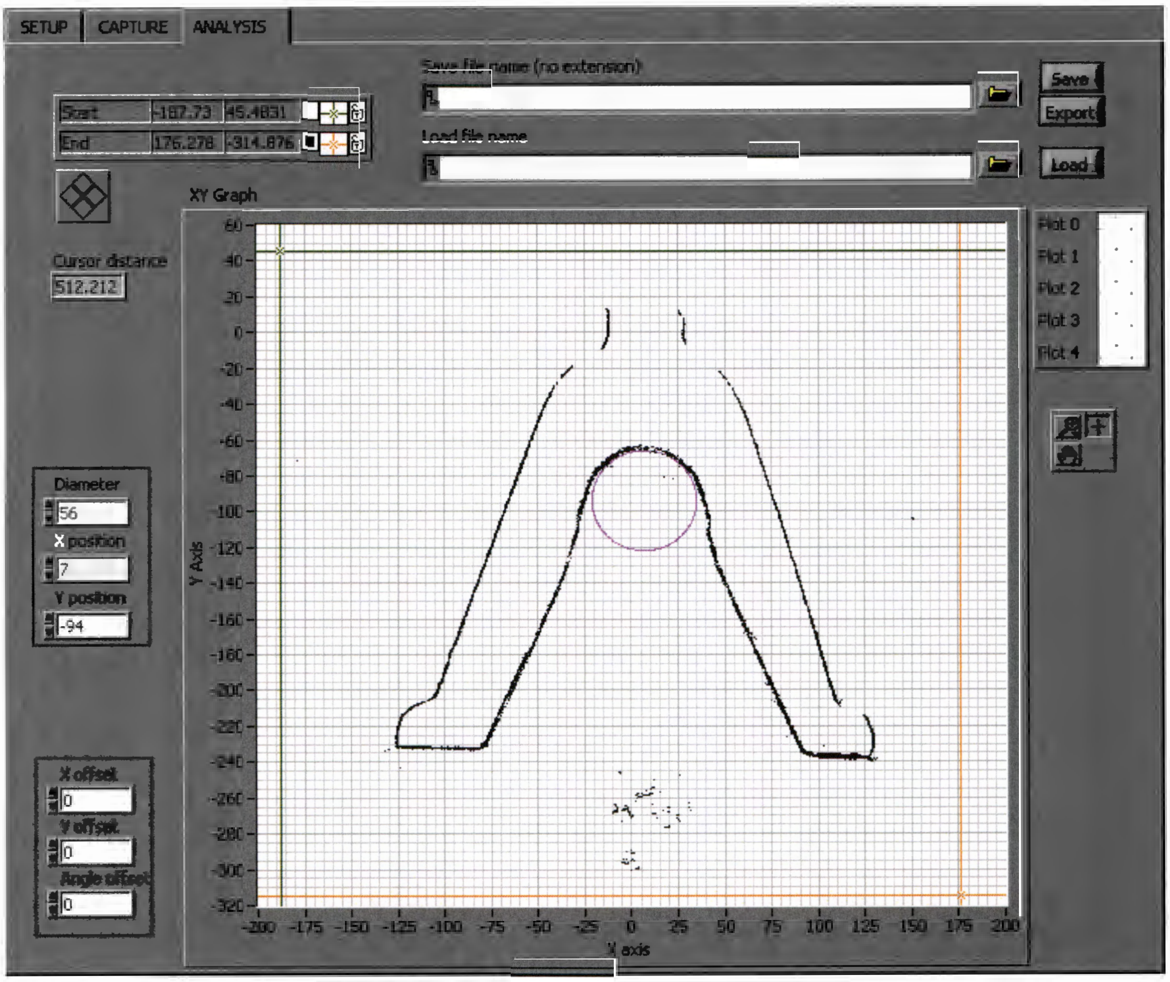

FIGURE 24: RESULTS FROM THE LASER PROFILER

When the system was examined closely, some concerning fundamental errors became apparent:

Surface profile acquisition method:

The laser profiler uses a point laser and a set of encoders to acquire the surface profile. Because it is a non-contact method, the manufacturer specifies that the points can be acquired in any order, as long as the laser beam is roughly at a right angle with the surface area to be scanned. These two facts combined mean that in the end, you have a point cloud which represents the surface profile, but no way to determine which points belong to which section of the surface. Therefore it is not possible to join the dots into a single curve. This introduces a bias into the results. The "human factor" is therefore always present and therefore, the maximum accuracy of the system is limited to the thickness of the line (set of points).

Accuracy, precision and significant digits:

"Accuracy is the agreement of a measurement with the accepted value of the quantity"

(Kotz & Treichel, 2003)

The stated accuracy of this profiler could not be found from publications by the manufacturer. It will be determined during the experimental section of this report. For the sake of argument, it will momentarily be assumed that the accuracy of this profiler is spot-on.

"The precision of a measurement indicates how well several determinations of the same quantity agree"

(Kotz & Treichel, 2003)

Since the manufacturer has left the points as they were acquired, it is possible to comment on the precision of the profiles just by looking at the distribution of the points that are to represent a single point since this represents several determinations of the same quantity.

Looking at Figure 25, one block in the y-axis represents 4mm. Since it is known that the set of points is to represent a single surface (which for this section should be roughly horizontal), the thickness of the collection of points in the y-axis can be taken to represent a single actual value. This implies that even if one could assume the profiler to be 100% accurate (which it cannot be), it could not possibly be more precise than ±4mm.

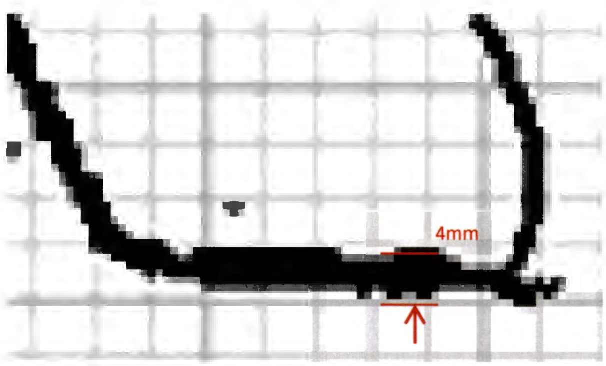

Figure 25: Thickness of line

"Unless indicated otherwise, the standard convention used in science is that the final digit in a number is uncertain to the extent of ±1."

(Kotz & Treichel, 2003)

Looking at Figure 26 on the right, there is an implicit precision of measurement of ±0.001mm. This does not agree with the ±4mm that was seen above.

Therefore, regardless of the accuracy of the instrument, it cannot possibly be more precise than the thickness of the line represented by the multitude of points that determine it.

Figure 26: Precision of laser profiler

2.6. Conclusion

In this chapter the following has been determined:

- Sheave wheels are subject to both natural and accelerated wear.
- If accelerated wear in sheave wheels can be detected early on, it is often possible to remedy the situation while keeping costs and downtime to the minimum.
- It is a legislative and OEM requirement that sheave wheels be inspected at certain intervals for the sake of both the wheel and the steel wire rope.
- There are several techniques for determining the profiles of sheave wheels.
- Each of these techniques has some concerning deficiencies.

An interesting observation made by the author during the writing of this section was about the precision of the various methods. Aside from the Microscribe® there appears to be no form of verification or validation on the measurement precision and ultimate accuracy that could be achieved with any of the modalities. This is cause for concern since these are, after all, measurement instruments and the veracity of the results obtained by them need to be established before they are used as an input for go/no-go criteria on multi-million Rand (or worse, potentially fatal-critical) decisions.

The current methods of testing seem to be no more than a false sense of security for the mines and for other users of sheave wheels.

CHAPTER 3: DIGITISERS AND IMAGE ACQUISITION

By now we have identified that a problem exists and have provided sufficient background information to allow the reader to fully comprehend the problem. In the next chapter we will be formally defining what an ideal solution would look like. Hopefully some of the solution's properties have been alluded to through the shortcomings of the current state of the art. Before formally stating the problem and defining the ideal solution, it is necessary to delve into one last theoretical section which will address one of the properties required of an ideal solution. This chapter is about digitisation of measured values and in it the author attempts to offer a concise summary of the world of digitisers so as to provide the reader with the final piece of information required before the solution can be formally defined.

Looking at a combination of definitions from various dictionaries, a digitiser can be defined as:

A device for converting continuous/analogue signals into discrete digital (binary) signals for processing by a computer.

Although this is technically correct, it would be more appropriate (for the purposes of this document) to focus on a specific type of digitiser. The new document-specific definition of a digitiser would then be:

A device for converting physical objects into their digital representations.

These types of digitisers are used in various applications including medical diagnostics, quality control and reverse engineering. They all have different ways of collecting the information and are based on several different data acquisition modalities. There are two main categories of digitisers namely contact and non-contact digitisers. A distinction is made in Figure 27 below.

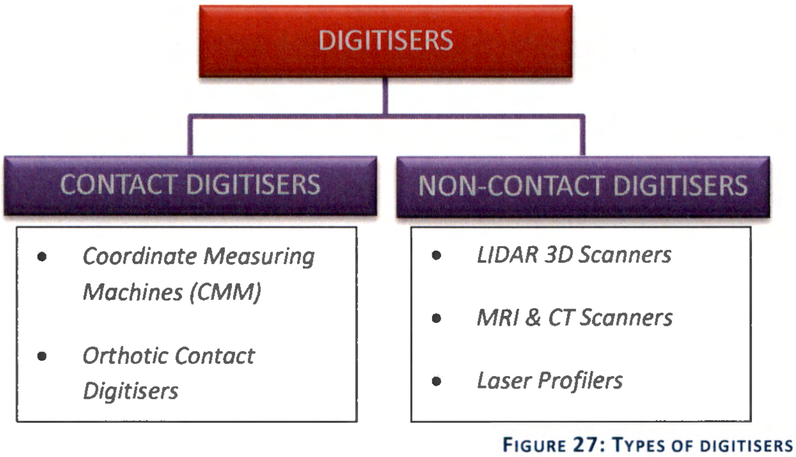

FIGURE 27: TYPES OF DIGITISERS

3.1. CONTACT DIGITISERS

FIGURE 28: A FEW TYPES OF CONTACT DIGITISERS. A) MOBILE CMM B) CMM AND C) ORTHOTIC CONTACT DIGITISER

Contact digitisers (see Figure 28) work on a fairly straight forward principle: a mechanical device with a stylus that is brought into contact with the surface of an object. The position of the stylus is then recorded by measurement sensors (e.g. distance or angle measurement) and sent to a processor for interpretation and digital reconstruction of the measured surface. Figure 29 shows the process of acquiring data with a contact digitiser.

FIGURE 29: THE PROCESS OF DIGITISING COORDINATES WITH A CONTACT DIGITISER

This technique suffers from various drawbacks. The main shortcoming is that since the stylus needs to be in contact with the surface it is measuring, there will be some loading effects either on the surface or in the profiler members (Elmas, Islam, Jackson, & Parkin, 2011). This will have an effect on the accuracy of the measurement as well as the speed at which profiles can be obtained. Another drawback with contact methods is that the stylus tip has a finite radius which affects the maximum accuracy of the measured values (Wong & Li, 1999).

These contact digitisers have a valuable place in industry and are widely used in applications where the shortcomings are not true constraints as shown in the figure above. The stylus is sometimes replaced by a non-contact sensor while keeping the architecture of the rest of the machine the same. For example, the CMM sometimes uses a triangulation laser or capacitive probe. It will still have the same drawback of being time consuming, but will address the other drawbacks of loading effects and stylus tip radius.

The Microscribe (Figure 30) mentioned in Chapter 2 is an example of a mobile CMM.

FIGURE 30: THE MICROSCRIBE MOBILE CMM

3.2. Non-contact digitisers

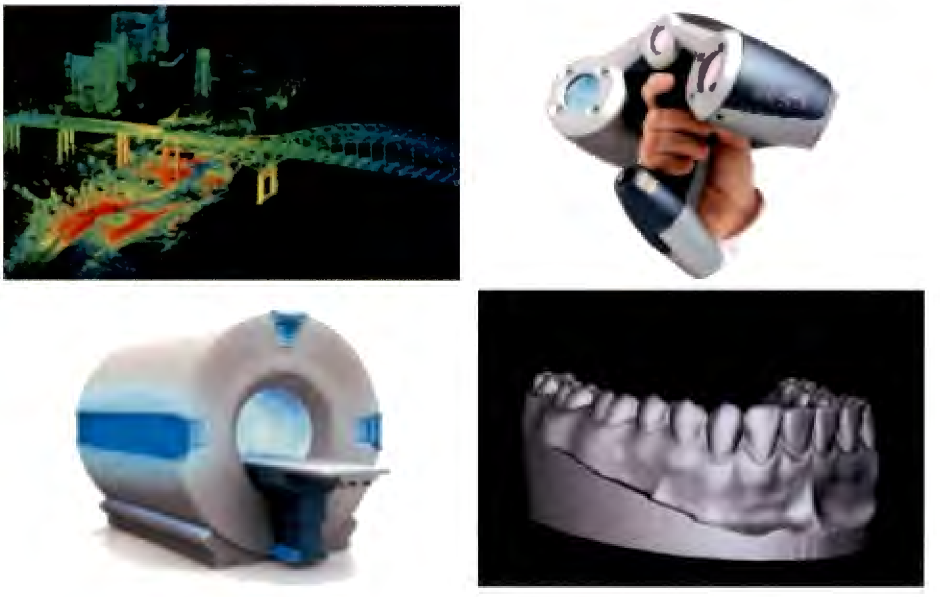

Figure 31: Non-contact digitisers / results a) LIDAR b) Stereoscopic Vision c) CAT scan and d) 3D Laser scanner point cloud

Non-contact digitisers (see Figure 31) work in a similar way to contact digitisers, except that instead of the use of a physical stylus, they use a source-sensor combination and electromagnetic waves of different frequencies to determine the responses to objects made by the waves. This is essentially an electromagnetic stylus.

Figure 32: The process of digitising coordinates with a non-contact digitisers

Different modalities use different sections of the electromagnetic spectrum. Some modalities are shown in the figure below.

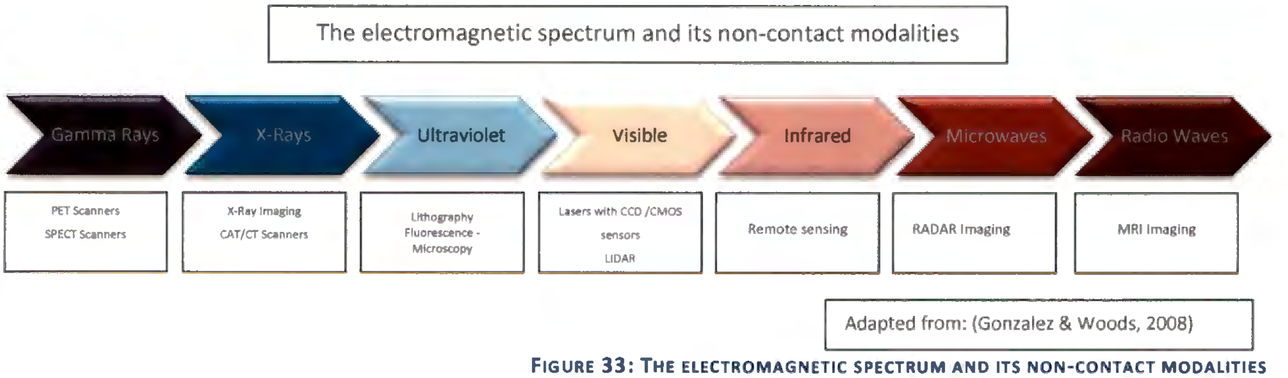

Figure 33: The electromagnetic spectrum and its non-contact modalities

Actually, the electromagnetic spectrum is not the only spectrum used for image acquisition. Other modalities include the Scanning Electron Microscope and acoustic-based methods like SONAR (Gonzalez & Woods, 2008). In the interest of brevity, these are not considered here and when non-contact data acquisition modalities are mentioned in this document, the implication is that they are of electromagnetic origin. More specifically, they are in the visible portion of the spectrum.

These optical non-contact methods can be divided into three distinct classes (Yang, Jackson, & Parkin, 2006) namely:

- Triangulation sensing,
- Light sectioning,
- Shadow analysis.

Triangulation sensing is typically used in laser profilers. In this case a laser diode projects a laser spot onto a surface and then uses a CCD chip to detect the reflection off of the surface. The distance between the object and the sensor can then be calculated by the position on the CCD sensor where the laser spot was detected. One of the main drawbacks of pure triangulation systems is that, as with contact profilers where the stylus is replaced by a non-contact sensor, it still has to physically trace the surface that is to be inspected. This means that although it has solved the problem of finite stylus size as well as the loading effects on the surface, it cannot do much for the speed problem.

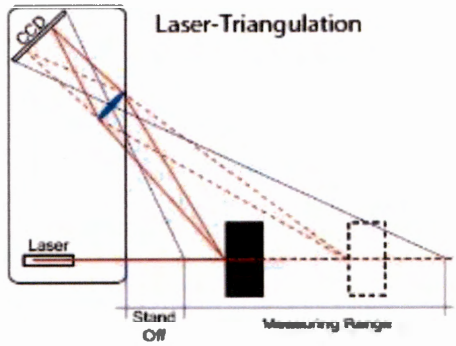

FIGURE 34: LASER TRIANGULATION PRINCIPLE

The laser profiler mentioned in earlier in Chapter 2 is an example of a non-contact digitiser that uses a point laser triangulation sensor to acquire the surface profiles.

Light sectioning is performed by projecting a line of light onto a surface and determining the surface profile by interpreting the resulting curve (Yang, Jackson, & Parkin, 2006) as shown in Figure 35. This is the modality used with line laser scanners.

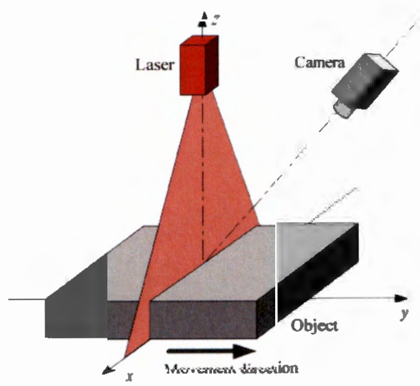

FIGURE 35: LIGHT SECTIONING WITH LASER LIGHT SHEET

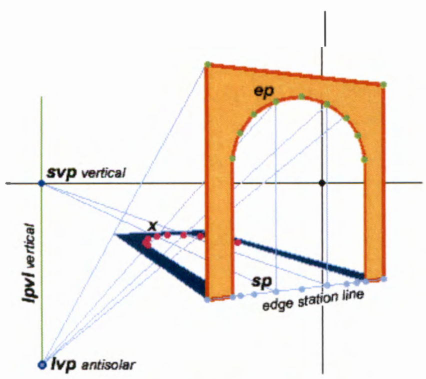

FIGURE 36: SHADOW ANALYSIS

Shadow analysis involves the determination of surface features by analysing the oblique shadow that is cast over an illuminated surface (Yang, Jackson, & Parkin, 2006). This is a very basic structured light approach that can be applied very cost effectively since all that is required is a light source, an obstruction of the light and a sensor to determine what the shadow looks like (a camera). An example of this approach is shown in Figure 36.

3.3. Conclusion

If one chose a method like light sectioning or shadow analysis, it would be possible to acquire the profile of the sheave wheel with minimal involvement of mechanical arms and linkages. This would rule out the need for extra sensors while reducing the possible areas of error introduced by finite mechanical tolerances within the members of the mechanism. It would further decrease profiling time since both of these methods remove the need for tracing the surface to acquire the profile.

CHAPTER 4: DESIGN OF PROTOTYPE DIGITAL SHEAVE PROFILER

"If I asked my customers what they wanted, they would have said they wanted a faster horse"

Henry Ford

4.1. INTRODUCTION

From the preceding chapters it was concluded that there exists a need for a new method to take profiles of sheave wheels. This method would need to adhere to a certain set of specifications to compensate for the shortfalls of the various other methods while staying within the prescribed capabilities as dictated by the relevant legislation. It would also need to be validated to give the operator an idea of the accuracy of the measurements taken.

4.2. THE DESIGN PROCESS FOLLOWED

FIGURE 37: A GENERIC PRODUCT DEVELOPMENT PROCESS (ULTICH & EPPINGER, 2008)

It was necessary to modify the design process shown in Figure 37, to be more applicable to this specific project. The "planning" section was replaced by "initial design specifications" since these were developed informally in previous chapters and serve as the start of the design process while the actual planning of a commercially viable project is not relevant for now.

FIGURE 38: THE DESIGN PROCESS FOLLOWED FOR THIS PROJECT.

"Concept development" and "system-level design" were swopped around since the output of the system level design is a set of final design requirements. It is the author's opinion that this is a suitable input for the concept development and selection phase. To distinguish between this project and a conventional engineering project, the "design verification" and "design validation" phases were added. Phases 1 – 4 are considered in Chapter 4.3 while the section on detail design will be handled in 4.4 and the design verification in Chapter 5. The prototype profiler was then manufactured and it was validated in Chapter 6.

The section where the profiler is manufactured is not discussed in detail since the actual manufacture of the profiler does not really form part of this dissertation. The following section (Figure 39) briefly puts the type of prototype that will be manufactured into perspective:

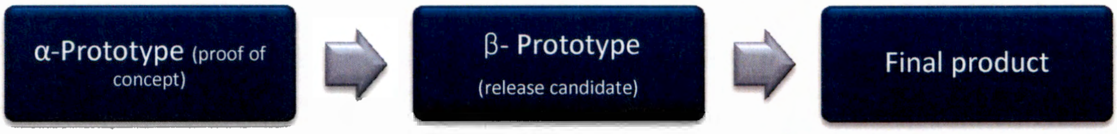

Figure 39: The prototyping cycle

An α-prototype is completed after the detail design specifications, but before the design is finalised. It is essentially a proof of concept prototype where the methodology behind the design can be verified and validated. It does not have to look like the proposed design, nor does it have to be made from the same material as the proposed design. It must be functionally equivalent to the proposed design (at least in the critical aspects). The β- prototype is both functionally and aesthetically equivalent to the proposed design. It differs only in the manufacturing method used (since the final release often makes use of mass production that would be impossible for small batches in the β- prototype. The β- prototype is often subjected to field tests and given to early adopters to try. After the feedback from this phase has been implemented, the final product can be produced.

4.3. User needs and design requirements

The first design parameter is that the profile must be available in digital format. That is part of the aim of this document.

4.3.1. User requirements

Most of the design specifications are decisions that will be made based on the background knowledge. These cannot be quantified and are therefore not to be verified or validated. The final specification concerns the accuracy of the profiler. This is the parameter that will be scrutinised and the one which will determine the ultimate success of the system.

How many operators are available to do a scan?

Two of the constraints in condition monitoring mentioned earlier (van der Walt, 2014) were safety precautions and consideration of the fact that many tests are done in remote locations. Both of these concerns can be addressed if the profiler requires only one person to operate.

How long does the operator have to scan a wheel?

Since the cost of stopping the machinery for inspections far outweighs the cost of the actual inspection, the inspections have become a grudge buy because of the time they take. To mitigate down-time losses the time allotted for a profile should be the absolute minimum that is possible.

Permanent or periodic system:

In the case of sheave wheels, the inspection interval has been determined in legislation to be roughly every six months to a year. Since these items are typically in service for many, many years and barring any serious abnormal conditions, will not wear unexpectedly fast, this time frame should be suitable. It is therefore not necessary to use a permanent monitoring system. The system will need to be taken to site to do the inspections either bi-annually or whenever new ropes are installed or whenever sheave grooves are cut.

Mass of the system:

As a periodic system will be used, the mass of the system becomes an important constraint as sheave wheels are usually located at the top of the headgear or high-up on draglines. The access to sheaves is usually by a flight of stairs to the top. The mass of the system should be comfortable for a single person to carry up several flights of stairs. Based on experience, it was decided that as long as the profiler weighs less than 5kg it would be suitable for on-site use.

Digital or analogue system:

If Condition Based Maintenance or just-in-time maintenance procedures were to be followed, it is important to try to predict not only the current condition of a component, but also to determine the rate of deterioration of the component. For this to be possible, trending of the wear rate of the sheave needs to be done. Trending of data is more easily and accurately done with digitised data and will thus be a requirement of the profiler.

Is there electricity available or should the system be fully battery operated?

On most sites where the author has been to in order to inspect sheave profiles, an electrical outlet has either not been available at all, or very difficult to arrange for. The system should thus be self-contained and should require nothing from the mine.

Follow through/condition monitoring for the sake of condition monitoring:

It was mentioned earlier that one of the constraints of implementing an effective condition monitoring strategy was the notion of follow through. The problem with many complicated, condition monitoring systems is that they produce mountains of data that cannot be readily interpreted. These systems often end up as white elephants while potential benefits of their use are never attained. The system should be designed in such a way as to ensure ease of use and interpretation of results for anyone to understand.

Accuracy/precision of the profiler:

Probably the most important design specification is the accuracy of the profiler. In order to be feasible, it must produce repeatable results that accurately determine the critical areas of the sheave wheel as outlined in Chapter 2. These results must be verified theoretically and validated experimentally. Finally, the profiler must be compared to the current state of the art through a similar validation process. The exact values of the required accuracy are determined later in this chapter.

4.3.2. FUNCTIONAL ANALYSIS

a. Overall functional diagram

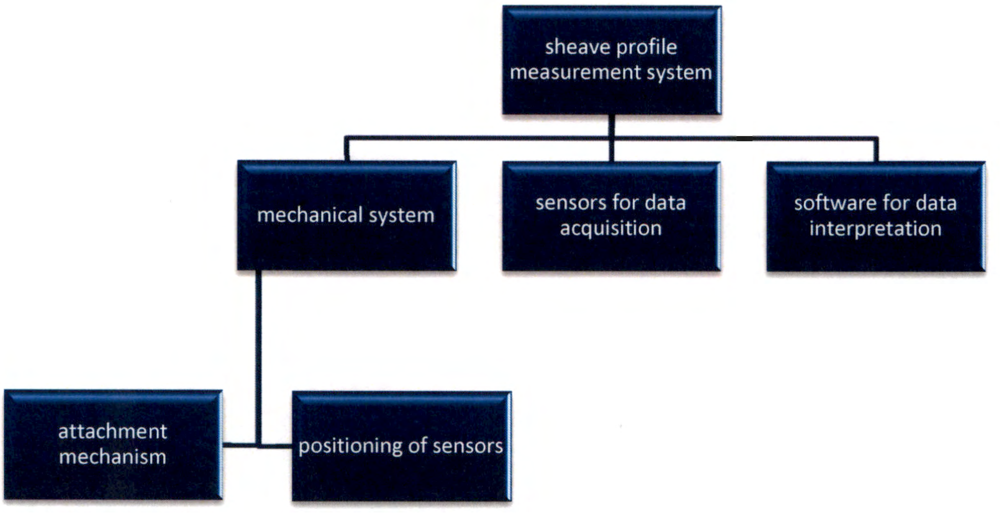

b. Mission-level functional diagram

- Where possible use existing, proven equipment and technology (must be able to verify accuracy)
- Acceptable life expectancy
- Maintainable/maintenance free
- Reliable and repeatable results
- Compact
- Light-weight
- Safe for operator

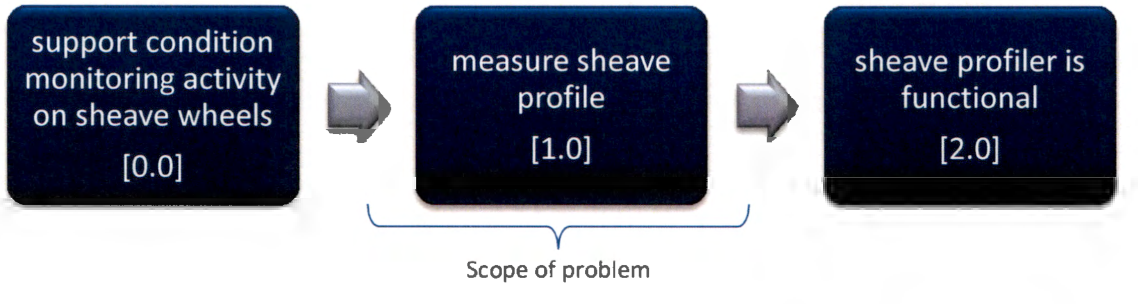

c. **System-level functional diagram**

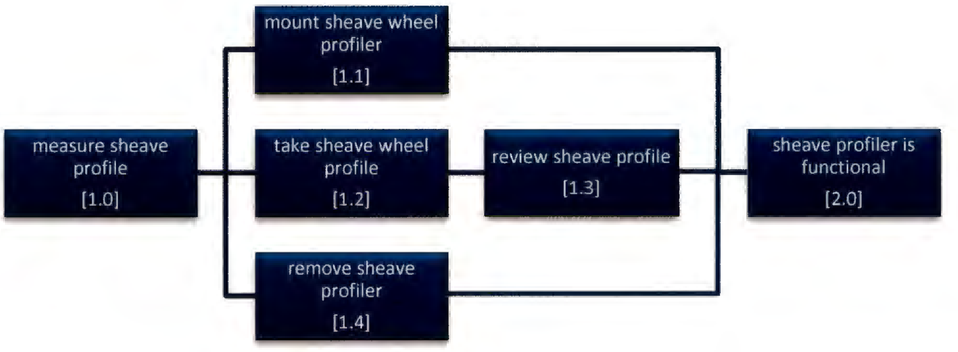

d. **First-level functional diagram**

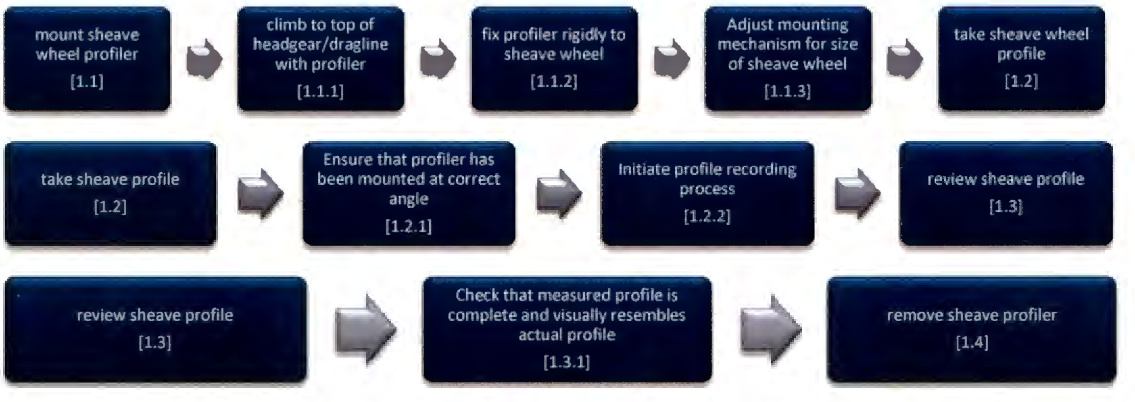

e. **Design parameters per function**

TABLE 1: DESIGN PARAMETERS PER FUNCTION

Number	Function	Design Parameter
1.1	**Mount sheave wheel profiler**	
1.1.1	Climb to top of headgear/dragline with profiler.	Light-weight. (<5kg)
1.1.2	Fix profiler rigidly to sheave wheel.	Sturdy mounting mechanism.
		Simple mounting for quick attachment.
1.1.3	Adjust mounting mechanism for size of sheave wheel.	Variable mounting mechanism.
1.2	**Take sheave wheel profile**	
1.2.1	Ensure that the profiler has been mounted at the correct angle.	One man operation. Short scan time.
1.2.2	Initiate profile recording process.	One handed process.
1.3	**Review sheave profile**	
1.3.1.	Check that measured profile is complete and visually resembles actual profile.	Some means must exist to immediately review profile briefly.
1.4	**Remove sheave profiler**	Simple mounting for quick release.

4.3.3. Other technical requirements

The requirement of the accuracy of the profiler is one that is not very well defined. Looking at the legislation one would quickly find that although they are adamant about the parameters of the sheave wheel that need to be inspected and the frequency of inspections, they make no mention of the desired accuracy of the methods to be used. It is left to the mine or the technician to determine the prescribed precision required. When asking technicians, you will get values anywhere from "less than 0.5mm" to "about 2mm should be sufficient". In the scope of a high-precision measurement instrument, this variation in requirements is significant. The author therefore decided that it was necessary to determine what the ideal accuracy would be. It would need to be related to the measurements that are expected to be made. The typical rope sizes range between 22mm and 110mm and there is an allowance for a 5% error on the rope size. If we use the 5% as a guideline for the measurement accuracy required, and consider the extreme scenarios we get the following:

$$T = Thickness\ of\ rope$$

$$R = Rope\ groove\ radius$$

$$R = T \pm 5\%\ from\ rope\ manufacturers$$

Therefore, looking at two of the extreme scenarios:

$$R = 22 \pm\ 22 \times \left(\frac{5}{100}\right) = 22 \pm 1.1\ mm\ worst\ case\ scenario$$

$$R = 110 \pm\ 110 \times \left(\frac{5}{100}\right) = 110 \pm 5.5\ mm\ best\ case\ scenario$$

Looking at the implicit required precision in the equation above and the definition of precision as shown earlier from (Kotz & Treichel, 2003) , it can be said that in order to obtain this measurement, the instrument would need to be accurate to within ±1 mm. As per the accepted convention, the confidence interval for the error shall be 95%.

4.3.4. Final design requirements

▪ Operation:	One man operation
▪ Mounting:	Sturdy for repeatable results
▪ Mounting:	Flexible for different size sheave wheels
▪ Mounting:	Quick attachment and quick release
▪ Data collection and storage:	Digital
▪ Power supply:	Self-supplied
▪ Mass:	< 5 kg
▪ Scan time:	< 5 minutes
▪ *Accuracy:*	$\pm 1\ mm\ with\ 95\%\ confidence$

4.3.5. Concept design and selection

Concept 1: Mobile 2D CMM

The first concept (see Figure 40 below) is for a device that is similar to the Microscribe® concept, but since it is an application specific profiler, the software and operation can be customised to compensate for the deficiencies mentioned in the Microscribe®. This concept relies on a stylus that can be moved forward and backward and rotated. It also relies on a sliding movement from left to right to give it the third degree of freedom to allow it to trace the profile. All the movements are recorded by encoders. The angle and position of each of the three encoders can be used to calculate the exact point of the tip of the stylus.

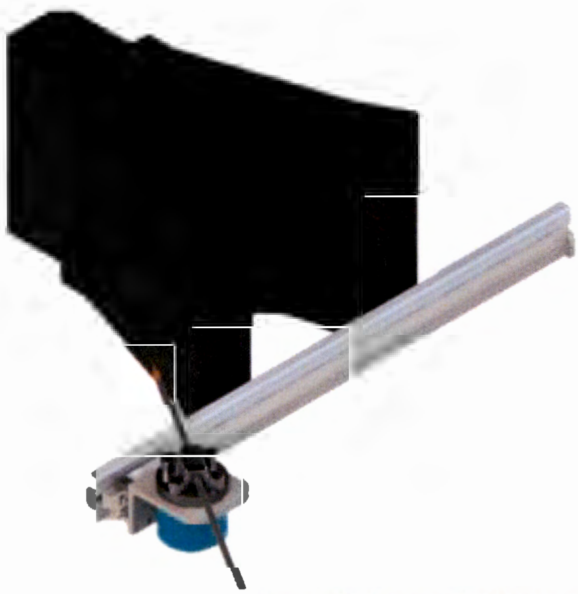

Figure 40: Concept 1 - Mechanical digital tracing mechanism

Concept 2: Shadow analysis profiler

The second concept proposes a system that is placed on the sheave wheel with three sensors which produce shadows on the profiler that form a line around the surface of the sheave wheel. These can then be interpreted to produce a digital representation of the cross section. Figure 41 shows this concept.

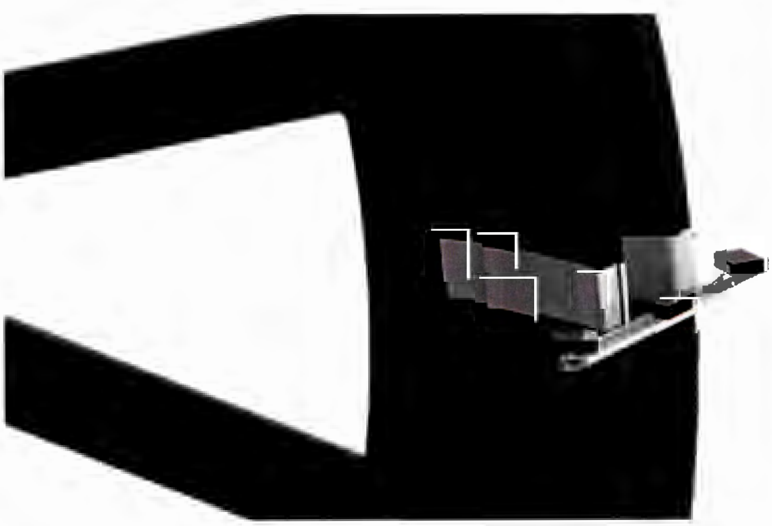

Figure 41: Concept 2 --Shadow analysis profiler

Concept 3: Line laser profiler

The line laser concept in Figure 42 is similar to the shadow analysis method in concept two. It differs in that, instead of using a shadow creation sensor, it uses a laser diode that is shone through a lens to produce a line. Three of these lasers shone around the surface of the sheave wheel should give a profile of the cross section of the sheave wheel.

FIGURE 42: CONCEPT 3 - LASER BASED PROFILER

In both of the last two instances, the shadow/ laser line is collected with a digital camera (webcam).

Concept Scoring Matrix:

This concept selection matrix is based on the matrix proposed by Ulrich & Eppinger (Ultich & Eppinger, 2008). The matrix they propose uses a reference design and scores the different concepts relative to the reference. Since the current state of the art for sheave profiling is not a single method/mechanism, it was decided that selecting one method as a reference value might bias the results of the concept scoring process. Instead, a variation is introduced where the concepts are only scored against each other. The scores go from 1 – 3 with three being the best and one being the worst. To force critical thinking each score may only be used once per parameter.

TABLE 2: CONCEPT SCORING MATRIX

		Mobile 2D CMM [#1]		Shadow analysis profiler [#2]		Line laser profiler [#3]	
Selection Criteria	Weight	Rating	Weighted Score	Rating	Weighted Score	Rating	Weighted Score
Theoretical Precision	40%	1	0.4	3	1.2	2	0.8
Cost	10%	1	0.1	2	0.2	3	0.3
Ease of Use	10%	1	0.1	2	0.2	3	0.3
Speed of taking profile	10%	1	0.1	2	0.2	3	0.3
Durability	10%	1	0.1	2	0.2	3	0.3
Ease of manufacture	10%	3	0.3	1	0.1	2	0.2
Safety for operator	10%	2	0.2	3	0.3	1	0.1
Total Score:		1.3		2.4		2.3	
Continue with development?		NO		YES		NO	

Concept selection matrices are inherently subjective. In an attempt to mitigate the effects of author's bias, it was decided that each selection criterion would be briefly described as well as the reasoning behind the scoring for each of the concepts.

- *Theoretical precision*

[#1] uses mechanical linkages which all cause reductions in accuracy. [#2] and [#3] actually have similar accuracies, but the fact that a laser line is made up of two interfaces (top and bottom of the line) that need to be interpolated, while a shadow is only a single interface (light to dark), [#2] was chosen as the best option here. Theoretical precision was weighted significantly higher than other options since it is the only parameter that is verified and validated in this document. It is therefore very important.

- *Cost*

The types of sensors used in [#1] include three encoders – these are relatively expensive. The costs for [#2] are reduced in that the sensors (which will need to be manufactured) are made up only of a high brightness LED and an obstruction. The laser diodes used in [#3] are readily available at a relatively low cost.

- *Ease of use*

[#1] requires that the user trace the surface of the sheave wheel. [#2] and [#3] have similar operational characteristics; they both simply require the user to place the profiler into position and press a button. It was decided that [#3] may be marginally easier to use since the visible laser line may help with the alignment of the profiler with the sheave.

- *Speed of taking profile*

Since [#1] requires the user to trace the profile manually, it will take the longest to record the profile. [#2] and [#3] will again be very similar, but [#3] may offer marginal improvements in speed of setup due to the clearly visible laser line.

- *Durability*

[#1] will likely wear out first since it has several mechanical components. [#2] and [#3] are again head-to-head, but since the duty cycle of the diode in the laser is less, it may be possible that the laser will last longer than the LED used in [#2].

- *Ease of manufacture*

[#1] is the simplest design since it is algorithmically much less intensive to produce. [#2] and [#3] have similar algorithms, but [#2] uses custom made sensors that add to the complexity of the design.

- *Safety for operator*

[#1] and [#2] are intrinsically safe, but since [#1] requires more operator intervention, it may be considered marginally more dangerous than [#2] due to the fact that the operator usually works in awkward positions an may need his hands to hold on. [#3] uses a laser which may pose a risk to the eyes of an uninformed or careless user.

Based on the concept selection matrix, it was decided that option 2, the Shadow Analysis sheave wheel profiler would be developed.

4.4. Detail design

The detail design of the profiler can be split into two sections namely hardware design and algorithm (and software) development. Although the hardware is discussed first, the two design processes were done simultaneously since they have a considerable effect on each other.

4.4.1. Hardware design

"The enemy of art is the absence of limitations."

Orson Welles

An analogy can be made with the quote above for the development of a product in that the absence of constraints is the enemy of design. During design of a new product, the author always tries to ensure that the problem is fully defined before commencing with the detail design. This is not always possible, but in the authors experience the better a design problem (and its generic ideal solution) is defined, the more elegant the design tends to be. Aside from the requirements, more design parameters can be found by critically evaluating the current state of the art. The following additional comments can be made in this regard:

(a) Contact methods

Most of the methods (aside from the laser profiler) are in contact with the sheave wheel during the recording of the profile. This is a fundamental limitation in the accuracy of the profiler since the stylus would tend to wear out, causing undetermined inaccuracies in the profile. It would therefore be more ideal to use a non-contact method.

(b) Movement (tracing)

All the methods (aside from the sheave gauges and plaster casts) are based on a movement of the scribe (whether digital or analogue) around the rim profile sheave wheel. This is a fundamental design limitation since it increases the time period over which the profile is taken. When the profile is taken over a relatively long period, the different points on the sheave wheel are measured at different times, meaning that if there is any interference (e.g. vibration on the headgear) the profile is affected negatively. Tracing the profile can also cause inaccuracies if the moving parts start to wear out. The proposed solution to this is that the profiler should be configured such that the entire rim profile is taken without physically touching the profiler and almost instantaneously.

Configuration of the system

With this in mind, it was decided that instead of a single, non-contact sensor that moves around the wheel, three sensors, placed at fixed positions will be used (as alluded to during the concept design phase). Error in the manufacturing and configuration of this system can easily be calibrated out after the profiler has been assembled.

Triangulation and the mathematics behind it will be discussed during the algorithm development section, for now it is sufficient to say that in order to keep the unit as simple and affordable as possible, the sensors for the acquisition of the profile will be included in the scope of this project. One sensor is made up of one CCD or CMOS sensor (webcam) and one shadow source (i.e. light source and obstruction source). The notion of using the shadow to trace the sheave wheel profile is analogous to the idea where the actual edge of a grinding wheel was used together with edge detection algorithms to determine the wear rate (Fan, Lee, & Mou, 2002)

Other researchers looked at using a similar photogrammetric setup with a CCD imaging sensor to determine the wear that occurs on train wheels and tracks.

Before describing the system as a whole and determining the design that would produce the ideal outcome, the specified components need to be discussed:

Webcam

The selection of the camera would be dictated by the following requirements: It would need to be low cost, it would need to have a manual focus[3] and it would need to have technical specifications that are made available to the consumer.

FIGURE 43: THE ASTRUM EYE USB WEB CAMERA

The camera that was selected for the prototype profiler is the *Astrum Eye 2 Eye USB Web Camera* ™ as shown in Figure 43. It was selected because of its low cost, manual focus and because it was the only webcam that the author could find that actually gave details about the lens and imaging sensor used. For the system as a whole, there are two sets of parameters that are of concern. The first is called extrinsic parameters. These have to do with the external factors of the set-up of the profiler. They are discussed during the calibration of the profiler. The second is intrinsic parameters. These are usually limited by the fundamental physics of the sensors used. These parameters cannot be changed easily and will therefore form part of the design

[3] A manual focus is required because the focal point of the camera is used to calculate the resolution of the data that is collected. If the focus is allowed to be automatically adjusted, it will not be able to predict the expected precision of the data.

uncertainty. It is important to factor in as many of these parameters as possible since they will increase the uncertainty with which a design is completed. From the specification sheet, the useful information that could be extracted is shown in Table 3 below.

TABLE 3: CAMERA SPECIFICATIONS AS PER MANUFACTURER

Sensor type	1/6.5" CMOS [GC0308]
Sensor resolution	640 x 480 pixels
Field of view	About 60°
Focal length	3.1 mm
Focus type	Manual focus
Lens material	Plastic and glass
Lens element	2g2p

More information on the sensor was required, since it will be needed during the algorithm development phase. This information was found in the Global Core 0308 CMOS sensor datasheet (see Appendix 4.1). The relevant sections are included in the table below.

TABLE 4: SENSOR SPECIFICATIONS AS PER MANUFACTURER

Optical format	1/6.5"
Pixel size	3.4 μm X 3.4 μm
Active pixel array	648 x 488 pixels

Shadow source (light source and obstruction source)

The purpose of the torch was to produce a shadow that is clear and has a well-defined, singular margin. It would also need to be a high-brightness, low-power device. It was decided that, to meet the latter requirement, it would be necessary to use a battery powered, high-brightness LED handheld torch. Regarding the former parameter, it was determined through informal experimentation that, to form a singular margin, the torch would only be allowed to have a single light source (thus the commonly available multi-LED torches could not be used as they produced multiple shadows). To form a well-defined margin proved to be a tricky problem since there is a strong correlation between the distance between the light source and the obstruction source and the plane onto which the shadow is projected: The obstruction source and the plane need to be as close as possible together, while the light source needs to be as far as possible away from the other pair. Figure 44 shows the different shadow configurations that can be obtained.

FIGURE 44: THE QUALITY OF THE SHADOW FOR DIFFERENT CONFIGURATIONS

In Figure 44, the effect of the positioning of the light and the obstruction source relative to the plane can be seen. In the first image from the left in Figure 44, the light source, obstruction source, and surface are all close together. Although the margin is fairly clear, this configuration causes the flooding of the unobstructed part of the surface with excessive glare, making it more difficult for the algorithm to detect the margin.

The second image shows a configuration where the obstruction and the light source are close together while the surface to be profiled is further away. This causes a fuzzy margin and in this case it will not be possible to detect it clearly.

The third image represents a configuration where the surface to be profiled and the obstruction source are close together, while the light source is further away. This appears to be the optimum configuration for the current application.

It was thought that the light beam from the torch would need to be able to focus between a concentrated point light to a flood light since the margin is influenced by this and the optimal configuration would need to be determined experimentally. It was determined that the light source should ideally be a flood light since it gives a more uniform shadow margin with less interference patterns. For the light sources on the sides of the profile it was necessary to adjust the focus of the beam slightly towards the spot-light since it allowed for a greater distance of consistent light.

Due to the points raised above, the *LED Lenser L7* depicted in Figure 45 was selected since it met all the requirements of focus, battery, led and brightness while still having a fairly low price.

FIGURE 45: LED LENSER L7 FOCUSING LED TORCH

Now that the components of the triangulation sensor have been individually discussed, they are assembled to form the sensor.

Single sensor setup

Figure 46 below shows the pinhole camera setup *(Faugeras, 1993)*. It is based on the notion that an image can be acquired without a lens by limiting the amount of light that enters the image plane. The image is inverted and scaled based on the focal distance (in this case the distance between the two screens).

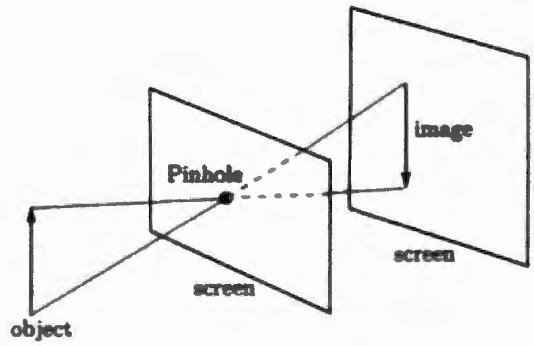

FIGURE 46: PINHOLE CAMERA MODE OF IMAGE FORMATION

Using the Pinhole Camera model allows for a very simplified calculation when the various parameters of the object are calculated. The position of any specific point on the CCD chip can be translated to a distance measurement by triangulating the coordinates of the point from the data collected by the CCD chip.

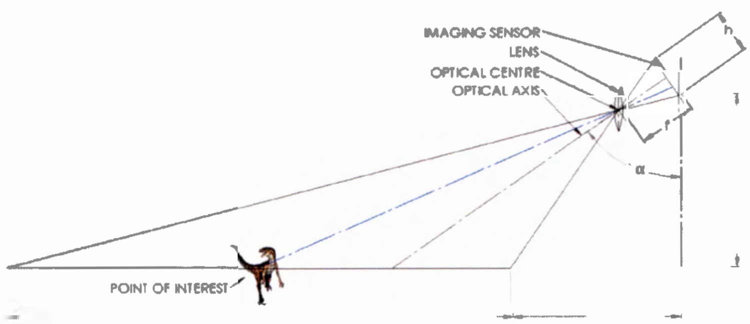

FIGURE 47: TRIANGULATION PRINCIPLE

Figure 47 above shows the basic layout of a triangulation based system. The required points can now be calculated using basic trigonometric identities. The parameter "d" is defined as the working area of the sensor (this is the "sweet-spot" where the sensor will perform optimally). Parameter "b" is known as the offset of the sensor (this is the "dead-spot" where data acquisition is not possible.)

Since the sensor is being designed specifically for this application, it is possible to vary the fixed values (like α and l) to ensure that the range of d and b are within the technical requirements of the project. Based on prior knowledge of the problem of sheave profiling, it was decided that the set-up would be done such that the working area would be between 200mm and 400mm from the triangulation sensor. It was also decided that practically, it would not be possible to lift the camera higher than about 70mm from the ground plane as it would introduce constraints for the manufacturing and operation of the profiler.

The requirement for the design of the sensor was only that it would need to allow for easy fixing to the manipulator, easy change of mounting angle (for side sensors) and a constant angle at which the camera should be mounted (more information on this later). The light source would need to be mounted parallel to the sensor mounting plane. The detail design of the sensor can be seen in Figure 48 below.

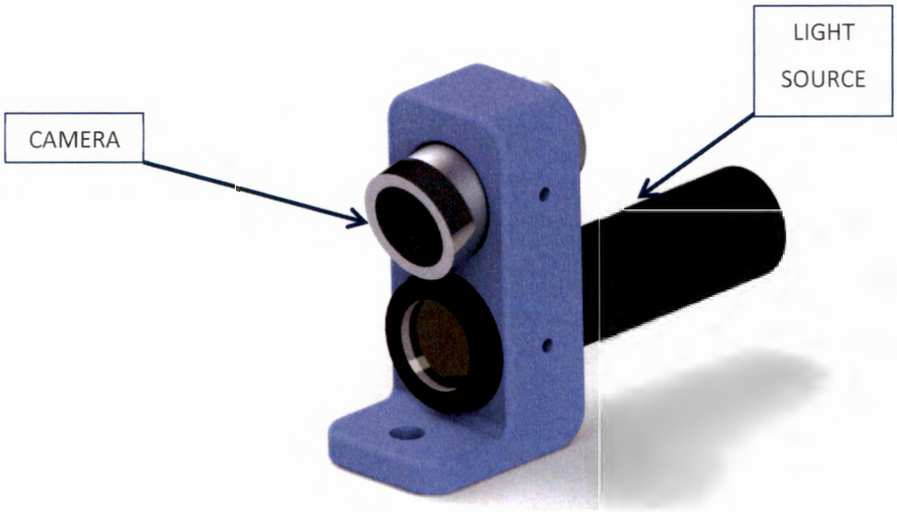

FIGURE 48: TRIANGULATION SENSOR DETAIL DESIGN

As mentioned earlier the size of the working area was defined to be 200mm. Based on the optimal shadow margin that could be obtained, the working area was defined to start at 200mm and therefore span between 200mm and 400mm from the sensor. From the camera specifications it is shown in 49 that the field of view (FOV) is 60°.

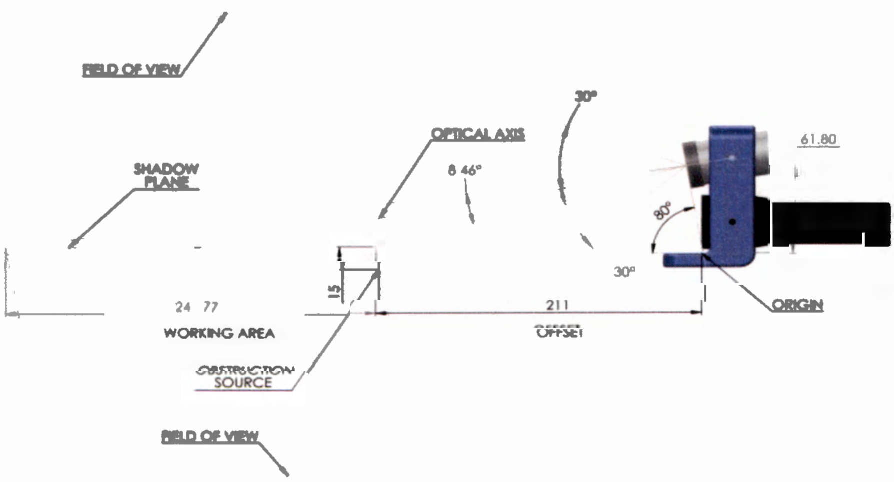

FIGURE 49: SCHEMATIC OF SENSOR DESIGN

To ensure that the working area is covered in all circumstances, the camera angle was set to 10° from the vertical. The position of the optical centre is then exactly in the middle of the working area. Looking at Figure 50 below, it is apparent that although the FOV of the camera is 60°, only 8.46° are required to cover the entire working area. This has fairly severe consequences on the accuracy of the profiler. This topic will be elaborated on more during the design verification section.

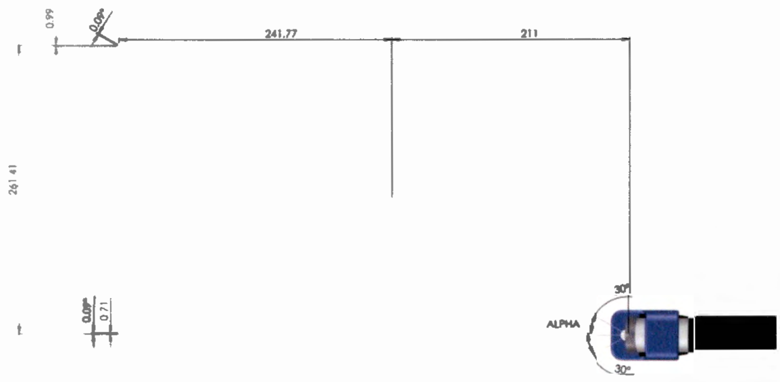

FIGURE 50: TOP VIEW OF TRIANGULATION SENSOR

Now that the sensor has been described completely, it is possible to consider the design of the complete system.

Complete system setup

In order to ensure that it is possible to take the profile of the entire cross section of the sheave wheel rim without having to move any components of the profiler, it is necessary to place the sensors in a way which facilitates this. The final setup can be seen in Figure 51.

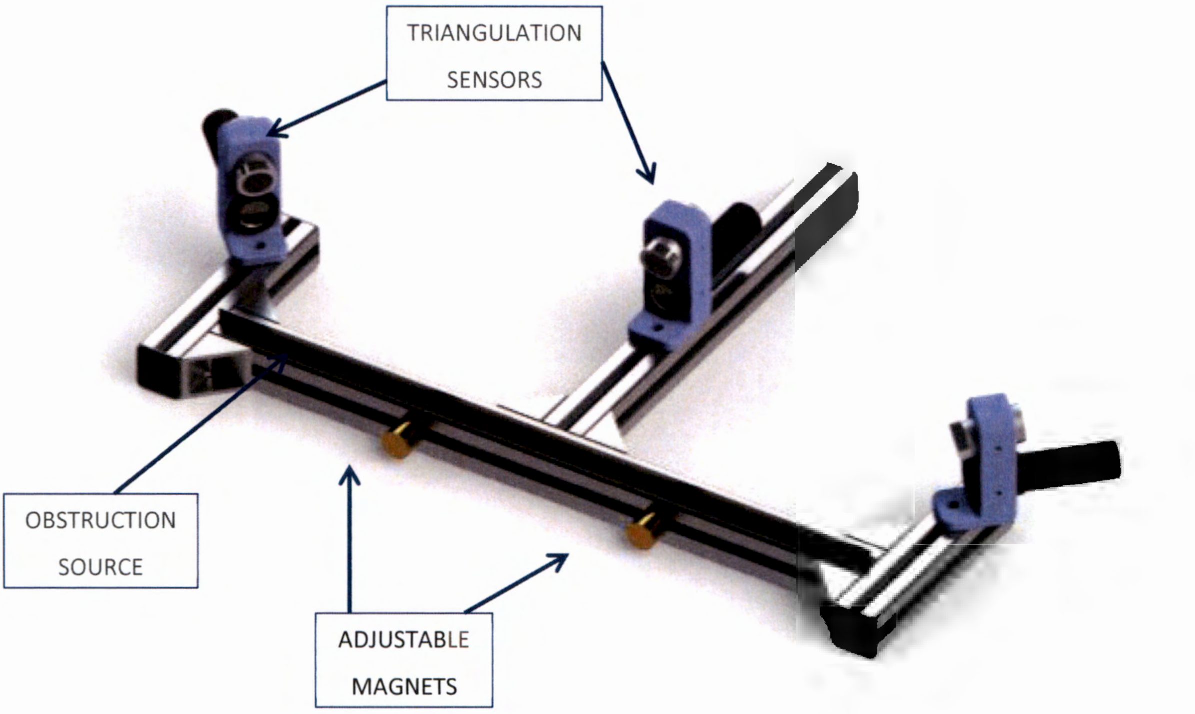

Figure 51: Final detail design of prototype profiler

More will be elaborated on the operational parameters of the profiler during the design verification section. For now it is time to look at the algorithm that will be able to provide the profiler we require.

4.4.2. Algorithm development

Now that we have an instrument, there needs to be a way for the instrument to detect and interpret the sheave profile and subsequently to present it in way that is useful to the user. Since this document is not destined for the computer science domain, the algorithmic development should not be judged form such an angle. Algorithmic development in this instance should merely be seen as a means to an end. There is much in the form of optimisation that could be done on the algorithm. Existing image processing algorithms were used from the MATLAB® image processing toolbox and were not custom-made. Syntax for the code was used from the MATLAB® help files and a textbook on the topic (Herniter, 2001).

Since this is an α-prototype only, the code for the acquisition of the images has not been included in the scope. For now they will be manually acquired from the hardware.

The approach of this section is to refrain from merely presenting the algorithm pseudo code, but rather to explain each concept simply and briefly. This should make the logic that was used to develop the algorithm easy to follow and replicate if required for academic purposes.

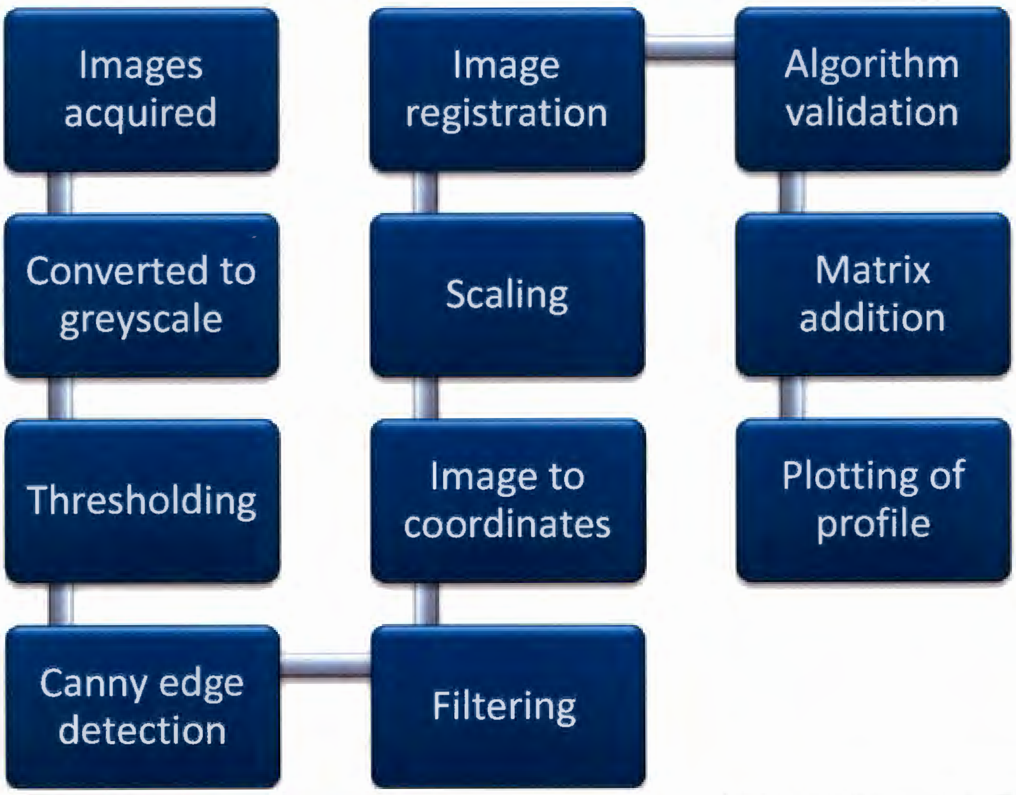

Figure 52: An overview of the algorithm

Images acquired

The images are acquired by the profiler. For now, a single image will be discussed, but each of the three images go through the same process, until they are added together later in the process.

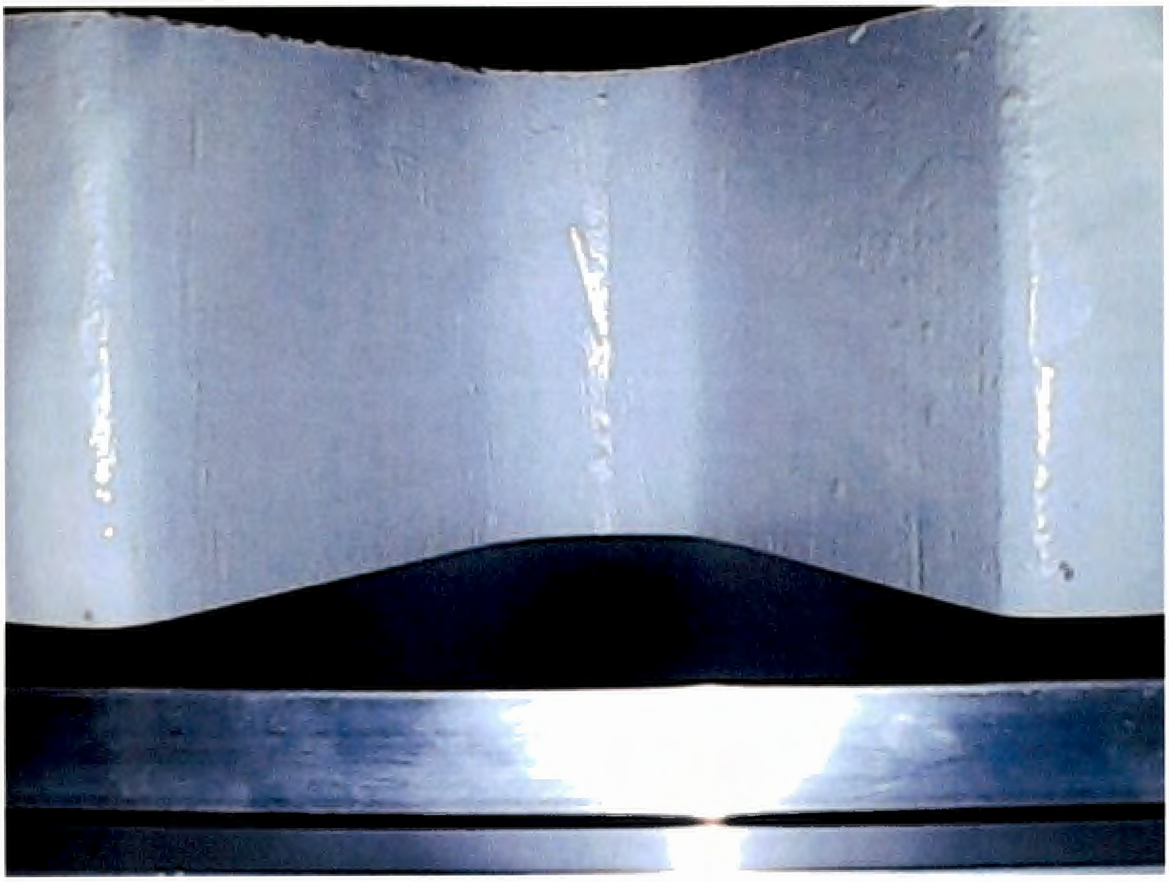

FIGURE 53: ORIGINAL IMAGE

Figure 53 above is the raw image as produced by the camera. It contains several areas that are not relevant and must be excluded. The region of interest (ROI) has been isolated manually and can be seen in the image below. If a commercial version of the profiler is developed, the ROI can be extracted automatically using regioning techniques.

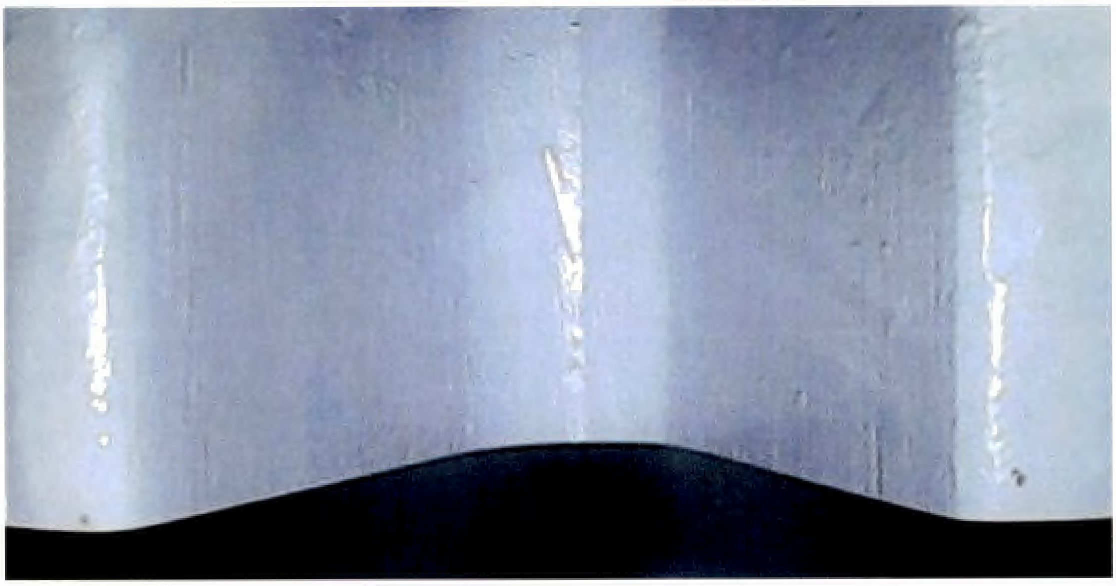

FIGURE 54: REGION OF INTEREST ISOLATED MANUALLY

As can be seen in Figure 54, the shadow causes almost total darkness, while the white contrast spray causes a distinctly white surface. This, although it looks like a black and white image, is still recorded as a colour image. This is significant because a digital colour image is represented by a 3D matrix representing the intensities of the various colour components (RGB, HSV etc.) while a greyscale image is represented by a 2D matrix of values representing the greyscale intensities of each pixel. A binary (pure black and white) image is represented by a 2D matrix of 0's and 1's in this case.

Since we are not really interested in the intensities, but rather in the coordinates represented by the various pixels (i.e. the position of the pixel instead of its exact value), it would be the easiest to convert the image to a binary value (this will become clear later).

Converted to greyscale

The image is then converted to a greyscale image using the following conversion equation based on the ITU-R 709-5 conversion recommendation known as the "Luma" algorithm for RGB to greyscale image conversion.

```
I = 0.2989*rgb_img (:,:1) + 0.58708*rgb_img (:,:,2) + 0.1140*rgb_img (:,:,3); (ITU-R, 2002)
```

There are many debates surrounding how to get an RGB image to a greyscale image in the best possible way and several algorithms for do this exist, but since we are still only ultimately interested in the binary values, a "pretty good" transformation equation has been used above.

FIGURE 55: NTSC GREYSCALE IMAGE

Image Thresholding

At this point, the image is converted to a pure black and white (binary) image. It is now represented as a 2D matrix of ones and zeros only. Figure 56 illustrates the binary image.

FIGURE 56: BINARY IMAGE

Canny edge detection

Since we are not actually interested in the whole image, we need to isolate the portion that we care about.

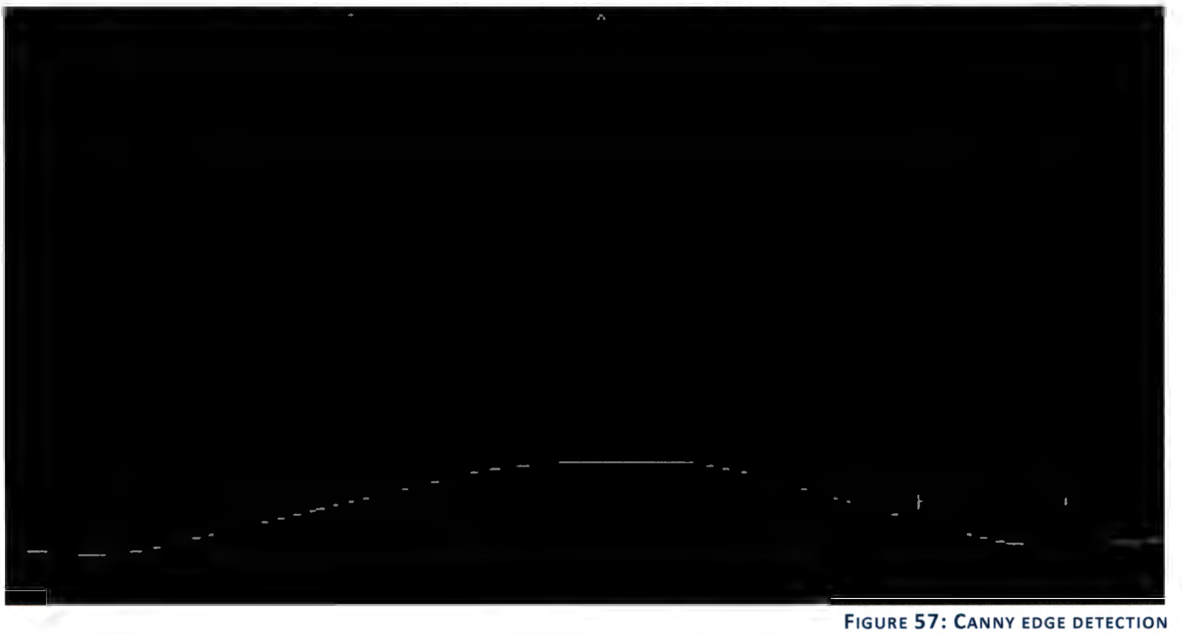

FIGURE 57: CANNY EDGE DETECTION

The interface between the black and the white section (i.e. the shadow margin), will give us an un-scaled sheave profile. The edges of the image are areas where there is a significant change in image brightness. This allows the computer to convert a complex image to a simplified version by only considering the step changes in brightness. (Russel & Norvig, 2010) This way, the computer will be able to process the correct data while ignoring irrelevant parts of the photograph.

There are numerous edge detection algorithms, each with positive and negative aspects. The Canny edge detection algorithm is a robust and very efficient algorithm to detect the edges sufficiently. It is very sensitive and noise tends to be an issue, but this will be addressed by filtering the results.

On the right hand side of the image, just above the middle, there is a section where the algorithm picked up some noise. This must be filtered out.

In the Canny edges image (Figure 57), there are several sections on the main profile line where it appears as though there is missing data. It should be noted that since the Canny Edge Detection algorithm creates a line that is one pixel thick, it does not always appear to be a solid line but if one could zoom in further it would be noted that in fact it does display correctly.

Filtering

It is possible to implement some sort of fancy filter to try to eliminate the "false positives" that were picked up by the algorithm in this case. The risk of doing this is that the filter may remove some of the true edges. The filtering technique applied in this algorithm is a very crude one based on the following logic and background understanding of the problem:

The assumption is that there will not be any false positives in the shadow area since it is almost entirely black and the thresholding step should ensure that all the points here become pitch black. The section that is in the light may have very small shadows due to surface roughness. These will show up as minute yet pitch black sections within the white section. When the Canny edges algorithm is applied, it will draw an edge around the small black spots. Therefore, all noise should be located above the true line that has been detected and simply removing the data above the detected edge should provide sufficient filtering for this application and will ensure that no important data gets discarded in the process.

Converting the Canny edges image to coordinates

The image has now been cleaned up such that the only white pixels are those on the line that represent the sheave profile cross section. At this stage it should be noted that it is still an image and now needs to be converted to a collection of points before it can be scaled and manipulated and used for measurements.

4	0	0	0	0
3	0	1	1	0
2	1	0	0	1
1	0	0	0	0
R/C	1	2	3	4

x	y
1	2
2	3
3	3
4	2

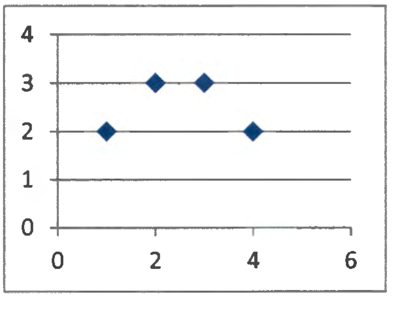

FIGURE 58: PROCEDURE FOR CONVERTING IMAGE TO COORDINATES

This is done by iterating through the entire matrix and whenever a value of "1" is found, using the address of the point, as a point in a new vector. This way a new vector is created that does not contain any ones or zeros, but only the coordinates of the ones in the original image. This can then be plotted as a graph as shown in Figure 58.

Figure 59 shows the scatter plot of the image that has been converted from a matrix of ones and zeros (a binary image) to a vector with coordinates where all the ones were.

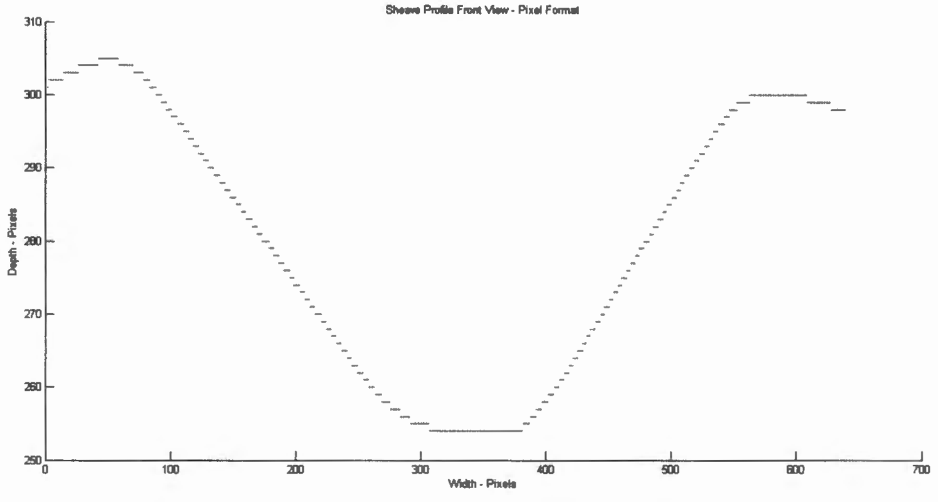

FIGURE 59: IMAGE NOW CONVERTED TO GRAPH

It should be noted that at this stage, even though the graph in Figure 59 vaguely resembles the sheave wheel profile, it is not yet an accurate representation of the sheave wheel since the units of the coordinates are in pixels and not in mm.

Scaling of the points

An image has a finite number of pixels. The further away the object is from the camera, the fewer pixels are available to represent a particular image. This affects the scaling of the measurements of distances for the profiler. Before looking into more detail on the scaling of the actual measurements, it is perhaps prudent to digress for a moment to elaborate on the concept of digital zoom.

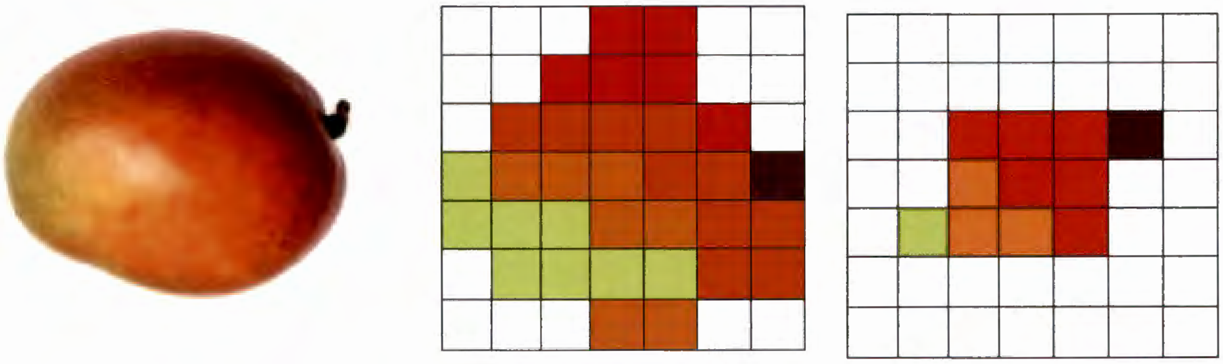

FIGURE 60: FEWER PIXELS AVAILABLE FOR DIGITISING A PARTICULAR OBJECT

When an object is photographed from up close, more pixels are used to represent the object, as can be seen with the crude descriptive images shown in Figure 60. The image in the centre is the same as the image on the right (both are a representation of the mango on the left), but the image on the right is taken from further away.

What this implies, is that the pixel density over the surface of an object is dependent on the distance that the sensor is away from the object. This is relevant because we are trying to determine the size of an object based on an image (from its shadow). Moreover, the surface of the sheave wheel has sections that are further away from the camera than others (that is, changes in depth). It therefore becomes necessary to derive a transform that scales the image based on the distance between respective points and the camera.

Because of the way the profiler is designed, points that are higher on the y-axis are further away from the profiler than points that are closer to the x-axis (y=0). Therefore, the resolution would be worse for a point that is located higher on the y-axis (and thus further away from the camera). The scaling would need to be such that every point is scaled by a certain factor (when converted to mm) depending on its position. Initially the scaling would be linear, but there is another aspect of the design that requires scaling to take place. To understand this it is necessary to look at the sensor configuration and how the image projection falls on the shadow plane. The second scaling algorithm is actually just a transform to "tilt" the image to a plane perpendicular to the optical axis.

It would be best to look at the characteristics of a single triangulation sensor as shown in Figure 61 before looking at the combined effect on the profiler and the result as a whole.

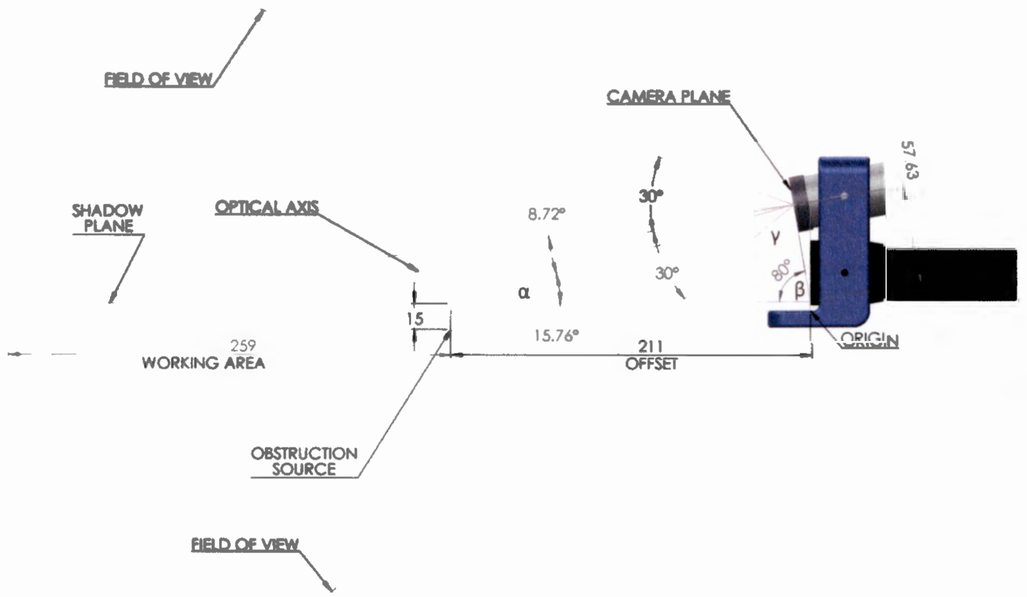

FIGURE 61: SINGLE IMAGING SENSOR SCHEMATIC

Assumptions & initial conditions:

$Field\ of\ view: FOV = 60°$

$Active\ field\ of\ view: FOV_{active} = 8.72°$

$Distance\ from\ sensor\ to\ obstruction\ source: d = 211\ mm$

$Angle\ between\ camera\ plane\ and\ shadow\ plane: \beta = 80°$

$Vertical\ distance\ between\ camera\ plane\ to\ shadow\ plane: a = 57.63\ mm$

$Active\ CCD\ pixels\ (veritcal): P_{vert} = 480\ pixels$[4]

$Starting\ point\ of\ working\ area: W_0 = 211\ mm$

$Length\ of\ working\ area: W = 259\ mm$

[4] See Appendix 4.1 for camera details

$Last\ point\ measured: W_f = 470\ mm$

$Angle\ of\ first\ incedence\ of\ FOV_{active}\ with\ W: \alpha_0 = 15.76°$

Calculations:

Active pixels (local): p_{vert}

$$p_{vert} = \frac{FOV_{active}}{FOV} \times P_{vert} = \frac{8.72}{60} \times 480 = 69.76\ pixels \cong 70 pixels$$

Step size (angle): Δα

$$\Delta\alpha = \frac{FOV_{active}}{p_{vert}} = \frac{8.72°}{69.76\ pixels} = 0.125°/pixel$$

Angle between camera and ray line: γ

$$\gamma = 180 - 15.76 - 80 = 84.24°$$

The goal of this calculation is to calculate the next value of d_n based on the step size and the angle step Δ α.

Using the sine rule, it can be shown that:

$$\frac{sin\gamma_n}{d_n} = \frac{\sin\alpha_n}{a}$$

$$d_n = \frac{a \times \sin\gamma_n}{\sin\alpha_n}$$

$$\alpha_n = \alpha_{n-1} + \Delta\alpha$$

$$\gamma_n = 180 - 80 - \alpha_n$$

$$a = 57.63\ mm\ [constant]$$

Repeating this calculation for all values of α, the scaling graph shown in Figure 62 has been developed.

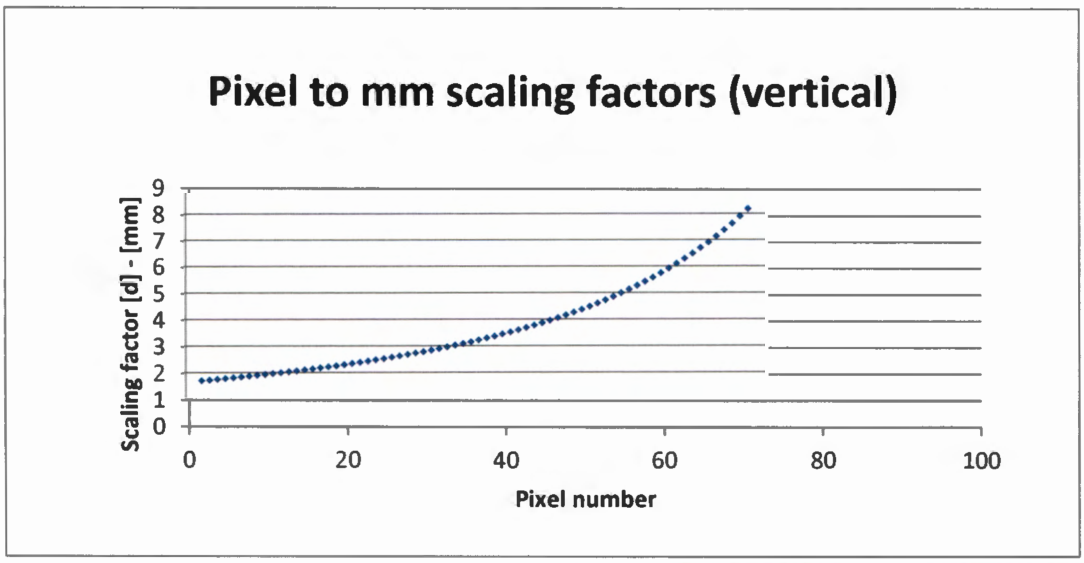

FIGURE 62: PIXEL TO MM SCALING FACTORS (VERTICAL)

Using this graph, the un-scaled graph of the sheave profile can now be scaled by multiplying every point with the appropriate scaling factor based on the position of the detected pixel above the zero line of the image.

Figure 63 indicates that a similar, but somewhat more complicated, problem exists for the horizontal scaling of the points:

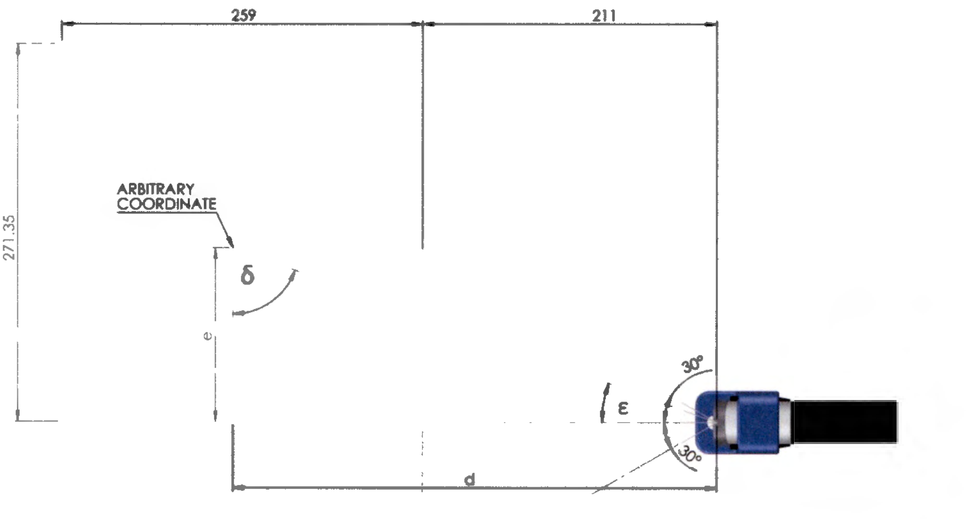

FIGURE 63: HORIZONTAL PROFILE OF IMAGING SENSOR

Assumptions & initial conditions:

$Field\ of\ view: FOVh = 60°$

$Active\ field\ of\ view: FOVh_{active} = 60°$

$Active\ CCD\ pixels\ (hor): P_{hor} = 640\ pixels$[5]

$Depth\ value: d = get\ from\ previous\ calculation$

Calculations:

Active pixels (local): p_{hor}

[5] See Appendix 4.1 for camera details

$$p_{hor} = \frac{FOVh_{active}}{FOVh} \times P_{hor} = \frac{60}{60} \times 640 = 640\ pixels$$

Step size (angle): Δ ε

$$\Delta\varepsilon = \frac{FOV_{active}}{p_{hor}} = \frac{60°}{640\ pixels} = 0.09375°/pixel$$

Angle between ray line and vertical plane:

$$\delta_n = 90° - |\varepsilon_n|$$

Using the sine rule, it can be shown that:

$$\frac{sin\delta_n}{d_n} = \frac{\sin\varepsilon_n}{e_n}$$

$$e_n = \frac{d_n \times \sin\varepsilon_n}{\sin\delta_n}$$

$$and\ \varepsilon_n = \varepsilon_{n-1} + \Delta\varepsilon$$

This calculation must be repeated for all combinations of ε and d. This would technically deliver a matrix of scaling factors, which would be fairly difficult to display intuitively. It was therefore decided that although the entire matrix is used in the calculations, only a few sample points will be displayed. The points at the start and end of the working area (d=211 mm and d = 470mm) were selected to give an envelope. The other points were selected at random to show the trend between the initial and final points. This is shown in Figure 64.

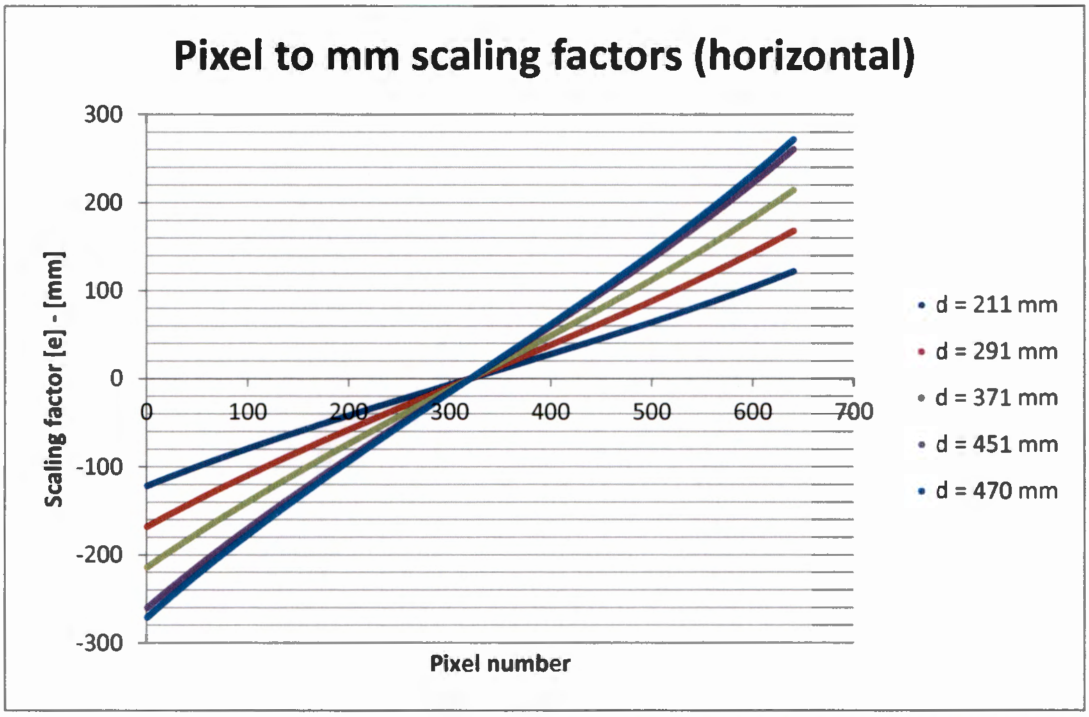

FIGURE 64: PIXEL TO MM SCALING FACTORS (HORIZONTAL)

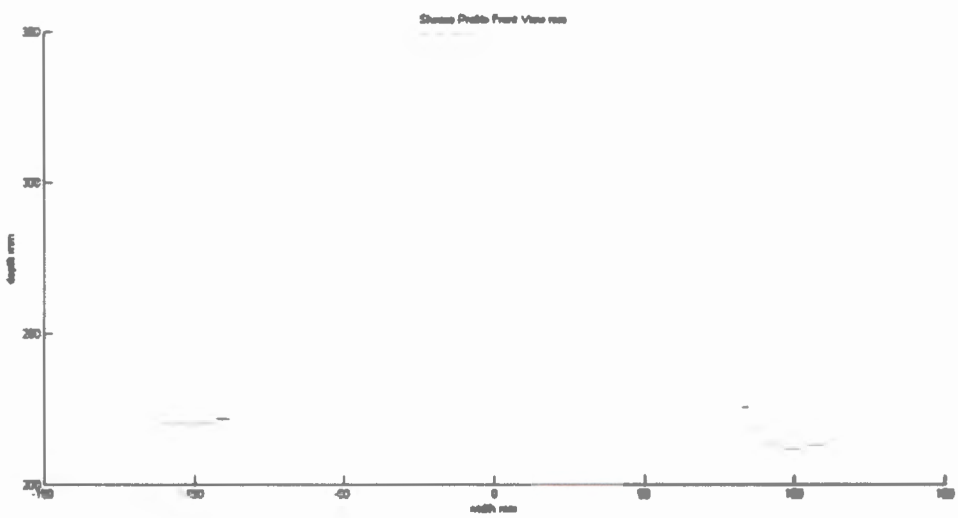

FIGURE 65: THE MIDDLE PROFILE OF THE SHEAVE WHEEL, CONVERTED TO A SCATTER PLOT

When scaling for the horizontal and vertical planes have been implemented, the resulting image looks like the one in Figure 65.

Without elaborating on the results too much, at this stage the author would like to point out the "steps" in the data. This is interesting and expected, although not ideal. The steps are due to the fact that a low number of pixels are used to digitise the profile. This is equivalent to using a low resolution camera to take a photograph. It is essentially a pixellation of the result. It was in a way predicted during the design calculations above where it was shown that at the maximum depth, the resolution of the data is as low as 8.17mm. This can only be solved by making use of a lens with a smaller focal length (so that more pixels are concentrated on the surface in question) or by making use of a camera with a larger CCD sensor (also to increase the number of pixels available to digitise the profile). This will be discussed further during the section where suggestions for improvements to the profiler are made at the end of the document.

Algorithm Validation:

Before calibrating the images based on the profiler setup, it is necessary to validate that the algorithm produces the desired result. The validation has to be done at this stage because once the image has been unskewed and the matrices added together, the validation will be completely different. Validation of the next parts of the algorithm is done under each of the sub headings. The final part of the algorithm (which is done in the mm domain as opposed to the pixel domain) is validated experimentally.

The validation was done by making an arbitrary sample image in bitmap format. The idea was to test the algorithm by comparing the input and the desired output with the actual output from the algorithm. The image was given arbitrary geometry and in order to allow it to represent the expected image more accurately, it was given arbitrary colours. The image progression can be seen in the image below:

From Figure 66, it can be seen that all three main functions operate as intended.

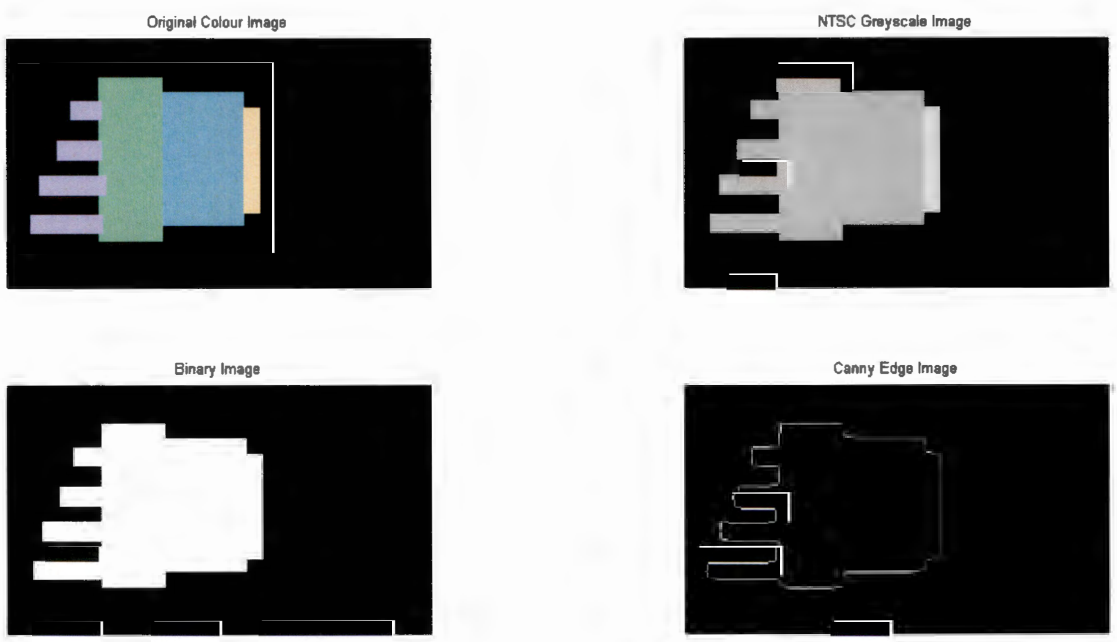

FIGURE 65: ALGORITHM VALIDATION

Next, it needs to be determined whether the "Canny-edges" image can be converted to an accurate scatter plot. This step is important since it represents the step where the algorithm has migrated from working with images to working with vectors.

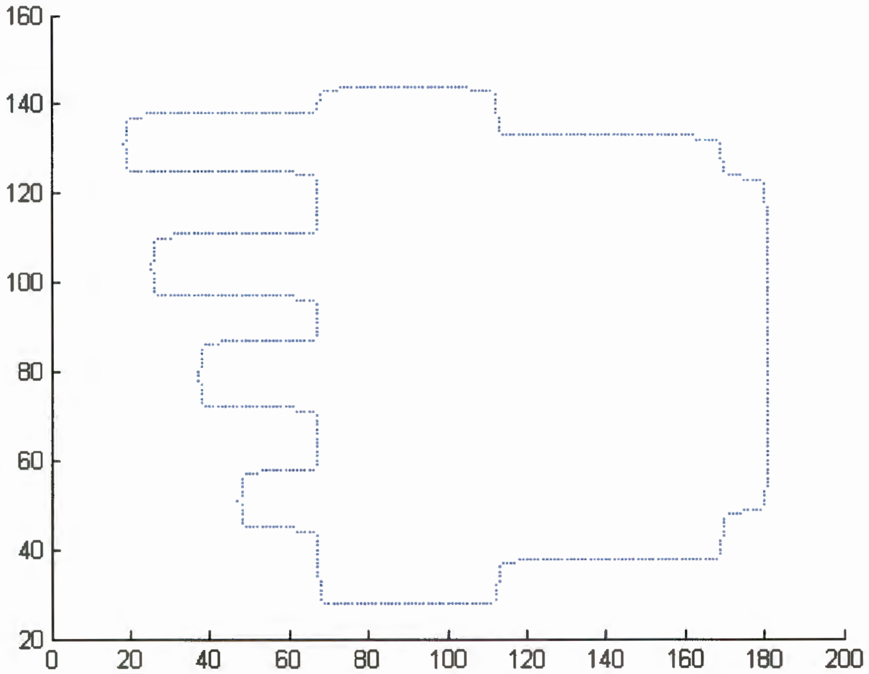

FIGURE 66: THE VALIDATION IMAGE CONVERTED TO A GRAPH

From the Figure 67 above it can be seen that the edges image was successfully converted to a graph. The resulting combined accuracy of the algorithm and hardware will be determined experimentally. At this stage it can be said that the algorithm performs the required functions as expected.

Image registration:

Since the images that are captured with the cameras on the left and right side are skewed it is first necessary to perform an image transformation to unskew them and get all the images into the same format.

Based on the calibration procedure presented by (Zhang, 2004) a **2D plane based calibration** procedure was performed to correct for the extrinsic parameters of the machine vision experimental prototype. The original, uncalibrated images are shown in Figure 68.

FIGURE 67: INITIAL UNCALIBRATED IMAGES. FROM THE TOP – LEFT, CENTRE, RIGHT

Therefore a transform had to be developed to get the images into the same "format" before they can be combined. The transform is developed on the checkers board and as long as there is no change between the camera setup between the images taken of the checkers board and the subsequent images taken of the sheave wheel, the exact same transform can be applied to the sheave wheel images.

The MATLAB® Image Processing Toolbox was used for the extraction of the transform. The process is briefly shown in Figure 69. It was done for left and right although only one side is shown. The correlating points are manually selected with the image set on the right (centre camera) used as the base image.

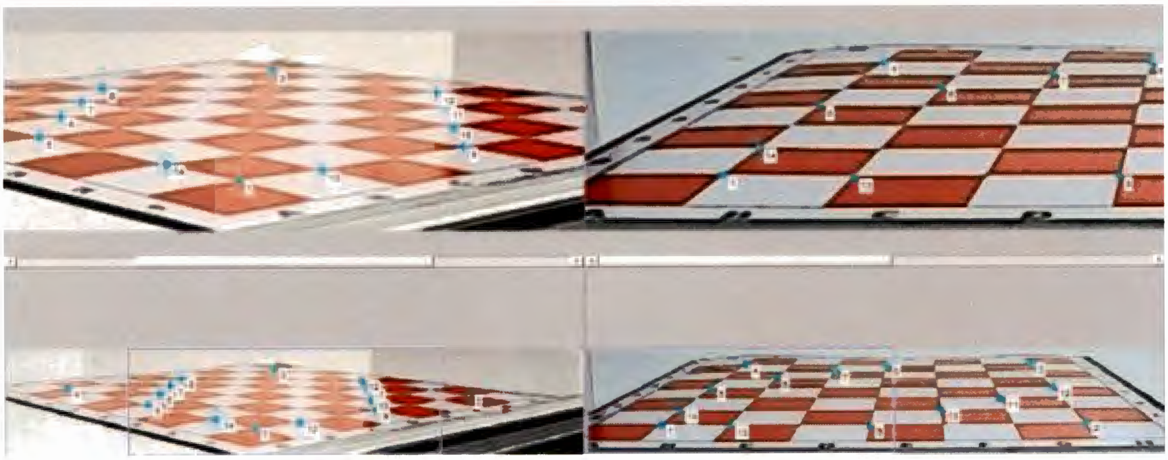

FIGURE 68: COORDINATE MAPPING FOR TRANSFORMATION FUNCTION

MATLAB® will then generate a set of transformation mapping coordinates as shown in Figure 70 below.

input_points =		base_points =	
272.7500	87.2500	81.2500	84.7500
505.2500	51.7500	552.2500	82.7500
292.2500	23.2500	491.2500	17.2500
66.7500	43.2500	175.7500	18.2500
155.7500	61.7500	138.2500	44.2500
168.7500	49.7500	209.2500	33.2500
180.2500	41.2500	274.7500	25.7500
192.7500	33.2500	331.7500	19.7500
404.2500	67.7500	312.7500	85.7500
398.2500	56.2500	391.2500	68.7500
393.2500	44.7500	457.7500	56.2500
388.2500	36.2500	514.7500	44.2500
321.2500	81.2500	157.7500	86.2500
230.2500	77.7500	101.7500	68.7500

FIGURE 69: TRANSFORMATION COORDINATES FOR LEFT IMAGE

These can be applied to the left checkers board image to complete the image registration process resulting in Figure 71.

FIGURE 70: LEFT SIDE IMAGE TRANSFORMED

This technique is also then applied to the image acquired by the camera on the right hand side of the profiler. The transformed image can be seen in Figure 72 below.

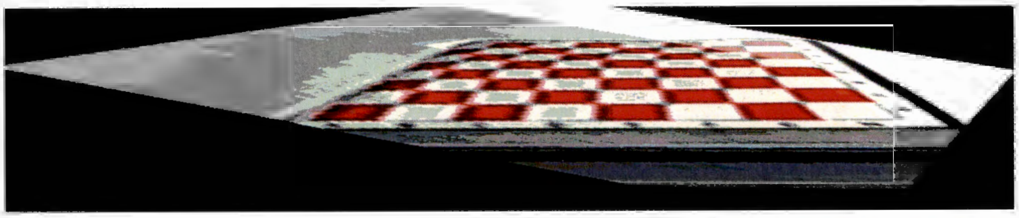

FIGURE 71: RIGHT SIDE IMAGE TRANSFORMED

Matrix addition

Using feature detection, the images can now be translated to overlap each other completely. However, due to the unsatisfactory resolution that was initially obtained with the cameras (as mentioned earlier), this will not be possible for this project. In order to still continue with the profiles, it was necessary to manually add the images and decide where each of the three data sets fit in. This is not ideal since introducing the "human factor" increases bias and reduces repeatability. The only saving grace here would be if the matrix addition was actually done while still in the pixel domain. This would ensure that operator bias is down to a minimum since the pixel domain is not intuitive (as far as actual measurements are concerned).

Figure 73 below is an attempt at manually adding the unscaled Canny edges images. The two side images were acquired by applying the transforms that were determined using the checkers board calibration technique above. The centre image is the unchanged Canny edges image shown earlier.

FIGURE 72: COMBINED CANNY EDGES IMAGE

This image should now appear as though the view is looking at the profile of the sheave wheel from the angle of the centre camera. An interesting observation can be made in that the outside two profiles appear to be incorrectly scaled. It would be expected that they were tilted more in if one were looking at the sheave wheel from the centre camera. This observation can be confirmed when the image is converted to a graph.

Figure 74 shows the converted image. It is still in the pixel domain, but at this stage it becomes apparent that the profile is not correct since the angles of the outside walls of the sheave wheel are a true representation of the sheave wheel profile. The resulting image could not be put through the final piece of the algorithm (converting from pixels to mm) since the inaccurate image cause divergent results.

The most likely cause for the incorrect transformation having been applied is the resolution of the cameras that were used. The checkers board pattern on the left and right (as in Figure 72 and 73) is not an exact reconstruction of the centre image (Figure 69 – middle). This transformation error is then compounded when the scaling is done to get the divergent results mentioned above. This will be discussed more during the recommendations for further study.

Plotting of the profile

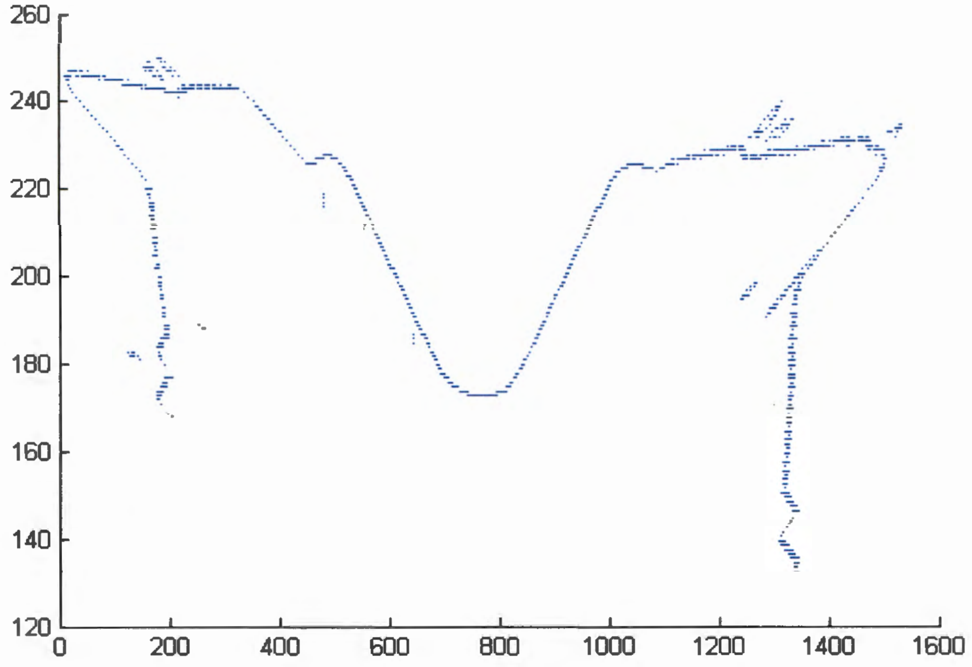

FIGURE 73: COMBINED IMAGE OF SHEAVE PROFILE (PIXEL FORMAT)

4.5. CONCLUSION

The author will refrain from jumping into an in-depth critique of the result for a moment since the purpose of this chapter was just to develop the profiler and the algorithm. Analysis of the results will be done in Chapter 7. Regarding the design process, the following can be concluded:

- From the objectives of the project, and the background research that was done, a set of design and user requirements were constructed. These were combined with the outputs from the functional analysis, to form the final design requirements. A detail mechanical design was done and shown. The algorithm was described in a step-by step fashion with intermediate results shown for each step.
- The process of calibrating the profiler was demonstrated and explained and the results for a calibrated profile were shown. At this stage it appears that the design has met some of the requirements as set out initially, but almost certainly not all. It will need to be manufactured, verified and validated to ensure that it complies fully (or to which degree it complies if not fully).

"Giving substance to shadows, giving substance evermore"

Rodriguez

Chapter 5: Design verification

Based on the requirements set out in the previous chapter, a profiler was designed. Before manufacturing can commence, it needs to be ascertained, theoretically (numerically or analytically where possible), whether the designed profiler will meet the requirements as set out. Just to recap, the requirements were as follows:

- Operation: One man operation
- Mounting: Sturdy for repeatable results
- Mounting: Flexible for different size sheave wheels
- Mounting: Quick attach and quick release
- Data collection and storage: Digital
- Power supply: Self-supplied
- Mass: < 5 kg
- Scan time: < 5 minutes
- Accuracy: $\pm 1\ mm\ with\ 95\%\ confidence$

5.1. Operation

By design, the profiler only needs a single person to operate it. The profiler therefore meets this design requirement. This parameter will be validated at a later stage.

5.2. Mounting – sturdy

The profiler mounts rigidly to the sheave wheel by design and therefore meets this requirement. Also, the profiler takes the profile in a very short time frame. This is important because it frees the profiler from the external, transient influences that conventional profilers are subjected to. These include vibrations from the other sheaves in the headgear, contact with the operator during the scan, wind effects etc.

5.3. Mounting – flexibility

By rotating the magnets they can be loosened and easily moved to accommodate various sizes of sheave wheel. The profiler uses a flexible mounting system to ensure that any sheave wheel between 95mm and 475mm wide can be inspected with it. This design requirement has been successfully met.

5.4. Mounting – quick attach/ release

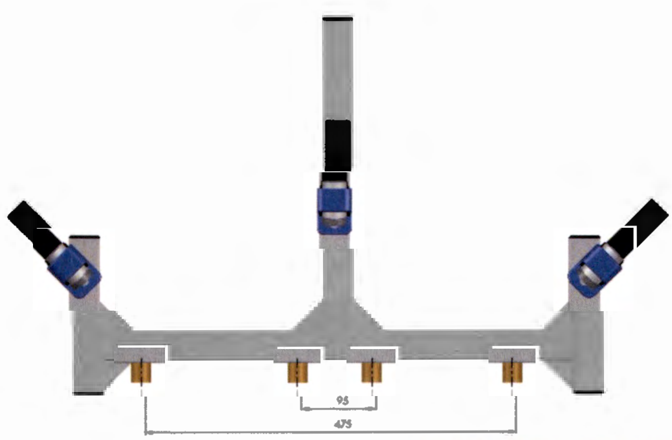

Figure 74: Extreme positions of the magnetic feet

The magnets allow for immediate attachment to the sheave wheel. Using a prying action to remove the profiler will allow the user to remove the profiler with ease. This requirement has thus been successfully met.

5.5. Data collection and storage

The profiler has been designed such that the profiles are collected digitally. The data is available in a *.csv format and can be interpreted by anyone with a computer. It has therefore met this requirement.

5.6. Power supply

The profiler uses batteries for the light sources and the cameras draw power from the laptop. The laptop computer has a rechargeable battery. The system therefore requires no external power supply for the duration of the scan and has thus met this requirement successfully.

5.7. Mass

The mass of the profiler (according to the summation of its various parts) is 3.47kg[6]. This will later be validated by weighing the actual profiler.

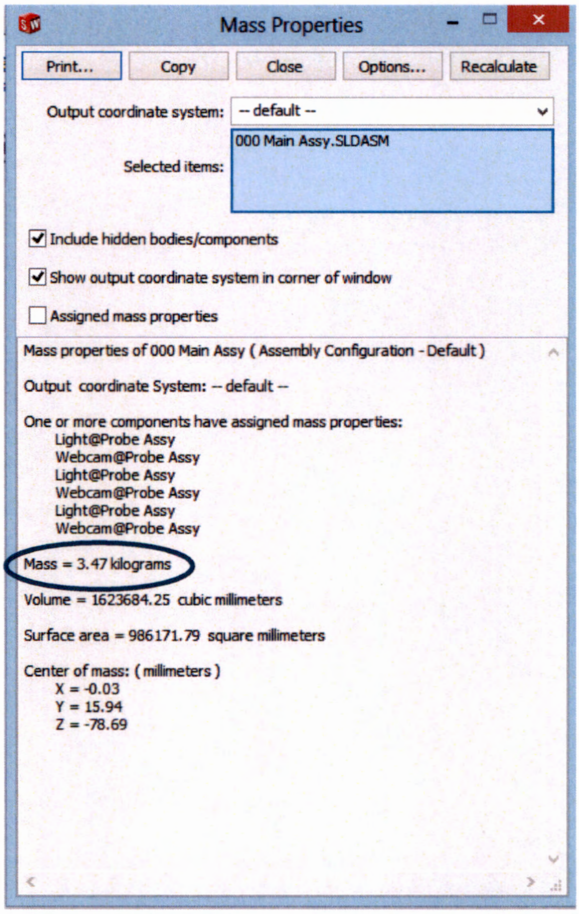

Figure 75: SolidWorks results of mass analysis

[6] The quoted mass necessarily excludes the mass of the laptop which does not form part of the scope of the design.

5.8. Scan time

The scan time is theoretically almost instantaneous. It must, however, be validated through experiment. It should be noted that the scan time mentioned here is the time for the actual scan. Since the time constraint imposed on the scan is not for the post processing, but only for the scan. The profiler can be removed from the sheave wheel which can then be put back into service while the operator continues to process the images.

5.9. Fit-for-purpose

The fit-for-purpose verification has been done graphically and attempts to answer the question: will the profiler be able to determine both the rim profile and the web thickness as required from industry and legislation? Because the profiler is generic enough to scan different shapes and sizes of sheave wheel, it was necessary to determine a new variable named the opportunity space. The opportunity space is made up of two variables namely the working distance and the field of view. Both of these parameters have been mentioned before, but for the sake of clarity, the following numbers are repeated:

- Field of view: About 60°
- Offset: 211 mm
- Maximum working distance: 259 mm

Looking at the image on the left in Figure 77, the portion of the opportunity space that can be attributed to the working distance can be seen while the portion of the working space due to the camera field of view can be seen on the right.

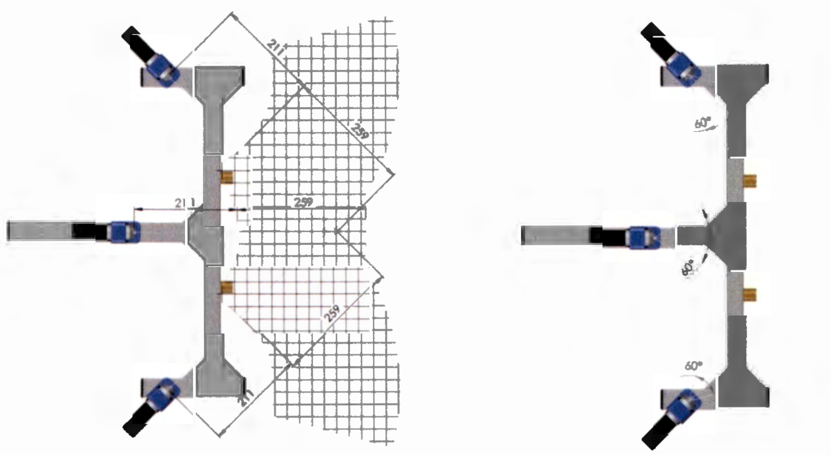

Figure 76: Opportunity space due to working distance (left), due to field of view (right)

Each sensor is able to take a profile that is shaped like a doughnut around it with the inner circle being the 211mm offset and the outer circle being the 259 mm maximum working distance. Looking at the image on the right, the field of view shows the shape of the opportunity space if one considers only the field of view. It could obviously have extended out much further, but in the same way that the circles in the previous image didn't actually go right around, it was decided to impose other constraints to ensure that the images display better. The constraints were just a trimming of the opportunity space by removing the areas that will obviously not be used while retaining all the areas that have even a small likelihood of falling within the final opportunity space.

A point must fall within both parameters in the opportunity space to be considered to be eligible for recording (this can be likened to an AND logical operator in Boolean algebra). The image below represents a superposition of both images above and the hatched rectangle is deemed as the largest obtainable opportunity space with the configuration of the sensors as it is designed at present. The rectangle is 245mm deep and 318mm wide. Now, since this is the design verification, the question is, will the designed profiler meet the requirements set out? In other words, is this opportunity space large enough to record the rim profile and the web thickness of most sheave wheels?

The sheave wheel sample that has been provided is roughly 260 mm wide and 250 mm deep (it should be noted that this sheave is on the larger side of the spectrum). The profiler would be able to measure the entire width of the wheel and 98% (245/250 x 100% = 98%) of the depth (see Figure 78). This is sufficient since the web thickness can be determined within the first +- 150 mm of the depth of the wheel. This design requirement shall be deemed to have been met.

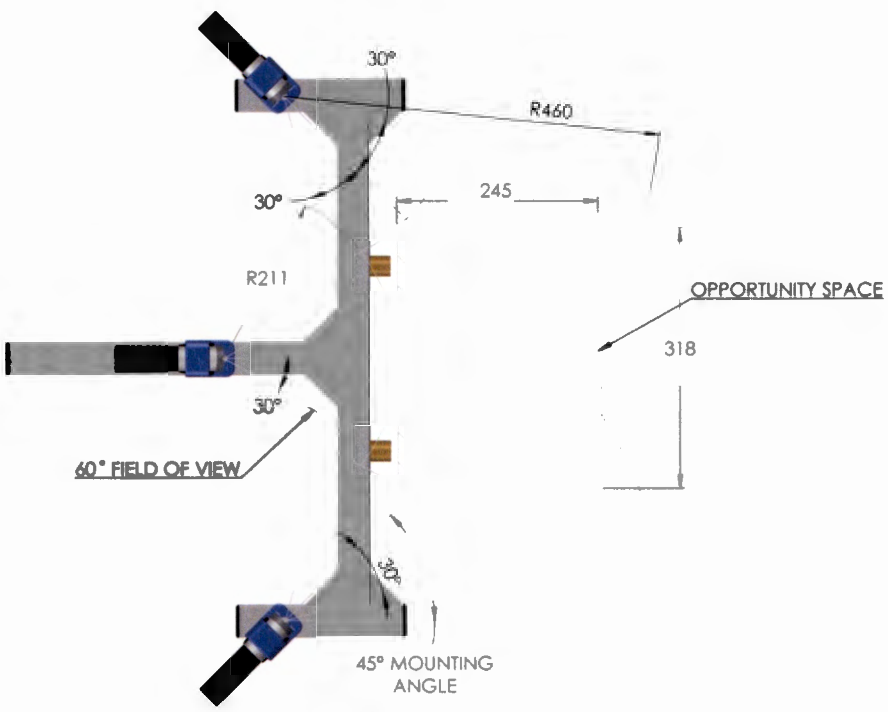

FIGURE 77: COMBINED OPPORTUNITY SPACE

5.10. ACCURACY

The following section is dedicated to uncovering all the hidden sources of uncertainty in the design itself. Those factors will be combined to form a generic design uncertainty which will be the accuracy of the proposed profiler. If this is within the limits set out by the final design requirements, the parameter shall be deemed to be verified.

The following sources of uncertainty with regards to the accuracy of the profiler have been identified:

- Extrinsic parameters
- Intrinsic parameters

5.10.1. Possible manufacturing discrepancies – extrinsic parameters

Is the distance from the camera to the zero point what it should be?

The profiler was designed to start measuring at 211 mm so it is important to ensure that the sensor is located at 211 mm from the point where data acquisition starts. It should be noted, however, that the profiler takes relative measurements with 211 mm as a baseline. This means that, even if the 211 mm was completely wrong, the profile would still be correct since it would be relative to 211 mm. A good idea would be to change the algorithm to take the first data point as a local origin for the profile, irrespective of profiler mounting configuration.

Is the mounting angle between the three cameras what it was expected to be?

This is an important parameter that will undoubtedly not be entirely perfect since the mounting angle is not very easy to ensure. Incorrect mounting will have an effect on the matrix addition step since the lines will not add up correctly if the angles are incorrect. In light of this, a calibration routine has been implemented to ensure that the data is scaled according to the actual mounting as opposed to theoretical ideal mounting configuration.

Is the angle for the camera mounting what it should be?

As mentioned in earlier sections, the profiler does not use the entire CCD chip of the camera and thus if there is a minor misalignment of the camera, it should not have too much of an effect on the data since it will just use a different portion of the CCD chip.

5.10.2. Camera inadequacies - intrinsic parameters

Finite number of pixels in an image and the number of pixels used

Camera manufacturers regularly quote impressive values for their equipment. The cameras used in this profiler were said to be "Up to 8 Megapixels". When examining the actual sensor data, these statements seem misleading since the sensor is only 640 X 480 pixels which amounts to only 307 200 pixels, that is: 0.3 Megapixels. Upon reading the fine print, it becomes clear. They use software interpolation to produce an image that contains 8 Megapixels. In a measurement instrument however, it is not possible to use software manipulation to create data where there is none. This will be elaborated on this during the recommendations for further study. For now, it is necessary to consider the effect of this on the result. This will be done together with the bottom section on pixel density since they are inseparably interlinked.

Effect of pixel density as the distance from the sensor increases [in x and in y]

The resolution of the data decreases with an increase in measurement distance. Therefore, the data that is collected at the outermost point of the working area will have a different accuracy to that detected at the beginning of the working area. This was alluded to earlier in the graphs where pixel to mm scaling was done during algorithm development. In the interest of clarity, they are shown again in Figure 79.

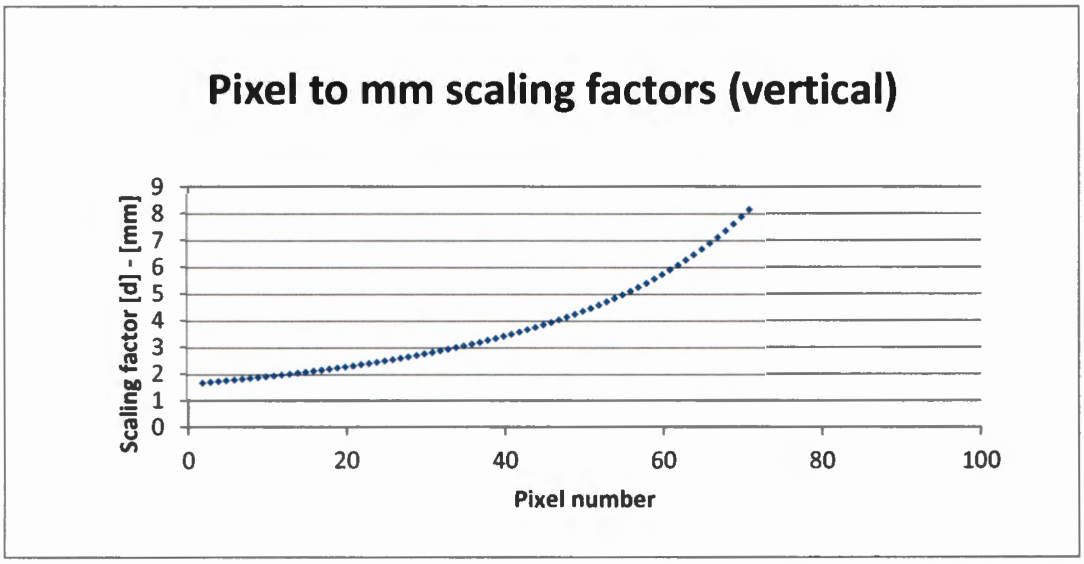

FIGURE 78: PIXEL TO MM SCALING FACTORS (VERTICAL)

Looking in the y-direction (depth value as seen in Figure 65), the maximum error in the working area is the maximum step size. It is found at the last point in the working area and is:

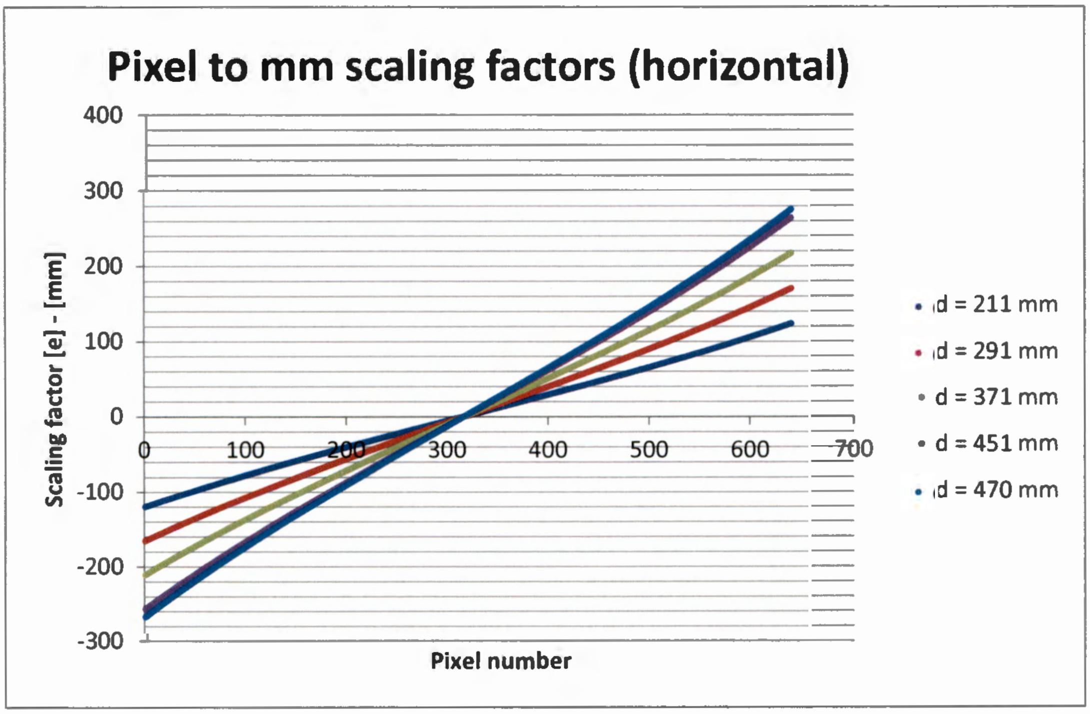

FIGURE 79: PIXEL TO MM SCALING FACTORS (HORIZONTAL)

$$e_{y,max} = 8.1682\ mm$$

The minimum error in the working area is at the lowest value of the depth and is:

$$e_{y,min} = 1.6915\ mm$$

It may be tempting to simply state that the overall error is the maximum error obtained (the worst case scenario) and thus: $e_y = e_{y,max}$ but this will inadvertently be selling the result short. Looking at the graph above, the error margin grows exponentially with the increase in distance. This means that for most of the first part of the working area the error is significantly less. For precisely that reason, the standard deviation cannot be used since it will be inaccurate for a large portion of the result. The only really feasible way to determine the accuracy of the profiler in the y-direction would be to write the error as a percentage of the measured value. To confirm this, it may be useful to plot the percentage error as a function of the distance (see Figure 67)

$$e_{y,max} = 1.73\ \%$$

$$e_{y,min} = 0.26\ \%$$

The mean of the error data in percentage format is: $\mu = 1.14\ \%$

The standard deviation of the error data is: $\sigma_y = 0.26\%$

To get to an acceptable confidence interval (95%), a coverage factor of $k = 2$ will be used. This means that we now have an error bound for the depth measurement that looks like this:

$$e_y = 1.14\% \ \pm (2 \times 0.26\%)$$

$$e_y = 1.14\% \ \pm \ 0.52\ \%\ with\ a\ 95\%\ confidence\ interval$$

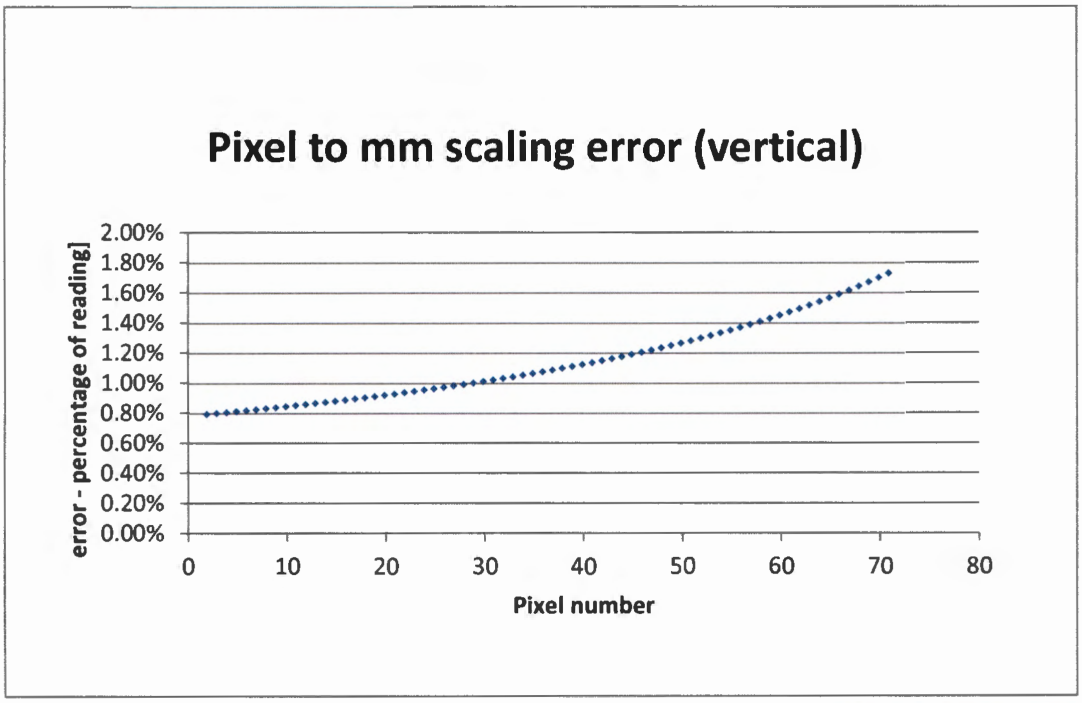

FIGURE 80: ERROR ON THE Y-AXIS

For the x-axis, the same will now be done, but since the scaling is now multifactorial, the maximum error will be used. This is acceptable in this case because the changes are very small for different values of d.

$$e_{x,max} = 0.22\ \%$$

$$e_{x,min} = 0.16\ \%$$

The mean of the error data in percentage format is: $\mu = 0.18\ \%$

The standard deviation of the error data is: $\sigma_y = 0.02\%$

Again, to get to an acceptable confidence interval (95%), a coverage factor of $k = 2$ will be used. This means that we now have an error bound for the depth measurement that looks like this:

$$e_x = 0.18\ \% \ \pm (2 \times 0.02\ \%)$$

$$e_x = 0.18\ \% \ \pm\ 0.04\ \%\ with\ a\ 95\%\ confidence\ interval$$

Since both coordinates contribute to the overall coordinate of a measured point R, it can be said that:

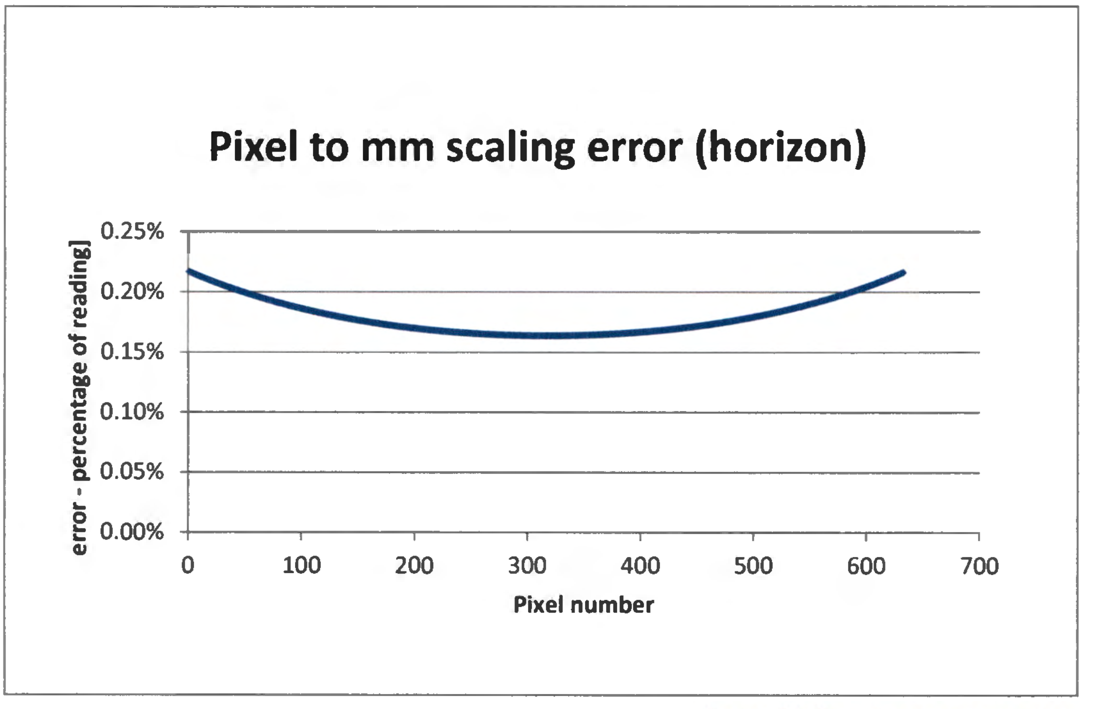

FIGURE 81: PIXEL TO MM SCALING ERROR

$$R(x, y) = \sqrt{x^2 + y^2}$$

$$\therefore e_R = \sqrt{{e_x}^2 + {e_y}^2}$$

$$\therefore e_R = \sqrt{(0.18\% \pm 0.04)^2 + (1.14\% \pm 0.52\%)^2}$$

$$e_R = \sqrt{0.0324\% \pm 0.0016\% + 1.2996\% \pm 0.2704\%}$$

$$e_R = \sqrt{1.332\% \pm 0.272\%}$$

$$e_R(d) = 1.15\% \pm 0.52\% \; with\ a\ 95\% \ confidence\ interval$$

Based on the equation developed above, the individual error for any point can be determined, based only on the depth value [d] associated with it.

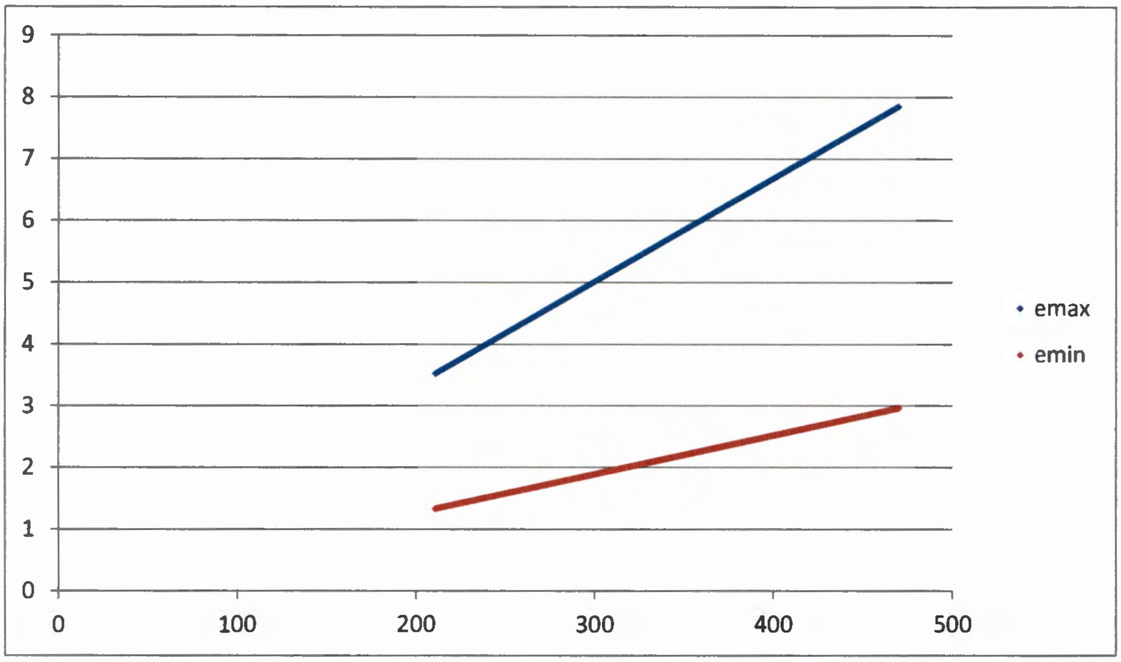

FIGURE 82: ERROR AS A FUNCTION OF DEPTH POSITION D

5.11. CONCLUSION

The following summary can be made about the verification of the profiler as it was designed in Chapter 4:

TABLE 5: DESIGN VERIFICATION SUMMARY

User/ Design Requirement	Required Value	Verification	YES/NO
Operation	One man operation	5.1	Yes
Mounting	Sturdy	5.2	Yes
Mounting	Flexible for different size wheels	5.3	Yes
Mounting	Quick attach and quick release	5.4	Yes
Data collection and storage	Digital	5.5	Yes
Power supply	Self-supplied	5.6	Yes
Mass	<4kg	5.7	Yes
Scan Time	< 5 minutes	5.8	Yes
Fit for purpose	Yes	5.9	Yes
Accuracy	$\pm 1\ mm\ with\ 95\%\ confidence$	5.10	No

CHAPTER 6: EXPERIMENTAL INVESTIGATION

"It doesn't matter how beautiful your theory is. It doesn't matter how smart you are, if it doesn't agree with experiment, its wrong."

Richard P. Feynman

6.1. INTRODUCTION

To recap, the aim of the project is as follows:

"To develop a method of digitally measuring the profile of a sheave wheel and to verify and validate the accuracy of this method while critically evaluating it against the current state of the art."

In the preceding chapters, the method (apparatus) for digitally measuring the profile of a sheave wheel was developed and theoretically verified. In order to comply with the aim, is validation and critical evaluation against the current state of the art is still outstanding. Therefore, there are two parts to the experimental investigation. The first is to attempt to validate the theoretical precision (from Chapter 5) of the newly developed profiler. The second experiment set aims to provide an objective comparison between the profiler developed earlier and the methods that have been identified as the current state of the art for sheave wheel profiling.

6.2. EXPERIMENT DESIGN

The experiment in this application is considered as the process of recording the sheave wheel profile. In the two figures below, this is demonstrated, first in a theoretical model and then it is shown in a practical interpretation of the model.

FIGURE 83: THEORETICAL EXPERIMENT MODEL

FIGURE 84: PRACTICAL INTERPRETATION OF THEORETICAL MODEL

The experiment has one input variable namely the method/instrument used to take the profile. There are two output variables that can be shown on the recorded profile. These are the x and the y coordinates of each point in the profile. During the experiment, the input variable will be changed while monitoring the effect on the output variables.

FIGURE 85: EXPERIMENT INPUT AND OUTPUT VARIABLES

For each experiment, two approaches were followed. The first approach consisted of measuring a discrete, known sample with each device/method. An experimental error bound could then be determined for each method and when combined with the experimental uncertainty analysis for each experiment, the overall error bound together with its confidence interval could be determined for each method/device. The second approach consisted of measuring an unknown sample that does not explicitly give information of the absolute accuracy of the profiler but will give an idea of the "fit-for-purpose" accuracy since the "unknown sample" is a cut-out section of a sheave wheel.

For each method, the experiment was conducted several times. The repeatability conditions from NIST (Taylor & Kuyatt, 1994) have been adhered to during the experimentation process in an attempt to reduce the probability of induced errors due to the experiment. These are:

- the same measurement procedure
- the same observer
- the same measuring instrument, used under the same conditions
- the same location
- repetition over a short period of time

6.2.1. Known sample experiments:

This series of experiments is based, to a certain extent, on the work done on the calibration of a 3D laser scanner (Chen, Shang, & Wei, 2011). Their experiment was generic enough to be used in most circumstances where a set of data points needs to be validated and a known sample is used. In their case, they have a 3D point cloud and use Geomagic Qualify software to perform the analysis. In this application though, the point cloud is only 2D and is much simpler and thus the need for complex comparison tools cannot be justified.

Two samples were profiled for the Known Sample experiment set. The first is a V1 Ultrasonic calibration block and the second is a Phoenix Phased Array calibration block. These particular blocks were selected because of their availability to the author, but they were deemed fit because they both consist of a good subset of different features that may be encountered during the profiling of a sheave wheel. These include:

- Straight edges
- 90° corners
- Step changes in height
- Radii

The blocks were also assumed to be good test samples since their dimensions are within the same order of magnitude of the expected dimensions for sheave profiles.

The experimental procedure for the profiling of these blocks entails taking the profile of as much of the block as possible (all methods will not be able to access equal parts of the block) and then performing a statistical comparison between the measured results and the known parameters of the block (as per the published values and tolerances).

The V1 Calibration block shown in Figure 87 can be made of steel or aluminium (they have different properties for ultrasonic applications, but are machined identically).

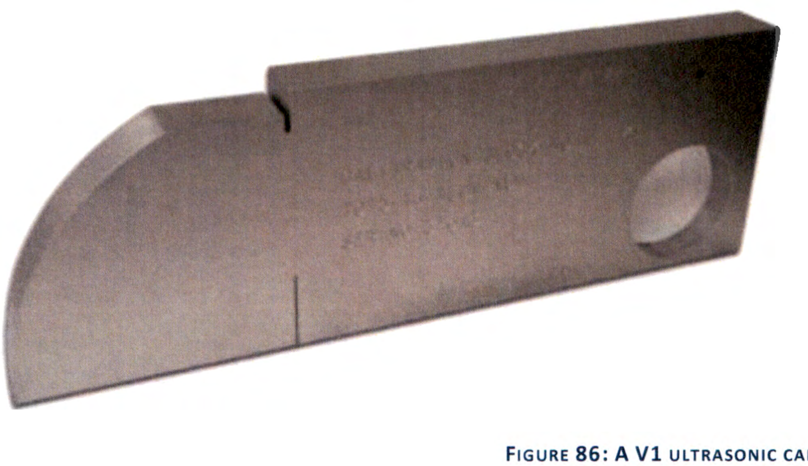

Figure 86: A V1 ultrasonic calibration block

The V1 calibration block has dimensions and manufacturing tolerances that are governed by BS EN 12223 and are as follows in Figure 88:

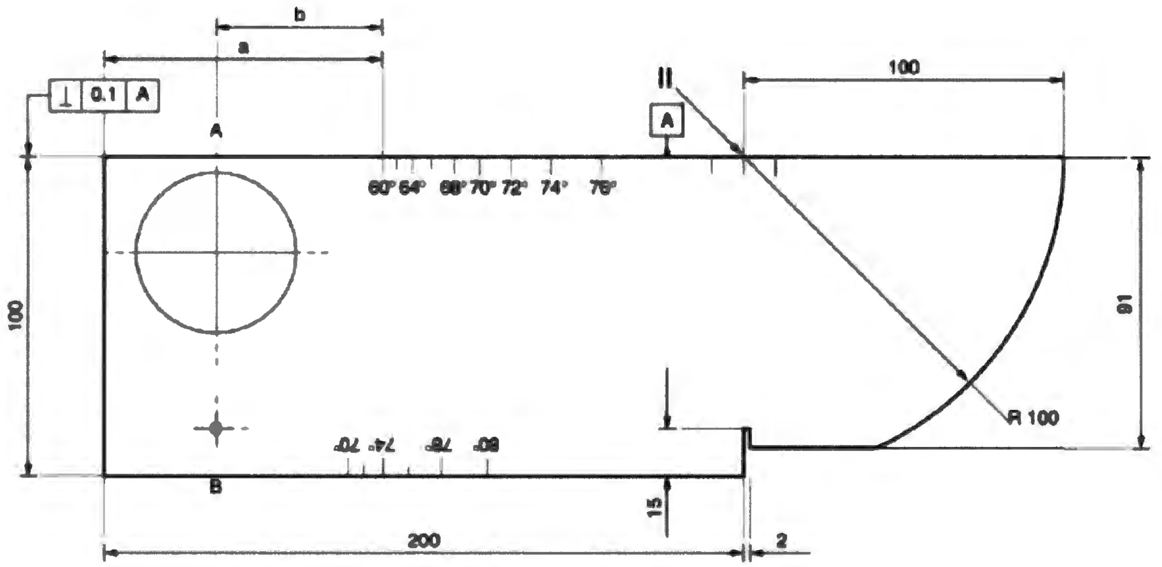

FIGURE 87: V1 CALIBRATION BLOCK SCHEMATIC (BSI, 1999)

According to the standard (BSi, 1999), the tolerance on machining of the block is to be ±0.1 mm and an allowance has been made for a surface roughness value of 0.8 μm. This will be discussed in more detail during the uncertainty analysis in Appendix 2.

The second block that was used has slightly different dimensions. It was hoped that a certain degree of data redundancy was introduced by the profiling of the second block. This sample is a calibration block for Phased Array Ultrasonics and is shown in Figure 89 below.

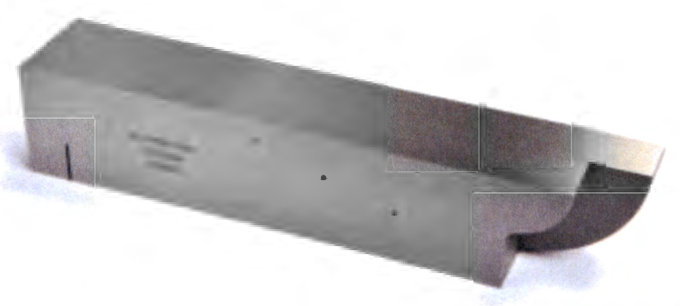

FIGURE 88: PHASED ARRAY TEST SAMPLE

This sample is issued with a certificate of compliance which can be found in Appendix 4.3. The dimensions of the block are shown in Figure 90.

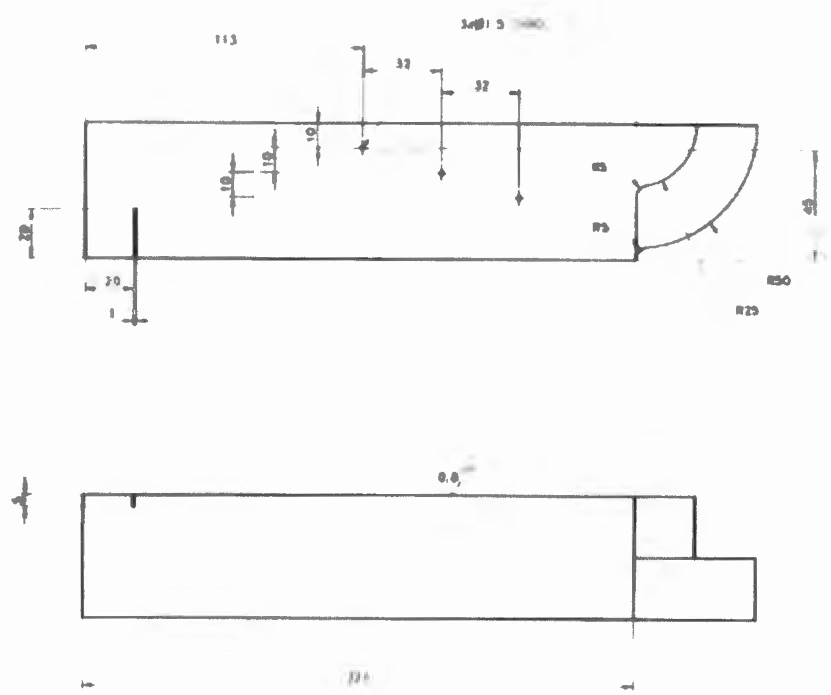

FIGURE 89: PA- CALIBRATION BLOCK SAMPLE DIMENSIONS

6.2.2. SHEAVE WHEEL EXPERIMENT:

The sheave wheel experiment (SWE) was done because, although the accuracy of the profile could be experimentally validated by only looking at known samples, there is an element of fit-for-purpose that needs to be evaluated. The profiler could be accurate, but is its particular design and construction suitable for the application it was intended for?

FIGURE 90: SHEAVE WHEEL SAMPLE THAT WILL BE PROFILED FOR SWE

To determine fit-for-purpose, each profiler/method will be evaluated against their ability to measure the critical areas of a sheave wheel profile (sample shown in Figure 91). In an earlier chapter, the critical areas for the safety of ropes have been shown as per the South African Bureau of Standards (SANS 10294, 2000). In Figure 94 that original image has been amended to include a measurement of web wear as per industry standard (W1 and W2 in the image below) which now implies that the sheave is inspected for rope safety and sheave safety.

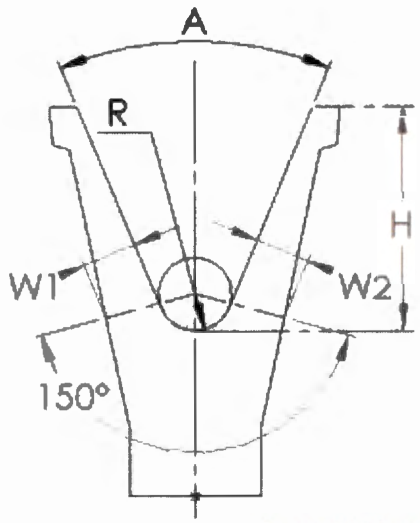

FIGURE 91: CRITICAL AREAS OF THE SHEAVE WHEEL PROFILE

The results from the sheave wheel experiments will not be compared to absolute values. Instead, the dispersion characteristics of multiple profiles obtained with the same method will be compared to quantitatively express the repeatability of the results as per the NIST Guidelines (Taylor & Kuyatt, 1994) .

6.3. EXPERIMENTAL PROCEDURE

The experimental investigation was divided into six experiments:

TABLE 6: EXPERIMENT SUBDIVISIONS

	Known Sample Experiments		Sheave Wheel Experiment
	V1 – Cal. Block	PA Cal. Block	
Validation of design	Experiment 1	Experiment 2	Experiment 3
Critical evaluation	Experiment 4	Experiment 5	Experiment 6

Since the critical evaluation experiment was done on several different profilers, experiments 4, 5 and 6 had to be subdivided as follows:

TABLE 7: FURTHER EXPERIMENT SUBDIVISIONS

	KSE – V1 Calibration Block	KSE–PA Calibration Block	Sheave Wheel Experiment
Plaster cast	Experiment 4 (a)	Experiment 5 (a)	Experiment 6 (a)
Laser profiler	Experiment 4 (b)	Experiment 5 (b)	Experiment 6 (b)
Pantograph	Experiment 4 (c)	Experiment 5 (c)	Experiment 6 (c)
Microscribe®	-	-	-
Sheave gauges	-	-	-

Lastly (to confirm the mass of the profiler as well as the time it takes to do a scan) two more experiments have been defined:

TABLE 8: EXPERIMENTS ON WORKING TIME AND MASS OF PROFILER

	Known Sample Experiment
Mass of profiler	Experiment 7
Time to take scan.	Experiment 8

The author was unable to obtain access to sheave gauges or to the Microscribe® for experiments. Sheave gauges, although a very important part of sheave profiling, cannot really be compared to the other methods since they can only actually measure the diameter of the rope groove. It would have been nice to be able to include the results from the Microscribe® but at least there is data published by the OEM on the validated accuracy of a properly calibrated Microscribe®.

Each experiment was done several times in an attempt to get convergence of the results and to reduce the local uncertainty of the experimental data.

6.4. Conclusion

The purpose of the set of experiments was twofold: The first goal was to validate the design of the new α-prototype profiler. The second goal was to do a critical evaluation of the new profiler against the current state of the art and also between different modalities within the current state of the art. The output of such an experiment should therefore in essence be a set of answers to the following questions:

Table 9: Experiment design summary

Question	Experiment
▪ How accurate is the α-prototype profiler?	1,2
▪ Is the α-prototype profiler able to take the profile of a sheave wheel such that the critical areas can be determined?	3
▪ If yes, are the results repeatable and to what degree?	3 - Analysis
▪ How accurate are the methods/profilers that are considered to be the current state of the art?	4(a-c), 5(a-c)
▪ Are they able to take the profile of a sheave wheel such that the critical areas can be determined?	6(a-c)
▪ If yes, are the results repeatable and to what degree?	6 - Analysis
▪ How does the accuracy of the α-prototype profiler compare to the current state of the art?	1,2,4(a-c), 5(a-c) - Analysis
▪ How does the α-prototype profiler's ability to repeatably profile sheave wheels compare to the current state of the art's ability?	3,6(a-c) Analysis

If the experiments that were designed in this chapter are carried out correctly, it should be possible to answer all the questions posed above. After looking at the experimental results in the following chapter, data reduction is done at which stage the experimental results will be produced in such a way as to answer the questions above.

CHAPTER 7: EXPERIMENTAL RESULTS

"No amount of experimentation can ever prove me right; a single experiment can prove me wrong."

Albert Einstein

7.1. INTRODUCTION

All the raw data of the profiles are not included in this report since it would simply be too much to present. The author has attempted, in the section below, to provide enough results to allow the reader to draw his/her own conclusions before they are formally discussed while refraining from drowning the reader in mountains of baffling, senseless data.

7.2. EXPERIMENTAL RESULTS

Since different methods of profiling were used and different experiment designs were used, it was decided that it would be best to discuss each method/profiler and under that heading discuss the different experiments that were done. It may sound strange because in essence we want to group the experiment types together for comparison (and we will), but since each profiler has its own quirks that need to be kept in mind when looking at the data it is better to first group the methods together.

7.2.1. ALPHA PROTOTYPE PROFILER

As the author has alluded to earlier, the α-prototype profiler that was developed in preceding chapters could not produce results that were of sufficient quality to be processed and evaluated. The author realised at the outset of this project that the decision to use low cost cameras might have negative implications for the precision of the profiler. It was decided that as long as a semi-high resolution camera could be used, the results would still be satisfactory. Unfortunately, it was later determined that the published values of the resolution of consumer-grade web cameras was not something that could be taken literally. Upon close inspection of the CCD sensor used, it was determined that the actual resolution of the sensor was roughly 15% of the published value. The author still believed that it would be possible to prove the concept with the low resolution camera while simply not meeting the requirement for the desired accuracy of the profiler. It later transpired that during the algorithm, certain steps caused an unavoidable decrease in resolution. By the time the image reconstruction had to be done, the resolution was such that accurate reconstruction matrices could not be created. This meant that even though all the steps from image acquisition through edge detection could be done with all the cameras, it was not possible to do the scaling and final reconstruction of the image. Therefore, no usable results could be obtained by the α-prototype.

In hindsight, it would be necessary to significantly increase the resolution of the camera that is used to record the profile. Unfortunately, due to time and financial constraints it is not possible to redo the experiments with the new information. The details have been added to the recommendations for further studies.

7.2.2. PLASTER CASTS

The plaster cast method discussed in Chapter 2 turned out to not be feasible at all. The profiles that were taken were not even rigid enough to trace onto a sheet of paper. The author discussed this with some practicing technicians and was informed that a second method of sheave profiling with plaster casts exists. It is similar to the technique discussed in Chapter 2, but instead of using plaster of paris bandages, a plaster of paris paste is used. Steps iv) – viii) are replaced with the following steps:

1. The cross section of the sheave is blocked off and filled with a plaster of paris paste.
2. When this has dried, it is removed and traced as per the instructions in Chapter 2.

Due to the disproportionate amount of time the plaster of paris takes to dry, it was only possible to do a single casting for each of the samples (there was a limited time within which the author had access to the calibration blocks). This was assumed to be acceptable since the main source of error for a plaster cast lies in the tracing of the profile onto a piece of paper and the measuring of the traced profile.

Experiment 4 (a): V1 – Calibration block

- Process Photos

As per the protocol from Chapter 2, the V1 block was greased very lightly after which the casting was done. The cast can was done on wax paper for practical purposes; the setup can be seen in the image below.

After drying, the profile was carefully removed by gently tapping the block with a hammer and then carefully lifting the block out.

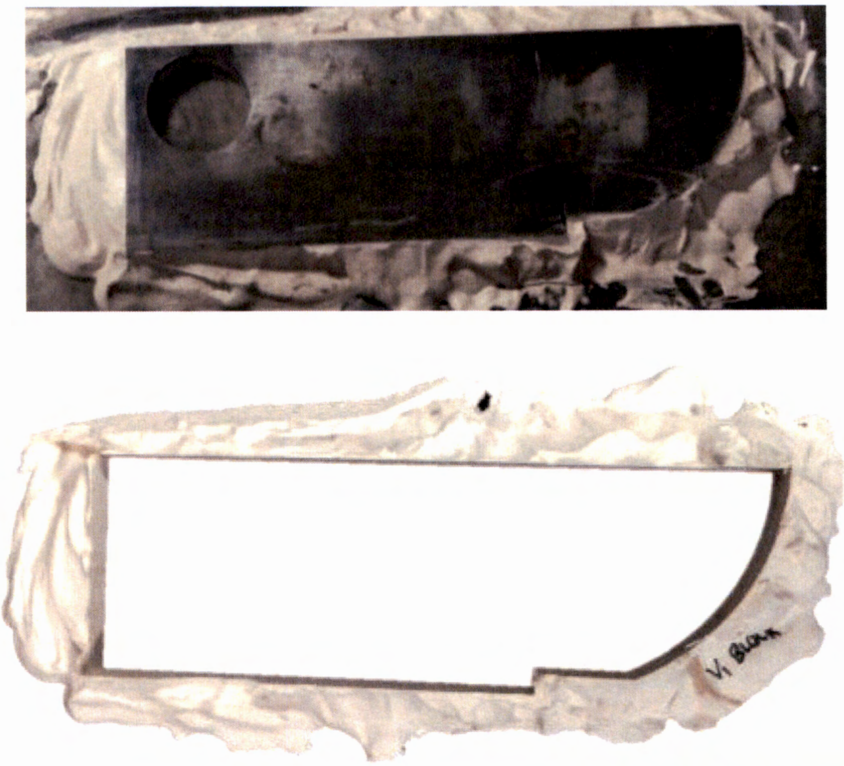

FIGURE 92: THE V1 BLOCK PLASTER CAST PROCESS

- Results

The resulting image was traced onto a sheet of paper and increments of 5mm were marked off on the length of the profile. These were used for the measurement data points. As per industry convention and HB 0.5mm pencil was used for the tracing of the profile which can be seen in Figure 94 below.

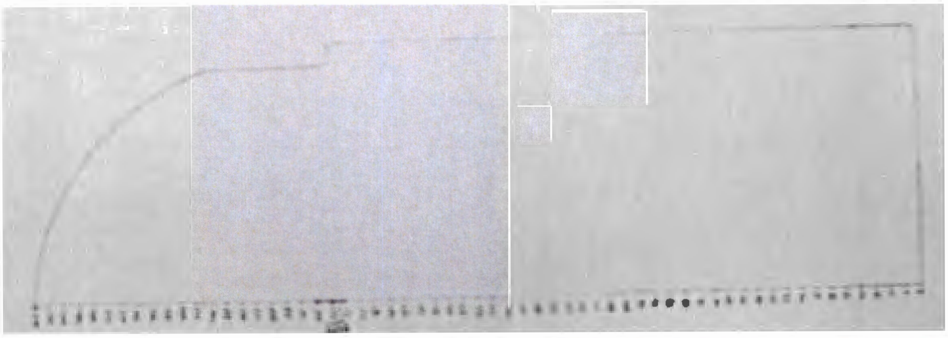

FIGURE 93: THE TRACED PROFILE OF THE PLASTER CAST [V1]

Each data point was measured using a calibrated digital calliper (see Appendix 4.2 for calibration certificate). These were then entered into an Excel® spreadsheet and processed to determine absolute error of the measurement and the dispersion factors. The relevant uncertainties were then applied (see Appendix 2.1 for detailed uncertainty calculations) so that accurate conclusions could be drawn.

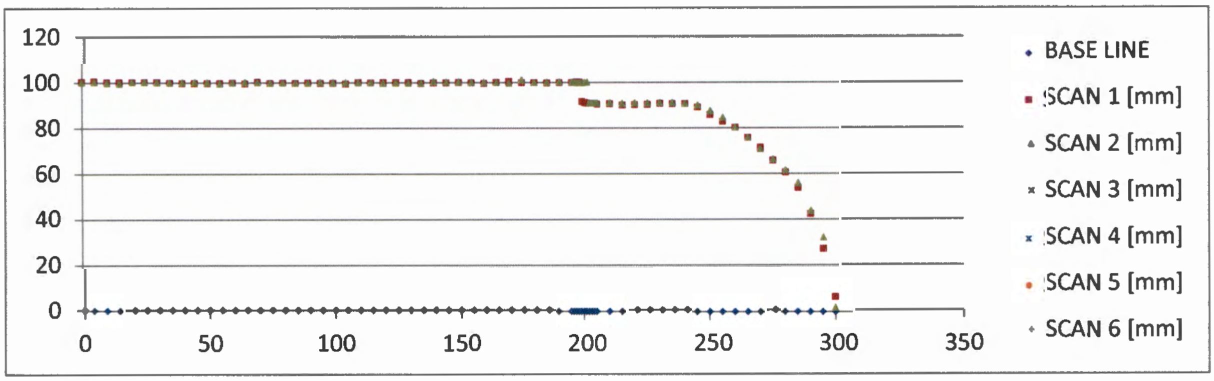

FIGURE 94: V1 BLOCK PROFILES BASED ON RAW DATA

For this experiment, the physical size of the sample based on the measurement does not matter as much as the error. The error was thus calculated for every point. This was done by subtracting the known actual size from the measured size. There are two experiment outputs namely the x and the y coordinate. Each has its own error margin. The average of all the errors was calculated as:

$$e_{pc,v1-y} = 0.66mm \pm 0.73\ mm\ within\ a\ 95\%\ confidence\ interval$$

$$e_{pc,v1-x} = 0.19mm \pm 0.66\ mm\ within\ a\ 95\%\ confidence\ interval$$

This result will be discussed more during the data reduction section.

- Remarks

It could be said that better methods exist for the extraction of the data from the plaster cast specimen, but since the goal of the experiment was to critically evaluate the current state of the art for sheave wheel profiling, the methods had to be used, as they are performed in industry. The effect of the decisions that were made is shown during the uncertainty analysis in Appendix 2.1.

Experiment 5 (a): PA Block

- Process Photos

The procedure for the PA Block sample is exactly the same as for the V1 block above. The experimental setup and the resulting plaster cast are shown in Figure 96 below.

Figure 95: PA Block plaster cast

- Results

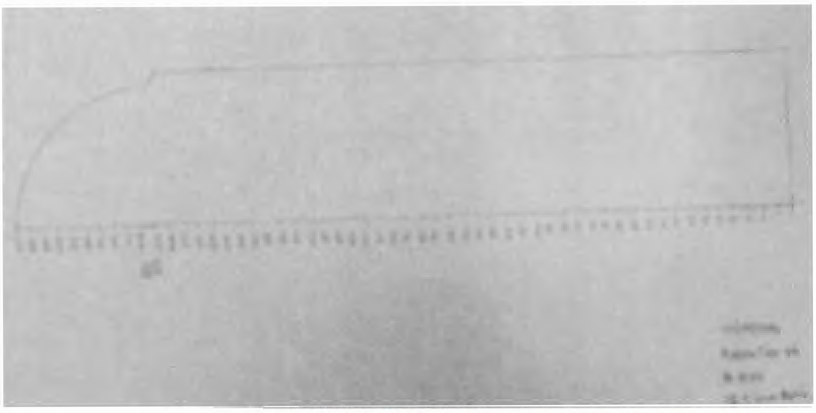

FIGURE 96: PA BLOCK TRACED PROFILE FROM PLASTER CAST

The profile was once again copied onto a sheet of paper with increments of 5 mm marked off for the recording of the measured data (see Figure 98 above) and copied onto an Excel® spreadsheet (see Figure 98 below).

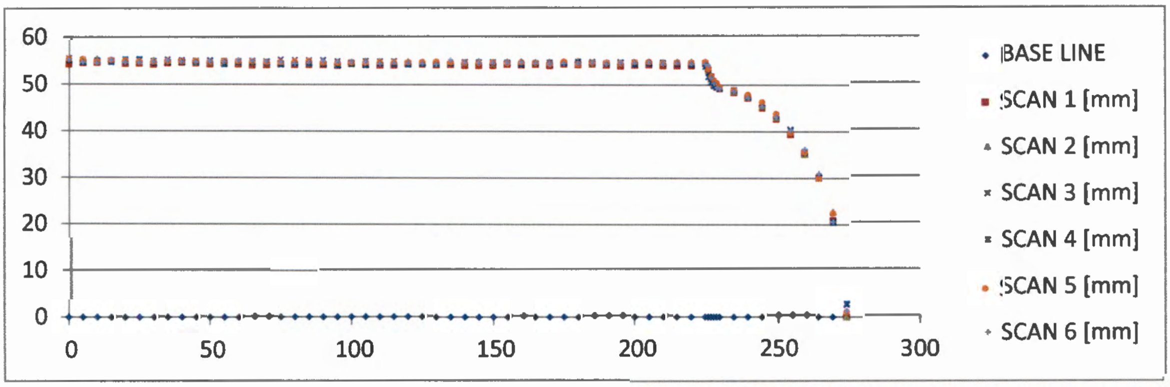

FIGURE 97: PA BLOCK RESULTS PLOT BASED ON RAW DATA

The averaged recorded values were compared with the absolute values known from the calibration certificate of the block (see Appendix 4.3) and absolute error was determined.

The error was calculated as follows:

$$e_{pc,pa-y} = 0.28mm \ \pm 0.66mm \ within\ a\ 95\% \ confidence\ interval$$

$$e_{pc,pa-x} = 0.29mm \ \pm 0.63mm \ within\ a\ 95\% \ confidence\ interval$$

- Remarks

It was noticed here that the error for this sample differs from that in the previous sample. It could be possible that the error is not a constant and should rather be expressed as a percentage of the measured value. This will be explored when all the data is put together.

Experiment 6 (a): Sheave Wheel

- Process Photos

The plaster cast of the sheave wheel is shown in the images below:

Figure 98: Sheave wheel profile plaster cast

- Results

Figure 99: Traced profile of sheave sample from plaster cast

The profile was traced onto a sheet of paper and the dimensions of the critical areas were determined by using the calibrated digital calliper as in earlier experiments. The following results were obtained:

TABLE 10: PLASTER CAST SHEAVE SAMPLE RESULTS

Critical Value	Variable	Units	Mean	ST DEV	Result Uncertainty	Experiment Uncertainty k = 2
Fleet Angle	A	°	45,92	0,19	0,08	0.60
Rope Groove	R	mm	55,66	1,40	0,57	1.28
Height of Groove	H	mm	111,10	1,02	0,41	1.00
Web thickness	W1	mm	56,27	0,34	0,14	0.64
Web thickness	W2	mm	54,05	0,28	0,11	0,62

- Remarks

For this experiment the absolute measured values were required. A comparison (and discussion) will therefore only be done during the data reduction stage when the absolute measurements for all the methods can be compared.

7.2.2. Laser profiler

Experiment 4 (b): V1 – Calibration block

- Process Photos

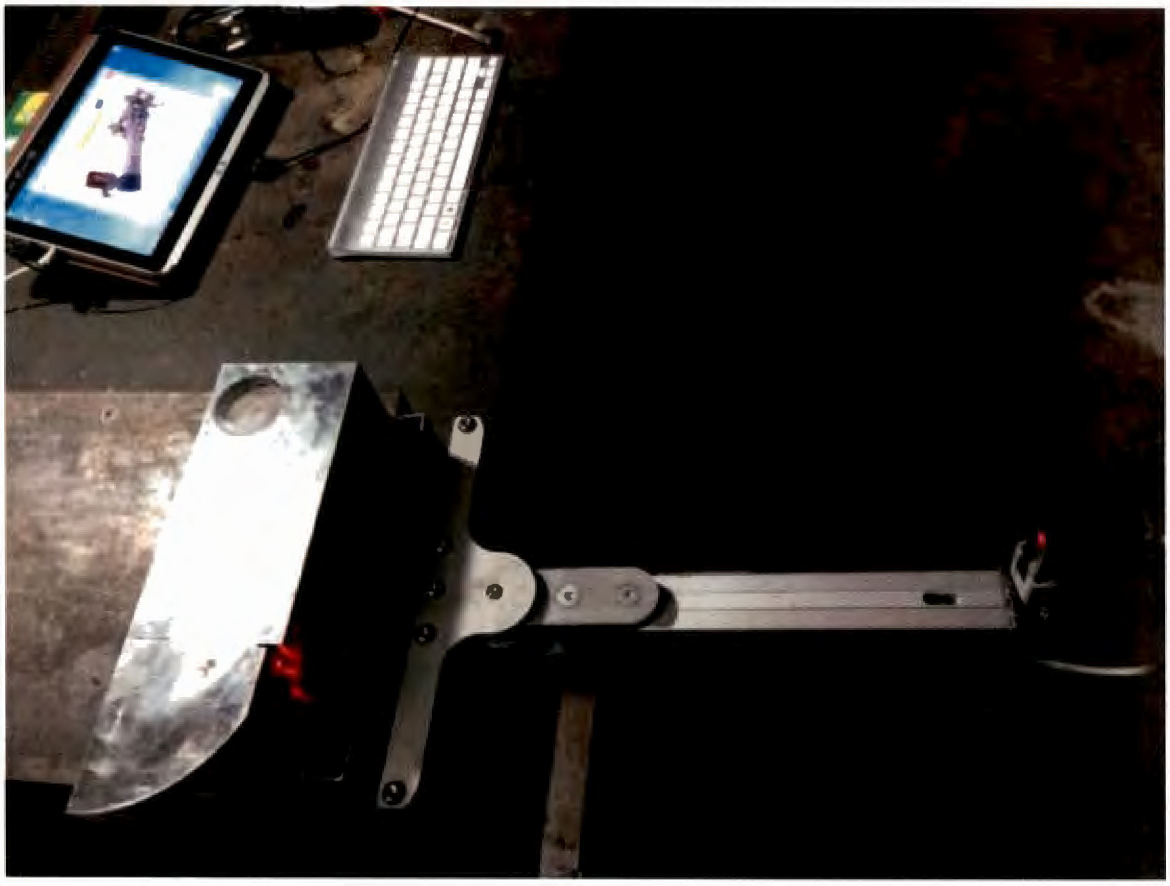

Figure 100: Laser profile of V1 block

- Results

The OEM software allowed the user to export the raw data into a point cloud (*.xyz) file. The point cloud was then imported into SolidWorks® for measurements to be done. In the interest of consistency, a procedure that resembles the one used for the plaster cast samples was used to collect the data from the laser profiler. In the SolidWorks® environment, it is possible to make measurements on a point cloud. The data was once again recorded at 5mm intervals and captured in an Excel® spreadsheet. The results can be seen in Figure 103 below.

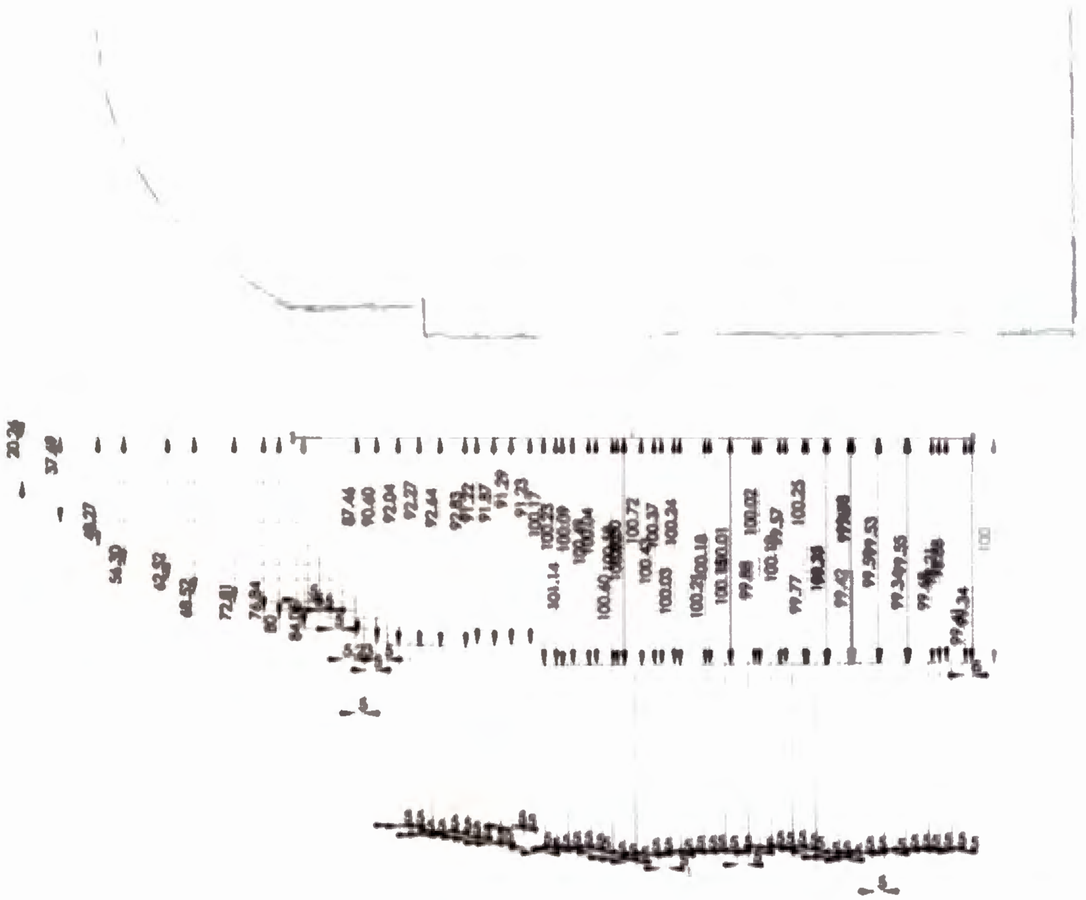

FIGURE 101: THE RAW POINT CLOUD (ABOVE) AND THE MEASURED DATA POINTS (BELOW)

The data was entered into an Excel® spreadsheet and plotted as in Figure 103 below.

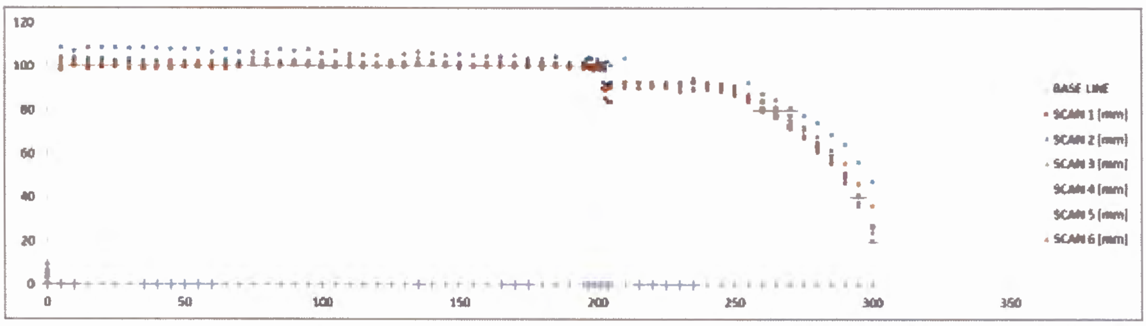

FIGURE 102: LASER PROFILER DATA OF V1 CALIBRATION BLOCK

The averaged recorded values were compared with the absolute values known from the calibration certificate of the block (see Appendix 4.3) and absolute error was determined using the uncertainty analysis in Appendix 2.2.

The error was calculated as follows:

$$e_{lp,v1-y} = 2.79\ mm\ \pm 2.10\ mm\ within\ a\ 95\%\ confidence\ interval$$

$$e_{lp,v1-x} = 3.43mm \pm 0.87\ mm\ within\ a\ 95\%\ confidence\ interval$$

- Remarks

There appears to be a large error as well as a large variance with the V1 block profiled with the laser profiler. This will be considered further when the error can be compared to other methods used on the same sample.

Experiment 5(b): PA Block

- Process Photos

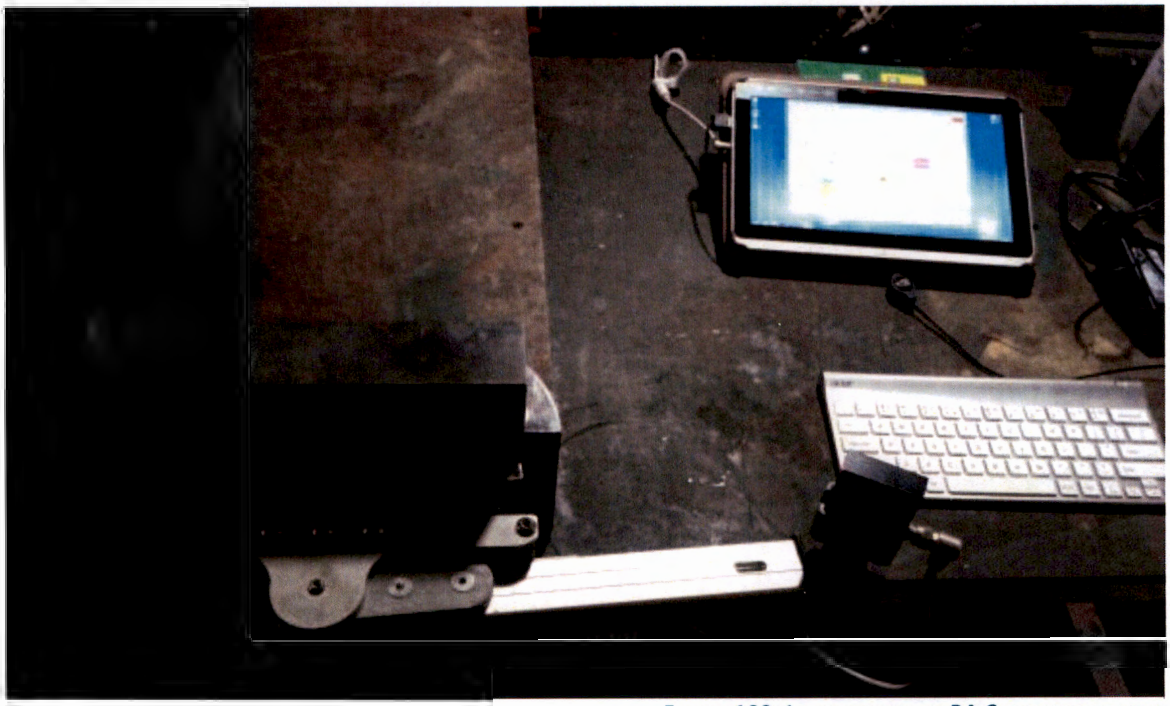

FIGURE 103: LASER PROFILE OF PA CALIBRATION BLOCK

The experimental setup for recording the profile of the PA calibration block is shown in Figure 104 above.

- Results

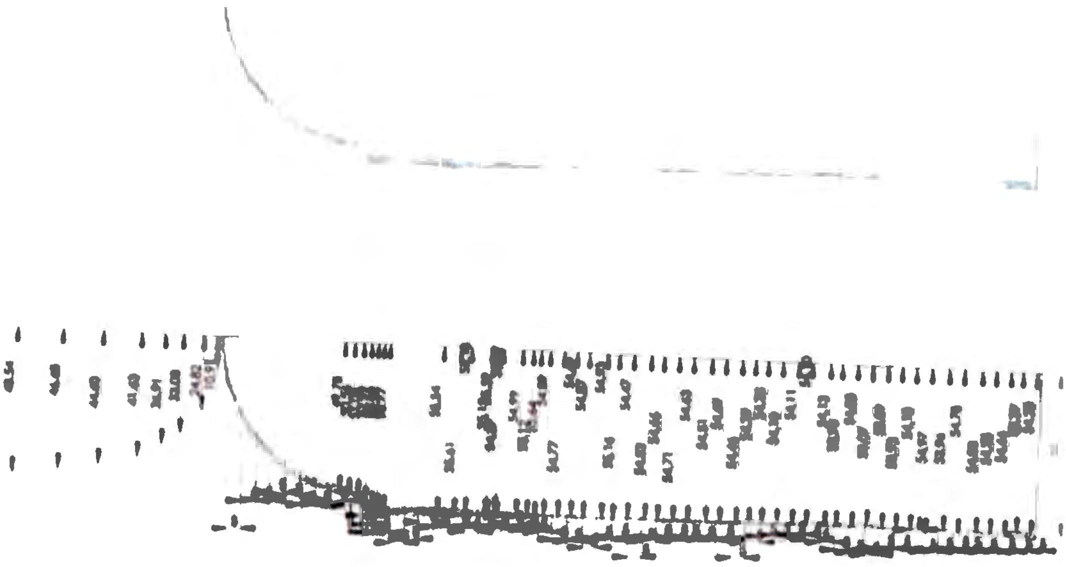

FIGURE 104: THE POINT CLOUD (ABOVE) THE ANALYSIS OF THE DATA (BELOW)

The point cloud data was exported to SolidWorks® where measurements were made as described for the V1 block earlier. The results are presented in Figure 106. The data was then entered into an Excel® spreadsheet and plotted as shown in Figure 106 below.

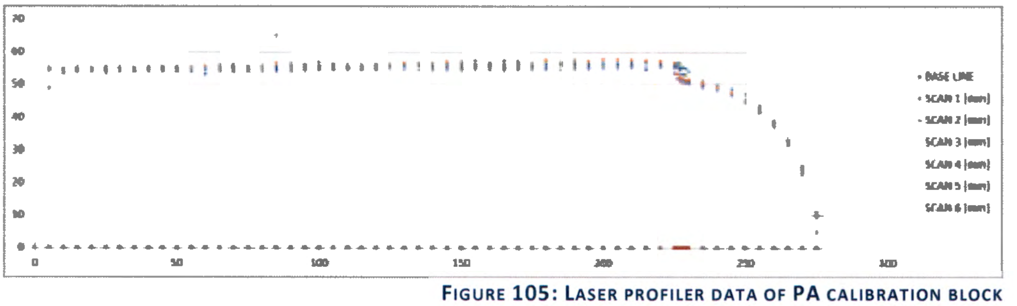

FIGURE 105: LASER PROFILER DATA OF PA CALIBRATION BLOCK

The averaged recorded values were compared with the absolute values known from the calibration certificate of the block (see Appendix 4.3) and absolute error was determined.

The error was calculated as follows:

$$e_{lp,pa-y} = 1.95mm \ \pm 0.73mm \ within \ a \ 95\% \ confidence \ interval$$
$$e_{lp,pa-x} = 0.50mm \ \pm 0.59mm \ within \ a \ 95\% \ confidence \ interval$$

- Remarks

There does not appear to be consistency between the errors that were obtained for the laser profiler measurements of the V1 block and the PA calibration block.

Experiment 6 (b): Sheave Wheel

- Process Photos

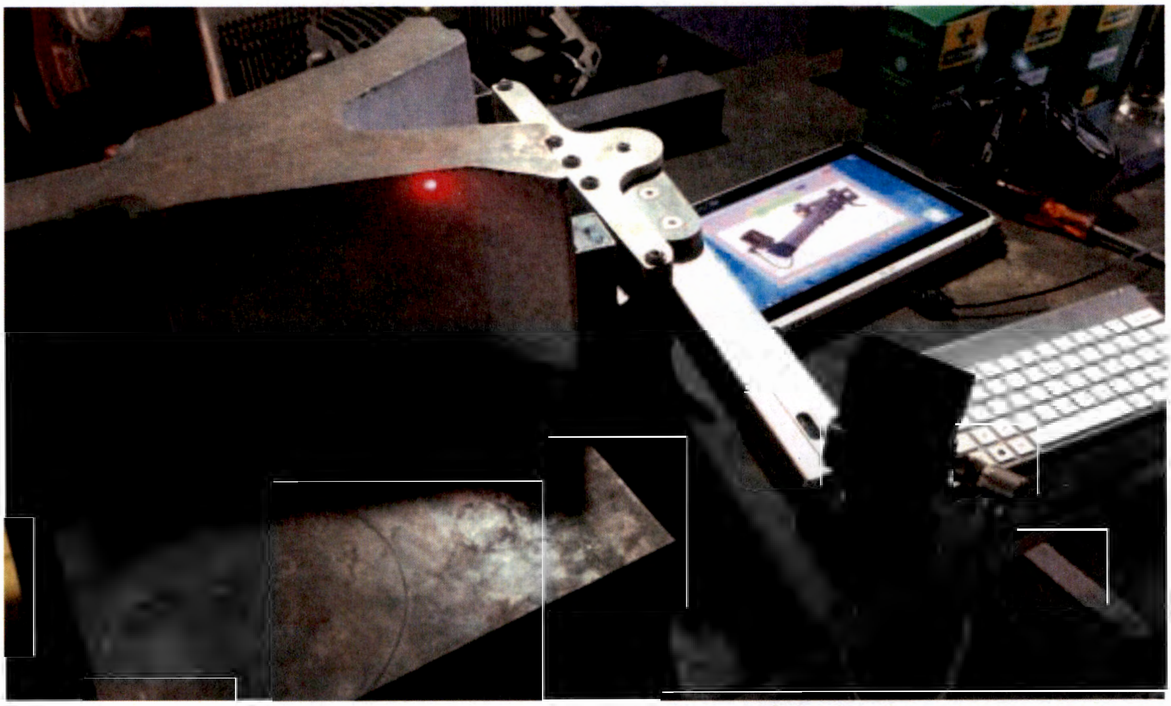

FIGURE 106: LASER PROFILE OF SHEAVE WHEEL SAMPLE

- Results

The relevant data points (as shown in Table 11) were measured directly in the SolidWorks® environment as shown in Figure 108.

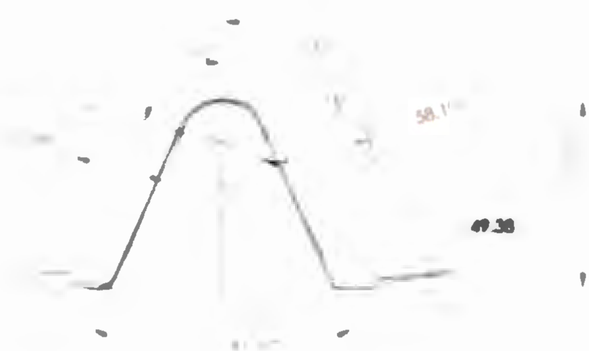

FIGURE 107: POINT CLOUD DATA FOR SHEAVE PROFILE

Table 11 represents the aggregate results from the 6 experiments that were done on the sheave wheel profile with the laser profiler.

TABLE 11: LASER PROFILER SHEAVE SAMPLE RESULTS

Critical Value	Variable	Units	Mean	ST DEV	Result Uncertainty	Experiment Uncertainty k = 2
Fleet Angle	A	°	46.94	0.50	0.21	0.42
Rope Groove	R	mm	51.59	1.07	0.44	0.88
Height of Groove	H	mm	110.90	0.69	0.28	0.56
Web thickness	W1	mm	57.20	1.14	0.47	0.94
Web thickness	W2	mm	55.83	0.63	0.26	0.52

- Remarks

For this experiment the absolute measured values were required. A comparison (and discussion) will therefore only be done during the data reduction stage when the absolute measurements for all the methods can be compared.

7.2.4. Pantograph

Experiment 4 (c): V1 – Calibration block

- Process Photos

The author appears to have neglected to take a photograph of this experiment. The setup was exactly the same (aside from the specimen used) as Experiment 5(c) below where the PA block was profiled using the pantograph.

- Results

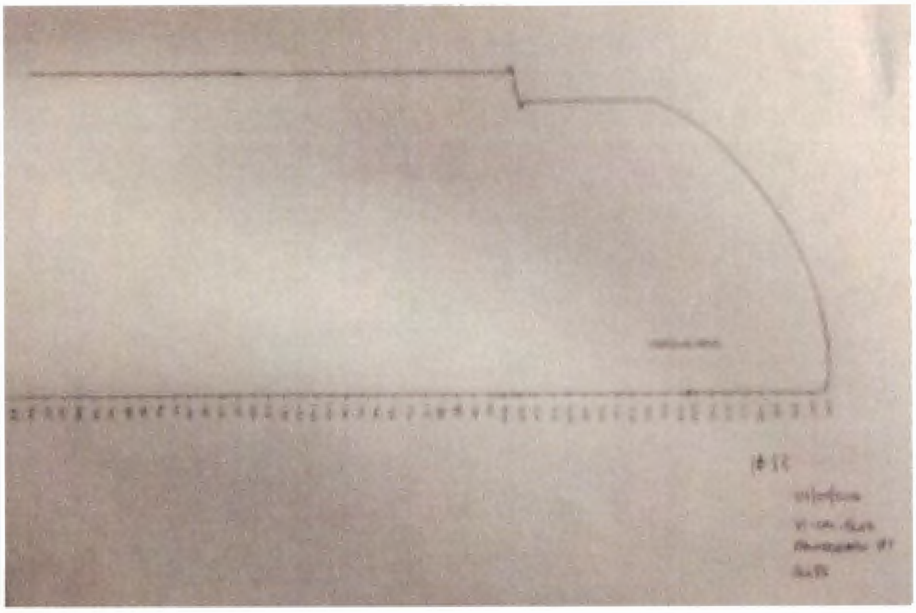

Figure 108: Pantograph experiment with V1 calibration block

The profile of the V1 calibration sample was digitised by measuring the Pantograph results in 5mm increments (to remain consistent with what was done with the plaster cast results). The data was once again entered into an Excel® spreadsheet and plotted. This plot can be seen in Figure 110 below.

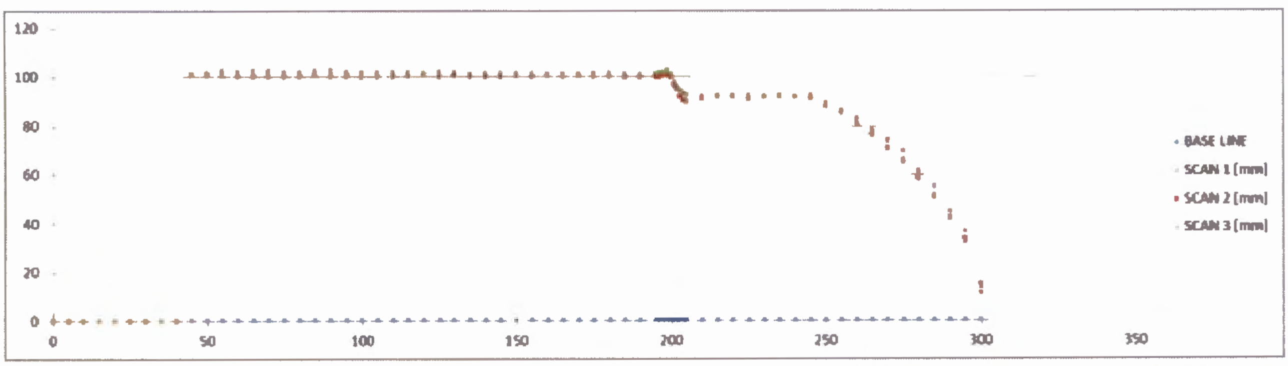

Figure 109: Data from pantograph profiles of V1 calibration block

The averaged recorded values were compared with the absolute values known from the calibration certificate of the block (see Appendix 4.3) and absolute error was determined using the uncertainty analysis in Appendix 2.3.

The error was calculated as follows:

$$e_{pg,v1-y} = 1.83mm \ \pm 0.91 \ mm \ within \ a \ 95\% \ confidence \ interval$$

$$e_{pg,v1-x} = 2.06mm \ \pm 0.86 \ mm \ within \ a \ 95\% \ confidence \ interval$$

- Remarks

Due to the size of the V1 calibration block it was not possible to get the profile of the whole block. This does not pose much of a problem for the depth readings (y-axis) since there are still many of them. It does however mean that the breadth readings (x-axis) could not be determined with a large degree of certainty since there were not many readings that could be used to take this profile.

Another factor that negatively impacted this experiment was that the author only did three experiments with the V1 block (this was due to limited time overlap available with the Pantograph and the V1 block as these are both used in industry on a daily basis). This is not too concerning for the y-axis readings since there are still many samples to get a good statistical interpretation of the quality of the data. It has however detrimentally affected the x-axis results. Therefore, more emphasis will be placed on the results from the PA block for the Pantograph analysis.

Experiment 5 (c): PA Block

- Process Photos

The PA calibration block was profiled using the pantograph. The experimental setup can be seen in Figure 111.

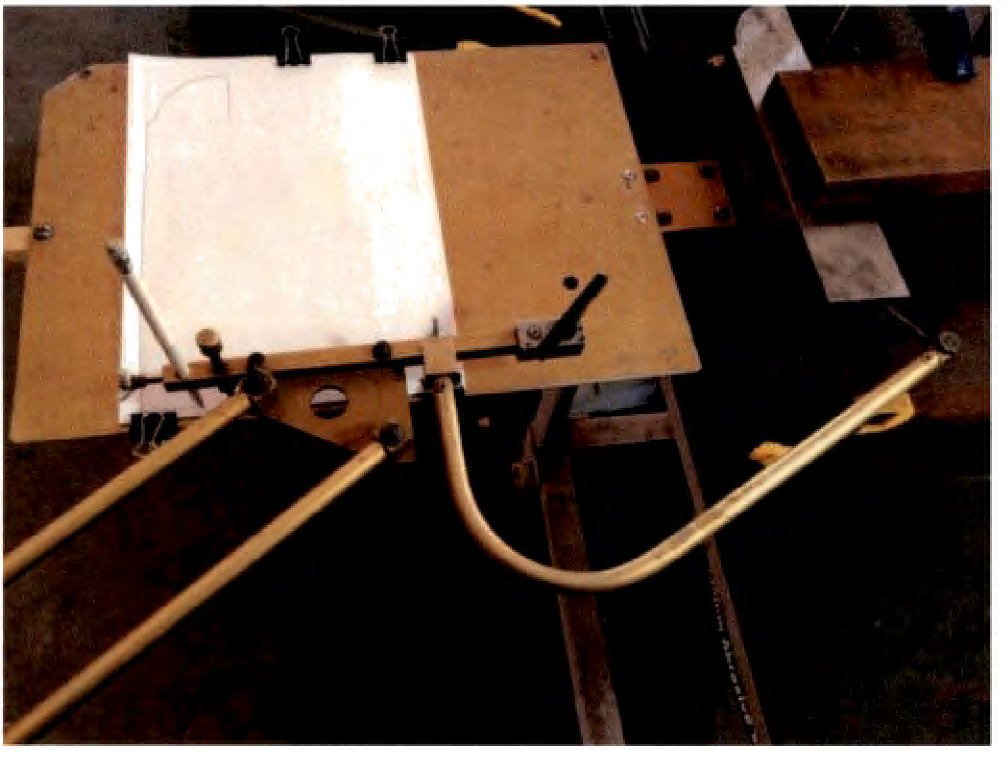

FIGURE 110: PANTOGRAPH PROFILE OF PA CALIBRATION BLOCK

- Results

Figure 112 below shows how the profiles looked and where the increments were made for measurements. These were again measured with a calibrated digital calliper (see certificate in Appendix 4.2).

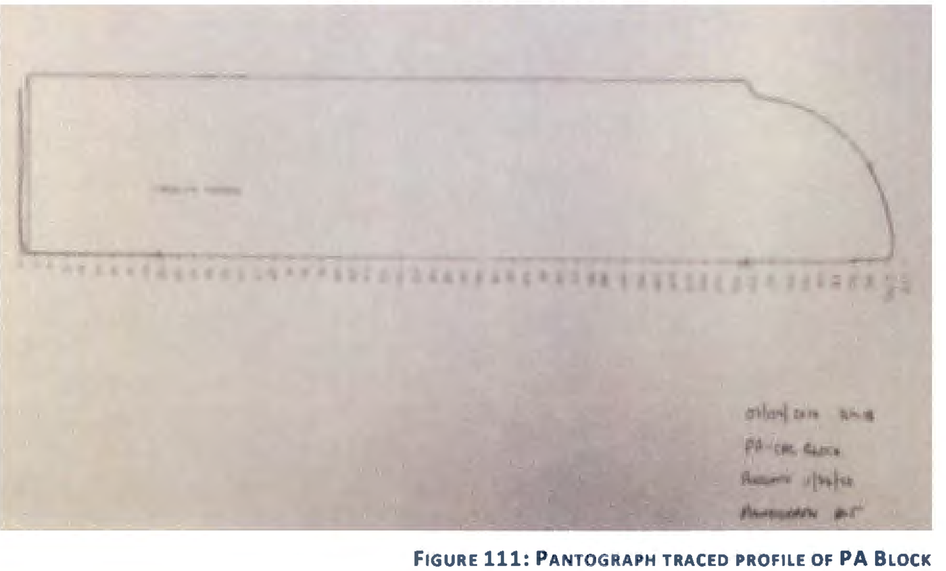

FIGURE 111: PANTOGRAPH TRACED PROFILE OF PA BLOCK

The results were entered into an Excel ® spreadsheet and plotted in Figure 113 below.

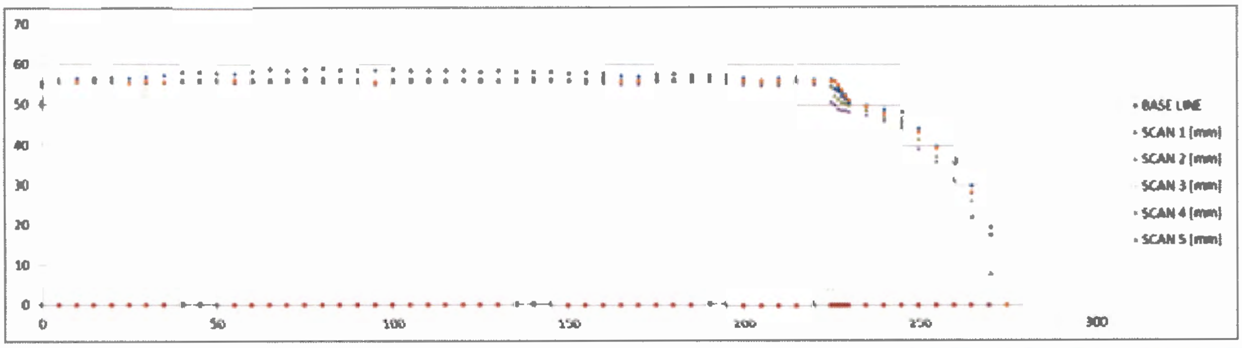

FIGURE 112: PA BLOCK PANTOGRAPH RESULTS

The averaged recorded values were compared with the absolute values known from the calibration certificate of the block (see Appendix 4.3) and absolute error was determined.

The error was calculated as follows:

$$e_{pg,pa-y} = 1.24\, mm\ \pm 1.15\, mm\ within\ a\ 95\%\ confidence\ interval$$

$$e_{pg,pa-x} = 1.93\, mm\ \pm 1.39\, mm\ within\ a\ 95\%\ confidence\ interval$$

- Remarks

There is still a deviation between the error values obtained from the results from the V1 block and those obtained with the PA block.

Experiment 6 (c): Sheave Wheel

- Process Photos

The experimental setup for the sheave wheel profile recording done with a pantograph can be seen in Figure 114 below.

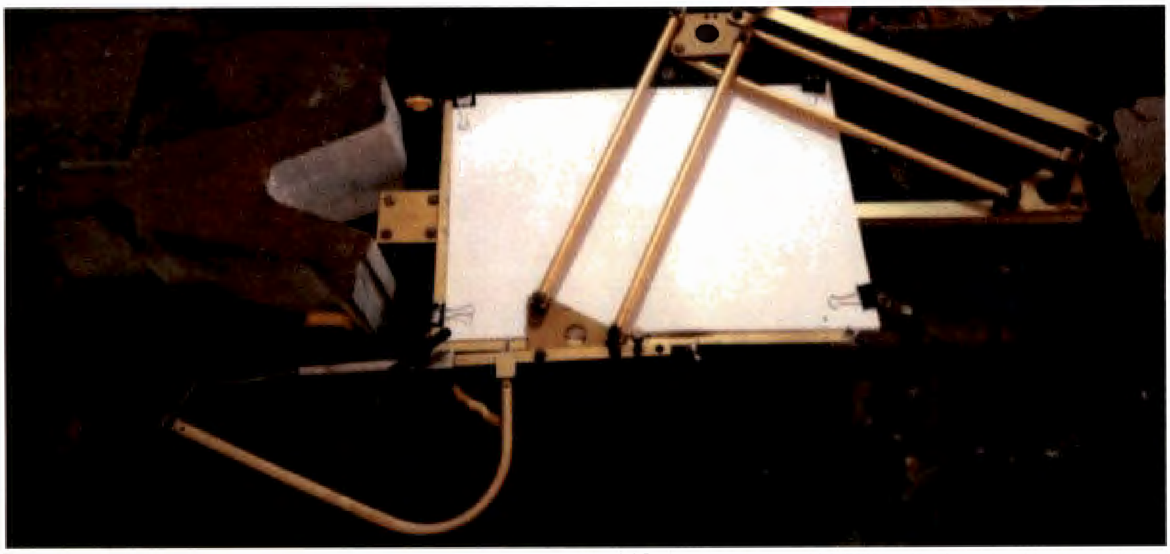

FIGURE 113: PANTOGRAPH USED FOR SHEAVE WHEEL SAMPLE PROFILE

- Results

Figure 115 shows one of the profiles and how the measurements were made on the recorded profile.

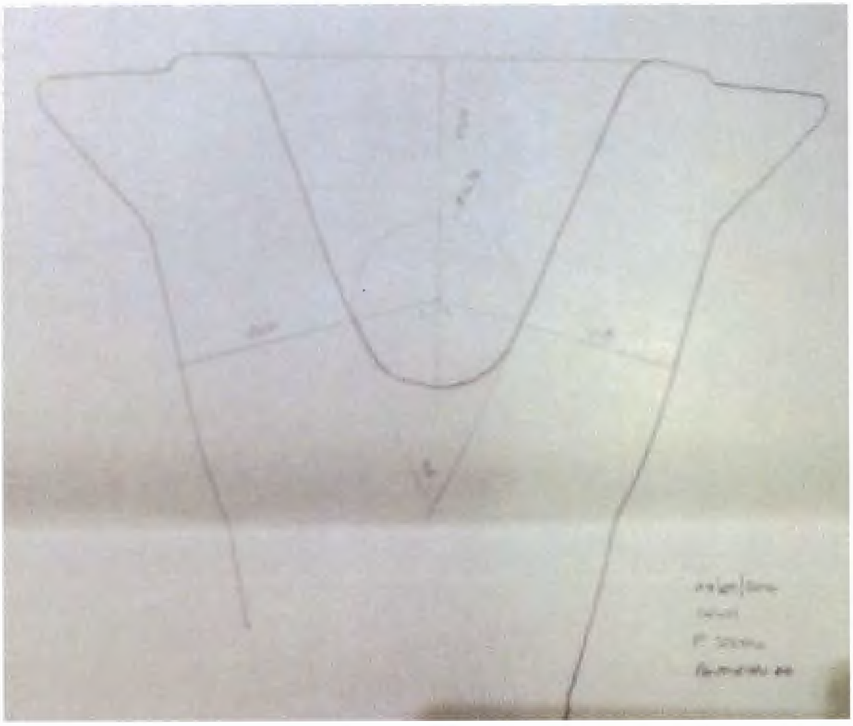

FIGURE 114: PANTOGRAPH TRACED PROFILE OF SHEAVE WHEEL SAMPLE

TABLE 12: PANTOGRAPH SHEAVE PROFILE RESULTS

Critical Value	Variable	Units	Mean	ST DEV	Result Uncertainty	Experiment Uncertainty k = 2
Fleet Angle	A	°	45.17	0.69	0.28	0.80
Rope Groove	R	mm	54.33	2.87	1.17	2.41
Height of Groove	H	mm	110.80	0.45	0.18	0.68
Web thickness	W1	mm	57.70	1.18	0.48	1.12
Web thickness	W2	mm	51.75	1.29	0.53	1.21

- Remarks

For this experiment the absolute measured values were required. A comparison (and discussion) will therefore only be done during the data reduction stage when the absolute measurements for all the methods can be compared.

7.2.5. EXPERIMENT 7: MASS OF PROFILER

The mass of the α-prototype profiler was determined by using a conventional home bathroom scale.

FIGURE 115: THE SCALE USED IN THE MASS MEASUREMENT EXPERIMENT

The experimental setup consisted of placing the profiler on a bathroom scale and recording the results. The experiment was repeated 10 times to be able to make suitable comments on the uncertainty and dispersion characteristics. The results are not very long and thus full results are presented here:

TABLE 13: RESULTS FROM MASS MEASUREMENT EXPERIMENT

Experiment No.	1	2	3	4	5	6	7	8	9	10	Mean	Standard Deviation
Mass [kg]	3.3	3.3	3.4	3.3	3.3	3.3	3.3	3.4	3.4	3.3	3.33	0.046

Based on the uncertainty of the data (as calculated in Appendix 2), it can be stated that the profiler has a mass of:

$$3.3 \text{ kg } \pm 0.2 \text{ kg within a 95\% confidence interval}$$

Referring back to the design mass of 3.47 kg, it will be seen that the actual mass of the profiler (within the confidence interval) correlates well with the design mass. Even the upper limit of the error margin for the mass is within the allowable mass. The profiler is therefore within the mass requirement given in the specifications with the mass having been verified and validated.

7.2.6. Experiment 8: Time to take profile

The experiment was conducted by setting up the α-prototype profiler on the sheave wheel sample, collecting the data to take a profile and then removing the profiler. It may be thought that the post-processing should be included in the analysis, but since this part does not form part of the work that needs to be done with the profiler still on the sheave wheel, it will not be included in the time it takes to record a sheave wheel profile.

The stopwatch that was used for the experiment is the standard stopwatch application that is supplied with an iPhone® 5s.

Table 14: Results from time measurement experiment

Experiment No.	1	2	3	4	5	6	7	8	9	10	Mean	Standard Deviation
Time [s]	40.76	46.95	42.02	39.08	51.28	42.60	31.16	42.02	38.72	49.12	42.37	5.46

Based on the uncertainty of the data (as calculated in Appendix 2), it can be stated that collecting the data for one sheave profile takes:

$$42.37\text{s} \pm 4.46\text{s within a 95\% confidence interval}$$

The initial specifications were for the profile to be taken in under 5 minutes. Therefore, the profiler meets the specifications comfortably.

7.3. DATA REDUCTION AND DISCUSSION OF RESULTS

"I don't even see the code anymore, all I see is blonde, brunette, redhead..."

Cypher – The Matrix

7.3.1. INTRODUCTION

Looking at a myriad of graphs and calculations can tend to distract one so much that they forget the aim of the experiments. There is an analogy about looking at a forest: you can either see the forest or the trees, but not both at the same time. In the results section, we have looked at the trees (zoomed in to detail). We will now attempt to place this into context in order to answer the questions initially set out to answer.

7.3.2. V1 BLOCK RESULT DISCUSSION:

Figure 117 and 118 represent the ordered, averaged measurement errors that were calculated from the raw data for each profiling method. These results will be further reduced by simply scoring the methods from best to worst.

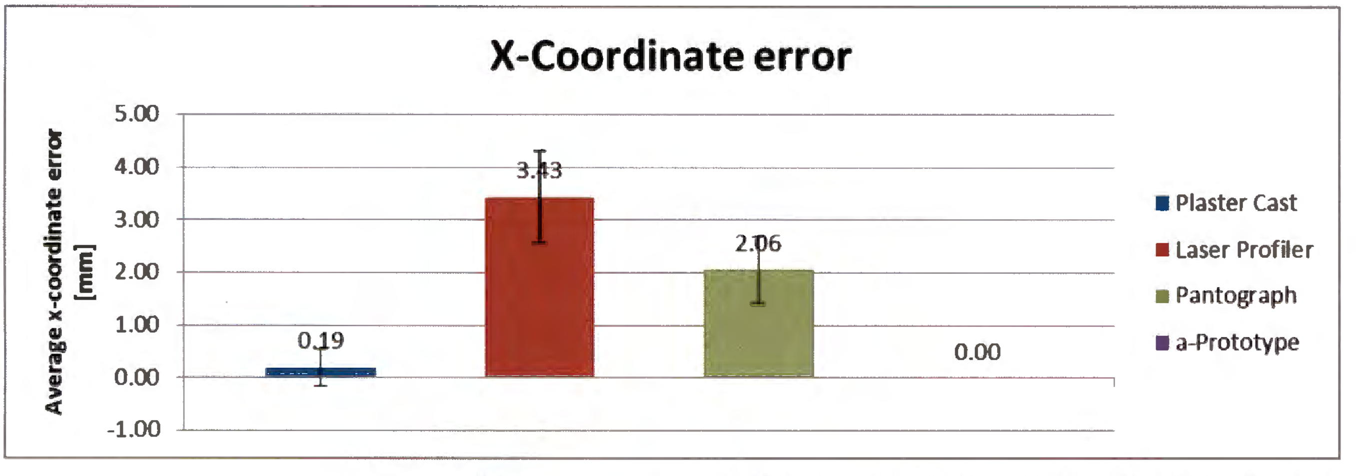

FIGURE 117: X-COORDINATE ERROR FOR MEASUREMENTS DONE ON THE V1 CALIBRATION SAMPLE

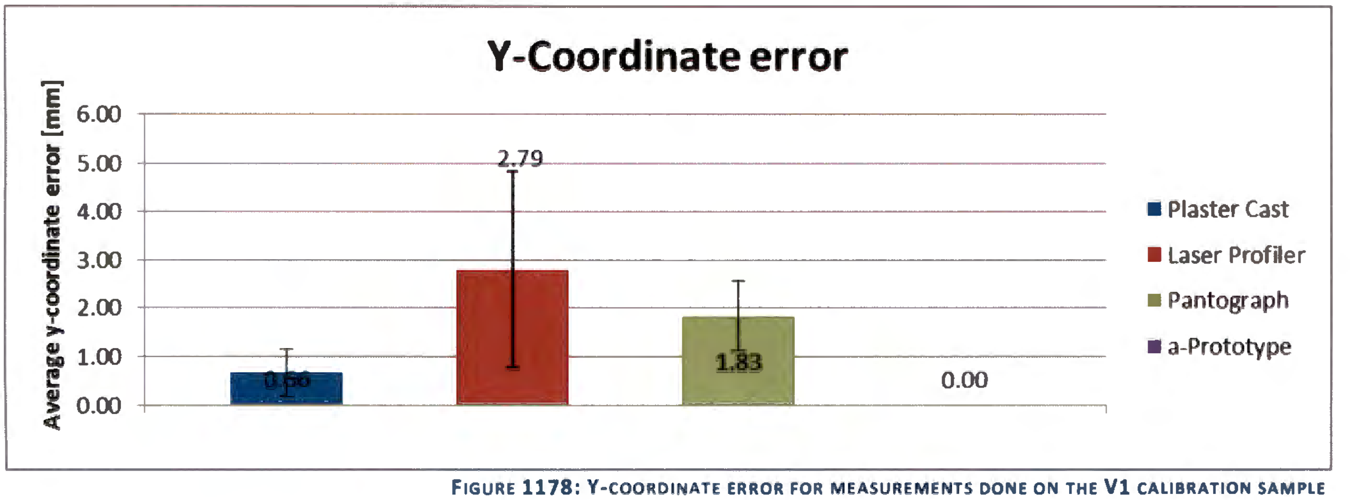

FIGURE 1178: Y-COORDINATE ERROR FOR MEASUREMENTS DONE ON THE V1 CALIBRATION SAMPLE

A test results matrix was developed as a means to compare the respective methods. This matrix evolves as other experiments and their results are added to it and shall serve as the critical evaluation of the methods.

Table 15: Test result matrix - V1 calibration block

Test results matrix				
	Plaster Cast	Laser Profiler	Pantograph	α-Prototype
x-coordinate	1	3	2	n/a
y-coordinate	1	3	2	n/a
Ultimate score[7]	2	6	4	n/a

7.3.3. PA calibration block result discussion:

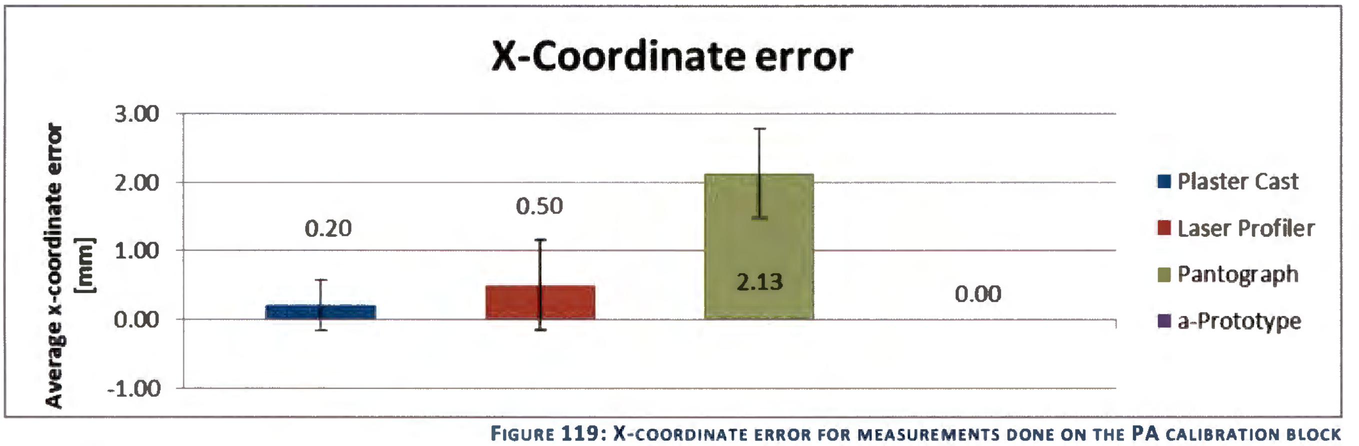

Figure 119: X-coordinate error for measurements done on the PA calibration block

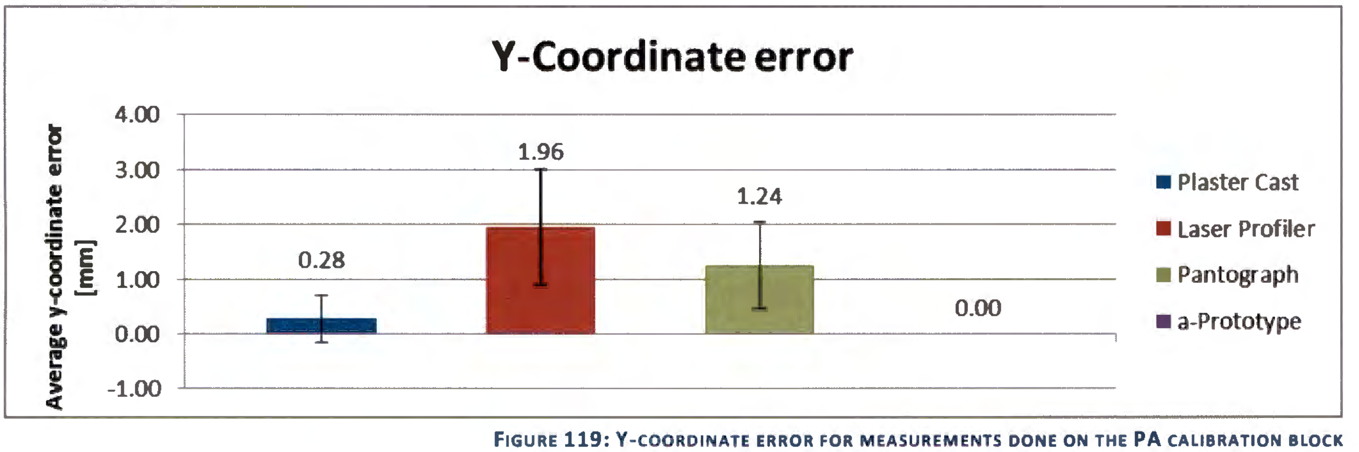

Figure 119: Y-coordinate error for measurements done on the PA calibration block

[7] The ultimate score assumes that the x- and y-coordinate error values carry equal weight and that the lowest ultimate score wins.

The updated test results matrix can be seen in table 16 below.

TABLE 16: TEST RESULT MATRIX - V1 + PA BLOCK

Test results matrix	Plaster Cast	Laser Profiler	Pantograph	α-Prototype
x - coordinate – V1	1	3	2	n/a
y - coordinate – V1	1	3	2	n/a
x - coordinate – PA	1	2	3	n/a
y – coordinate – PA	1	3	2	n/a
Ultimate score	4	11	9	n/a

7.3.4. SHEAVE WHEEL SAMPLE RESULT DISCUSSION:

In this experiment, the actual size of the sample did not really matter (since it is not known). The important aspects of this experiment are the ability of a profiler to record the profile of a sheave wheel (fit-for-purpose) and the repeatability of the data of each profile. The variance in the measurements shall serve as an indication of the repeatability of the various instruments/methods. Figure 122 and Figure 123 show the combined results of the Fleet Angle and the Height of the sheave wheel groove.

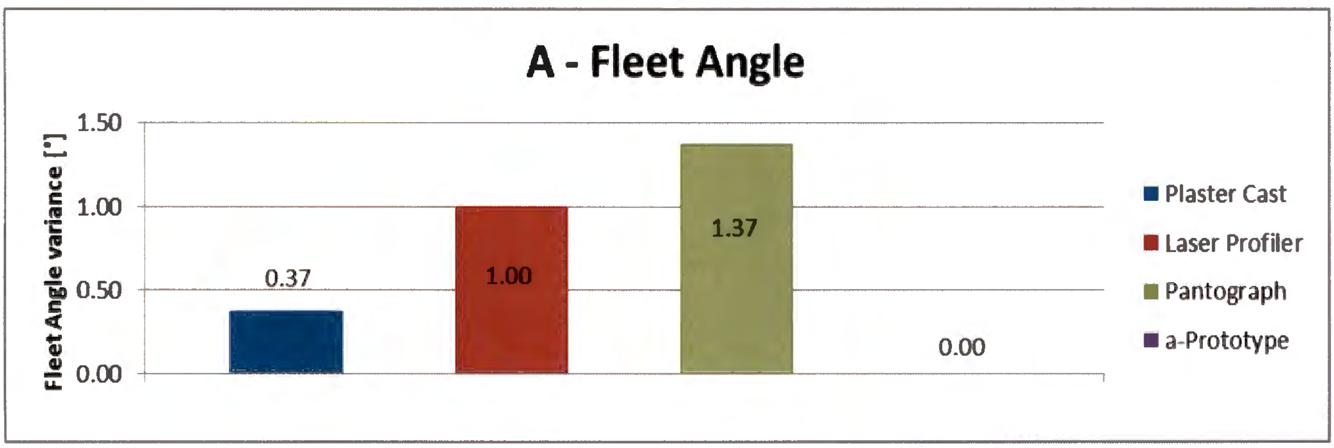

FIGURE 1211: FLEET ANGLE VARIANCE MEASUREMENT

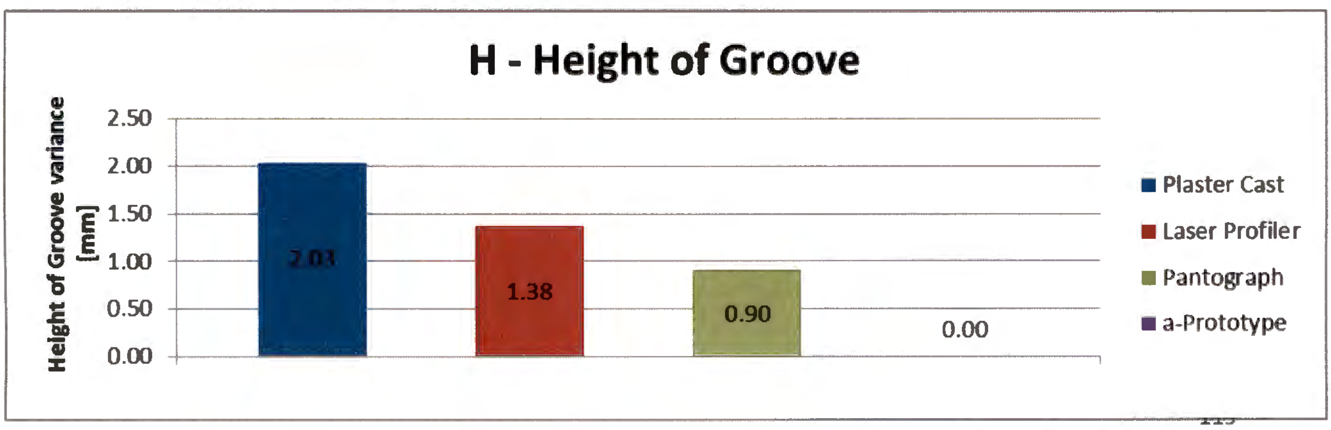

FIGURE 1202: HEIGHT OF GROOVE VARIANCE MEASUREMENT

Figure 124 shows the variability of the measurements when the profilers measured the rope groove radius.

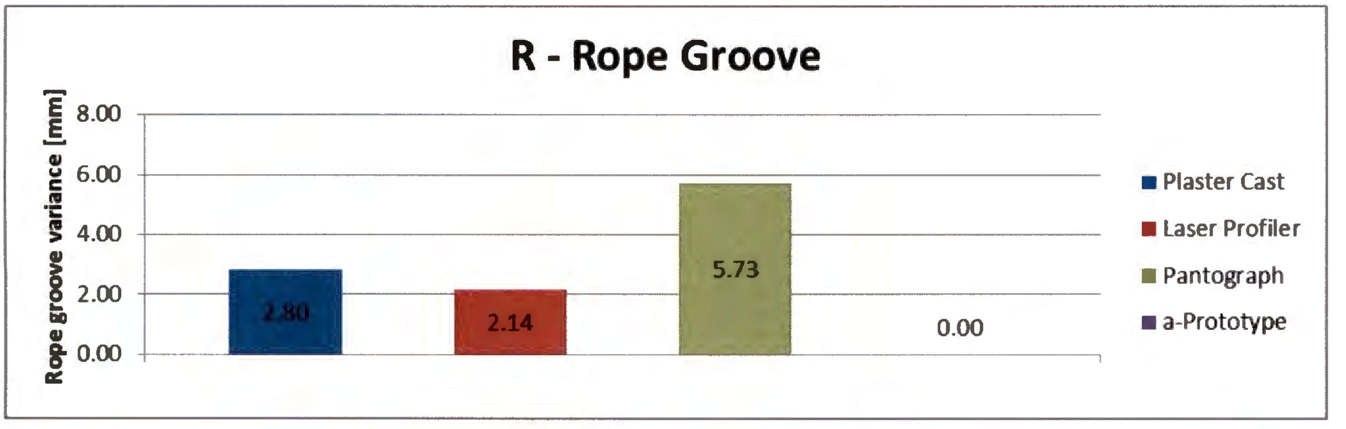

FIGURE 122: ROPE GROOVE RADIUS VARIANCE MEASUREMENT

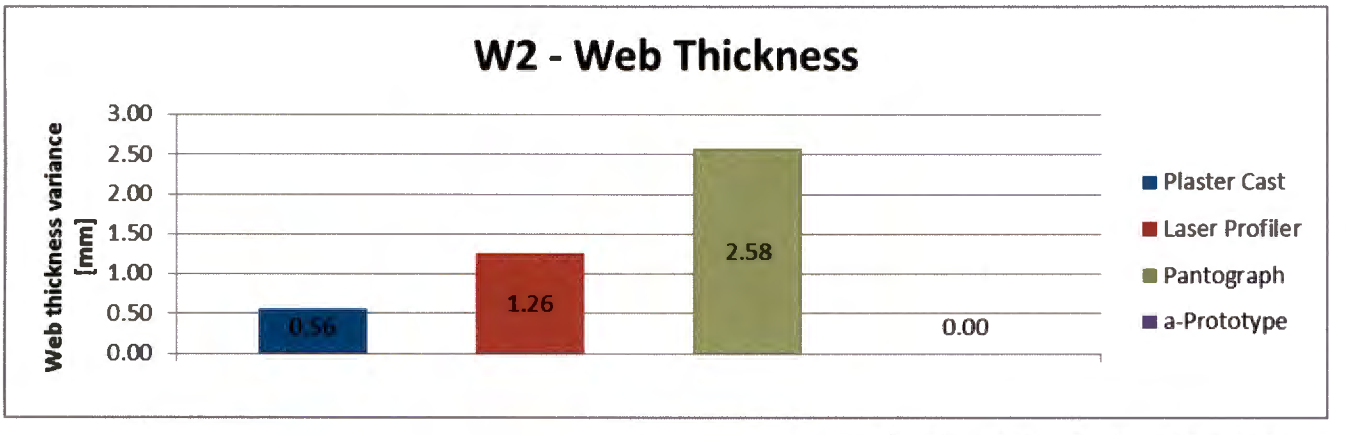

FIGURE 1244: THE WEB THICKNESS VARIANCE IN RESULTS

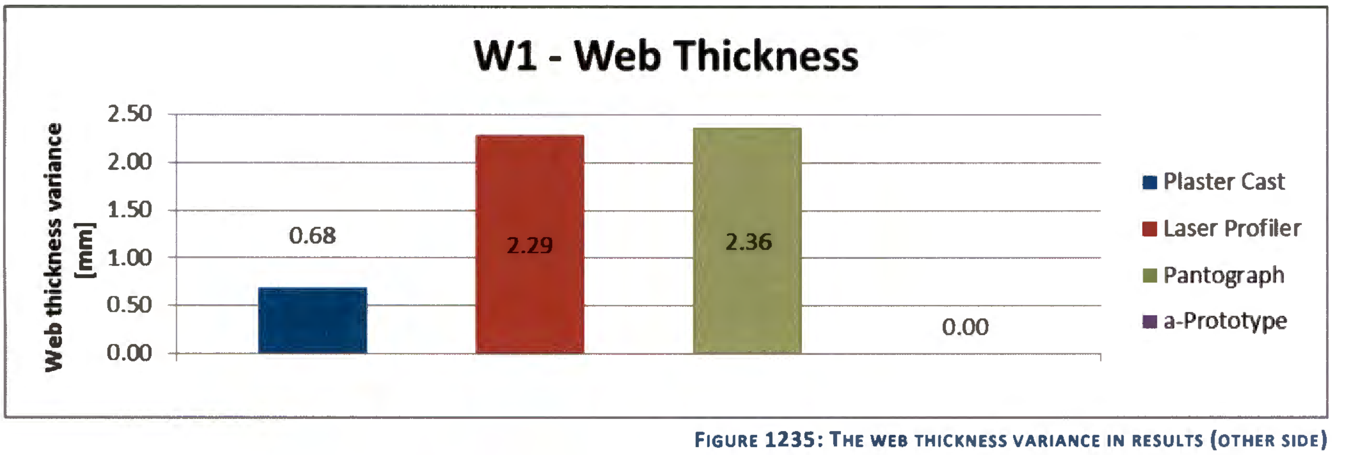

FIGURE 1235: THE WEB THICKNESS VARIANCE IN RESULTS (OTHER SIDE)

Figure 125 and Figure 126 show the variance in the web thickness of either side of the sheave wheel. The results from the five figures above have been added to the test result matrix which can be seen in Table 17.

Table 17: Test result matrix - V1 Block, PA Block and Sheave wheel sample

Test results matrix				
	Plaster Cast	Laser Profiler	Pantograph	α-Prototype
Accuracy of Profiler				
x - coordinate – V1	1	3	2	n/a
y - coordinate – V1	1	3	2	n/a
x - coordinate – PA	1	2	3	n/a
y – coordinate – PA	1	3	2	n/a
Ultimate score	4	11	9	n/a
Repeatability and fit-for-purpose of profiler				
Height of groove [H]	3	2	1	n/a
Fleet angle [A]	1	2	3	n/a
Rope groove [R]	2	1	3	n/a
Web thickness [W1]	1	2	3	n/a
Web thickness [W2]	1	2	3	n/a
Ultimate score	8	9	13	n/a

In the interest of clarity, the test result matrix has now been split up into two data sets. The first has to do with the absolute accuracy of the measurement device/method. The second has to do with the repeatability of the results obtained during the measurements done on the sheave wheel sample. It is necessary to split these two result sets because the different experiments were done in an attempt to answer different questions and by throwing together the last parts of the results, we may be losing valuable data.

7.4. Conclusion

The conclusion was done in what the author believes to be the most logical and simple way: The questions posed during Chapter 6 were repeated and an attempt was made to answer them based on the data presented and reduced in Chapter 7.

How accurate is the α-prototype profiler?

Since the experiments with the V1 calibration block and the PA calibration block using the α-prototype were not successfully executed, it is not possible to make a conclusion in this regard other than the theoretical conclusion made in Chapter 5.

Is the α-prototype profiler able to take the profile of a sheave wheel such that the critical areas can be determined?

Since it was shown that the profiler was able to provide the profile of the sheave wheel rim, it would be possible to extract three of the five critical areas namely:

- Rope groove radius
- Height of groove
- Flare angle

However, due to the insufficient quality of the data, these parameters cannot be extracted accurately or repeatably with the current setup.

If yes, are the results repeatable and to what degree?

With the current set-up of the α-prototype profiler, the results are not repeatable.

How accurate are the methods/profilers that are considered to be the current state of the art?

There was a large degree of inconsistency in the data that was obtained with the various profilers when it came to their respective absolute accuracies. It was noticed, however, that there was a trend between the relative accuracies of the profilers within the experiments. It was therefore decided that a recommendation would be made for further study for a deeper investigation into the absolute accuracy of the various methods.

In the meantime, the author took advantage of the clear trend and introduced the test result matrix which compares the methods to each other for the various experimental setups (as opposed to determining their absolute accuracy). The relative accuracy results are presented in Table 16 which rates the profiling methods as follows:

1. Plaster casts
2. Pantograph
3. Laser profiler

In this case the plaster casts produced the most accurate results and the laser profiler produced the least accurate results.

Are they able to take the profile of a sheave wheel such that the critical areas can be determined?

All three experimental methods that were used to represent the current state-of-the-art were able to yield results such that it was possible to obtain five out of five of the critical areas of the sheave wheel sample.

If yes, are the results repeatable and to what degree?

There was once again significant variability in the actual readings obtained. The test result matrix was once again utilised to get a relative comparison of the repeatability of the results. Something interesting was noted about the pantograph. It appears, from the data, as though the pantograph produced better results with the simple geometry of the calibration samples than it had done for the sheave wheel samples. Based on the results produced in Table 17, for fit-for-purpose and repeatability, the profiling methods are rated as follows:

1. Plaster casts
2. Laser profiler
3. Pantograph

How does the accuracy of the α-prototype profiler compare to the current state of the art?

A comparison could not be done since the α-prototype could not produce sufficient results for an analysis.

How does the α-prototype profiler's ability to repeatably profile sheave wheels compare to the current state of the art's ability?

A comparison could not be done since the α-prototype could not produce sufficient results for an analysis.

An assertion was made in Chapter 2 that, since none of the methods appear to be verified for accuracy, the author is of the opinion that all the methods currently employed in industry provide nothing more than a false sense of security for the responsible person on a mine. However, judging by the results of the experiments performed during this project, the author must modify his opinion to some extent to reflect the new knowledge that has been gained:

If plaster casts were done in the way they were done in the experiments in this document, the results would likely be within the requirement for a ± 1mm accuracy that was determined in Chapter 2. Neither the Laser profiler nor the Pantograph was able to produce results within this parameter within a suitable confidence interval.

Having said that, the method of taking plaster casts as performed in this document appeared to be inefficient since the set time for the plaster of paris was several hours. This is not practical unless the results are determined in a laboratory or on a sheave wheel that is not in service while the profiles are recorded. Using this method was messy and the application of the plaster of paris was time consuming.

The author concludes that although sheave profiling using plaster casts might be able to meet the accuracy requirements, the method is still not practical due to the long set time and the difficult set-up. It further does not lend itself to trending and wear rate prediction as hoped from a sheave profiling method.

CHAPTER 8: CONCLUSION AND FUTURE WORK

"It is important to always try to reason from first principles, rather than by analogy."

Elon Musk

8.1. INTRODUCTION

This chapter marks the culmination of all the other chapters. It is perhaps a good starting point to compare the inputs and goals of the project with the outcomes in an attempt to determine to what extent the author has achieved the goal as set out. It is then necessary to derive the relevant conclusions and apply the lessons learnt during the execution of the project and turn them into an actionable set of recommendations for further study. Figure 126 represents the comparison between the designed profiler and the manufactured profiler. Further consolidation of the work done follows below:

FIGURE 125: THE PROFILER THAT WAS DEVELOPED (LEFT) AND THE PROFILER THAT WAS DESIGNED (RIGHT)

8.2. CONSOLIDATION OF THE WORK DONE

There are five considerations that form the foundation of the argument the author has been trying to make with this document. They are summarised below:

1. **Sheave wheels are important for safety and economic reasons.**

In Chapter 2 the author investigated the field of sheave wheels and looked at the wear that occurs in sheave wheels. He considered the effect that a worn sheave wheel would have on a rope and discussed the implications of rope or sheave wheel failure (economic and safety).

2. **Many of the failures and much of the rope damage that occurs can be avoided by taking sheave wheel profiles regularly.**

This concept was investigated and discussed in Chapter 2. It was mentioned that although the legislation and recommendation only requires that sheave wheel profiles are recorded bi-annually (and quarterly for other parts of the wheel), it was noticed that wear in a rope can take place much quicker than the suggested interval. It therefore becomes necessary to decrease the size of the inspection interval, but due to the laborious nature of sheave wheel profiling (as determined in Chapter 2), the benefit of taking regular sheave wheel profiles does not yet justify the costs (in terms of downtime and labour).

3. **Sheave wheel profiles are being taken, but the methods are not of sufficient quality to draw useful conclusions about the condition of the sheave wheel or the rope.**

Chapter 2 further proposed that it might be necessary to perform experiments on the profilers that are considered the current state-of-the-art and validate their accuracy since this has not been done formally (not even by the manufacturers of the instruments). In Chapter 6, a set of experiments was designed in order to validate the profilers while the results were presented in Chapter 7.

4. **It is both possible and necessary to take sheave wheel profiles in digital format.**

Chapter 2 extolled the benefits of recording sheave wheel profiles in digital format (for trending and easy archiving) while Chapter 3 explored different methods by which digitisation of the data could be achieved.

5. **If a profiler is developed, as was attempted in this document, it would be able to record sheave wheel profiles to the standard that would be of sufficient quality to make comments regarding the condition of the sheave wheel.**

In Chapter 4, the author attempted to develop a profiler as was envisioned in Chapter 2 by using the added knowledge about digitisation that was gained in Chapter 3. In Chapter 5 the author attempted to theoretically prove point number 5 above. In Chapter 6 and 7 the author attempted to practically prove the statement made in point number 5 above. Although the experiments did not go as planned, the concept still remains valid and it would still be fair to make the point as above. The recommendations on how to adjust the experimental setup so as to improve the likelihood of a positive result have been added to the section on recommendations for further study.

Figure 128 is a summary of the work done during this project.

Figure 126: Consolidation of the work done

8.3. Validation in terms of objectives

Table 18 below summarises the verification and validation exercises that were done on the sheave wheel profiler.

Table 18: Verification and validation summary

User/ Design Requirement	Required Value	Verification	YES/ NO	Validation	YES/ NO
Operation	One man operation	5.1	Yes	n/a	
Mounting	Sturdy	5.2	Yes	n/a	
Mounting	Flexible for different size wheels	5.3	Yes	n/a	
Mounting	Quick attach and quick release	5.4	Yes	n/a	
Data collection and storage	Digital	5.5	Yes	n/a	
Power supply	Self-supplied	5.6	Yes	n/a	
Mass	<5 kg	5.7	Yes	Experiment 7	YES
Scan Time	< 5 minutes	5.8	Yes	Experiment 8	YES
Accuracy	± 1 mm	5.9	No	Experiment 1 Experiment 2	NO

Further validation in terms of the objectives of the study is included in Table 19 below:

Table 19: Validation in terms of objectives

Clarify the problem of what exactly needs to be scanned and the implications of such a scan using available literature and a survey of the people performing the scans.	Chapter 2 + Survey results in Appendix 3
Investigate the theory behind possible solutions to check for feasibility	Chapter 2
Use the information acquired in (1-2) to develop a clear set of design specifications.	Chapter 4
Use the design specifications to design and manufacture a prototype sheave wheel profiler.	Chapter 4
Verify that the designed profiler would be able to meet the design specifications (in theory).	Chapter 5
Validate that the manufactured profiler is able to meet the design specifications (in practice).	Chapter 6 and Chapter 7
Compare the scan data from the sample to other scans from other methods.	Chapter 7 – Experiment 2 and 4

8.4. Other fields of application

If the problem stated as the objective of this project were deconstructed to its most fundamental building blocks, several new applications become apparent. The new proposed objective may read:

"To develop a method of digitally measuring the profile of ***any surface subjected to wear*** *and to verify and validate the accuracy of this method while critically evaluating it against the current state of the art."*

If the mind is allowed to wander for a moment, thinking about all the different surfaces subjected to wear, the list would be extensive. Some of these possibilities include:

- **Winder Drum rope groove profiling**

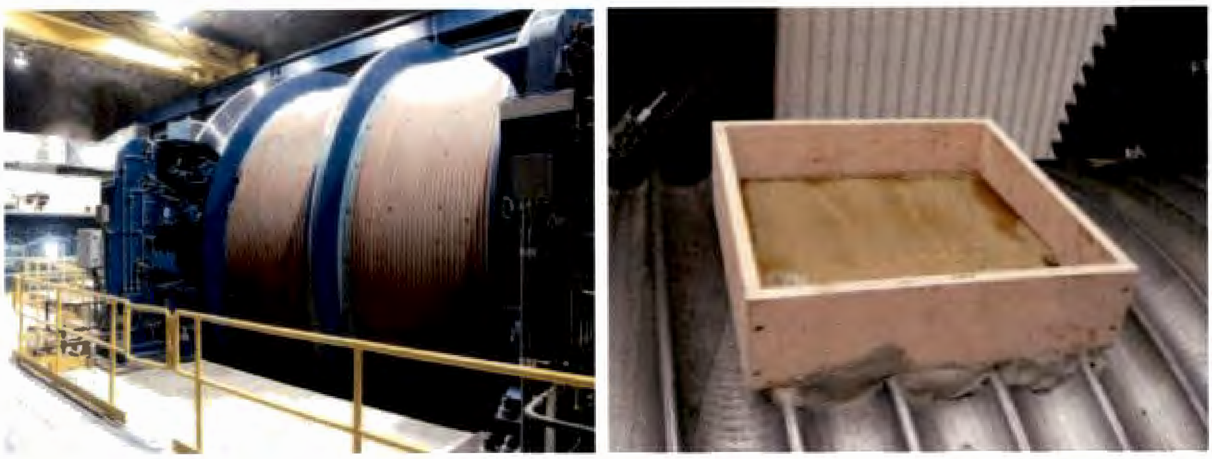

FIGURE 127: WINDER DRUM ROPE GROOVES

As mentioned in Chapter 2, the rope that passes over the sheave is driven by the winder. The winder consists of an electric motor, rigidly connected to a large drum onto which the rope is wound as the conveyance is lifted from the mine shaft. A similar method is used to lift the scoop of a dragline. The drum is profiled with several shallow rope grooves. These help to control the rope as it is wound back onto the drum. When they are worn out, the rope rolls up uncontrollably, causing unpredictable stresses as the rope rolls over itself. The image on the right shows that current state of the art (courtesy of Roland Verreet). Castings are made of the rope grooves. These are then drawn onto paper for reference and trending. This method is limited in that (aside from the limitations of plaster casts mentioned earlier) it does not allow for an easy sampling of all the rope grooves. This is significant because the entire drum does not wear at the same rate.

It would be feasible to use the technology developed in this dissertation to take profiles of all the rope grooves on the hoist drum, by reconfiguring the cameras and lights slightly.

- **Gear tooth profiling**

During normal operation, gears will wear out. This needs to be monitored fairly closely since a worn gear (or pinion) will cause vibration in the system, and possibly damage the gear it is mated to.

FIGURE 128: GIRTH GEAR

When a gear is misaligned or experiences a shock load, it may also be damaged and fatigue cracks could grow to a point where large sections or even entire teeth chip out. It should be possible to take 2D measurements at a few points on a gear to make a quick estimate of the condition of the gear.

FIGURE 129: BROKEN OUT SECTION OF GEAR

- **Corrosion Measurement on flat or rounded surfaces**

In theory, if it is known that a pipe or vessel did not corrode on the inside, and the original wall thickness is known, it would be possible to use the outside wall profile to determine the amount of wall thickness left over. This becomes very important since it is sometimes allowable for an engineer to extend the design life of pipes and pressure vessels if their physical condition can be proven to be within specific limits.

FIGURE 130: CORRODED PIPE

FIGURE 131: CORRODED PRESSURE VESSEL

FIGURE 132: TRAIN WHEEL

- **Train wheel profiles**

In conclusion the author is of the opinion that any surface that is subjected to wear (whether mechanical or chemical), that needs to have its condition inspected (whether to ensure that the profile is correct or to check for wall thickness) and possibly trended would benefit from applying the technology developed in this document. This statement warrants further investigation to be validated.

8.5. ASPECTS OF THE DESIGN MERITING FURTHER INVESTIGATION

Prototype Profiler:

8.5.1. The light source could be improved (for sunlight) by moving to infrared wavelength.

8.5.2. The algorithm could be significantly improved as far as speed and accuracy is concerned. It can also be updated.

8.5.3. A better camera with a larger CCD/CMOS sensor would result in better accuracy.

8.5.4. If a lens with a smaller field of view (telephoto) could be used, a larger percentage of the sensor could be used for acquisition of the profile, resulting in a more precise instrument. If the model that was developed in this document were used in reverse, one could decide on the required accuracy of the profiler and specify the lens and sensor combination that would give the desired result.

8.5.5. Future researchers in this area should not take published CCD resolution values for granted. It is recommended that any further experiments done in this arena should be prefaced with an in-depth photogrammetric analysis and calibration of the camera(s).

Experiments with other profilers

8.5.6. Techniques like the Laser Profiler, Pantograph, and Plaster Casts are dependent on user opinion of where a coordinate is located and thus a study could be done with different users scanning the same sample and giving results. This should give a better idea of the repeatability based on users. In this case, we have kept the users constant while varying the method only.

8.5.7. The sample that is used to determine the absolute accuracy of the profiler/method should be more rigorously planned. It was noticed that there was no correlation between the accuracy obtained while profiling the samples that were specified and the sheave wheel sample. This leads the author to believe that the samples used to determine the accuracy may not have been a true representation of the accuracy of measurements when looking at actual sheave wheels.

Further research to be done:

8.5.8. Once a profiler has been developed that is able to record sheave wheel profiles to within 1mm and with a 95% confidence interval, it is thought that a study should be conducted where case studies are done on actual sheave wheels and their wear rates are determined. From this, an estimate could be made and a prediction equation may be developed. This would allow the owner of the sheave wheel to simply plug in the required values and have advance warning of impending rope or sheave failure.

CHAPTER 9: REFERENCES

Barbero, B. R., & Ureta, E. S. (2010). Comparative study of different digitization techniques and their accuracy. *Computer-Aided Design*, 188-206.

Bell, S. (2001). *A Beginner's Guide to Uncertainty of Measurement.* Teddington: National Physical Laboratory.

Bridon Mining. (2011, 08). *Mining Rope Catalogue - Metric Edition.* Retrieved September 12, 2012, from http://www.bridon.com/x/downloads/undergroundmining/metric/MiningBrochure_Metric.pdf

BSi. (1999). *BS EN 12223:2000 Non-destructive testing - Ultrasonic Examination - Specification for block No. 1.* Brussels: European Committee for Standardisation.

Chamber of Mines of South Africa. (2012). *Facts and Figures 2012.* Johannesburg: Chamber of Mines of South Africa.

Chen, T., Shang, J., & Wei, L. (2011). Test method on Precision of the 3D Laser Scanner. *IEEE 3rd International Conference on Communication Software and Networks (ICCSN)* (pp. 417-420). Xi'an: IEEE.

Delorme, G. (2002). *The Effects of a Tight Groove in a Headsheave.* Retrieved 09 10, 2012, from Haggie Hints - Issue 4: http://www.camiro.org/Haggie_Hints/Issue%20_4%20The%20Effects%20of%20a%20Tight%20Groove%20in%20a%20Headsheave.pdf

Elmas, S., Islam, N., Jackson, M. R., & Parkin, R. M. (2011). Analysis of profile measurement techniques employed to surfaces planed. *Measurement*, 365–377.

Els, C. (2012, 09 04). Senior Machinery Inspector - Anglo Technical Solutions [0833088426]. (P. Steyn, Interviewer)

Fan, K. -C., Lee, M. -Z., & Mou, J. -I. (2002). On-Line Non-Contact System for Grinding Wheel Wear Measurement. *The International Journal of Advanced Manufacturing Technology*, 19: 14-22.

Faugeras, O. (1993). *Three-dimensional Computer Vision: A Geometric Viewpoint* (1st ed.). Cambridge, Mass.: MIT Press.

Gao, J., Chen, X., Zheng, D., Yilmaz, O., & Gindy, N. (2006). Adaptive restoration of complex geometry parts through reverse engineering application. *Advances in Engineering Software*, 592-599.

Goncalves, J. K. (2009). Sheave Wheels: Critical components for effective mining operations. In R. B. Media, *Engineers Technical Handbook* (pp. 229-233). Melville: Red Bird Media.

Gonzalez, R. C., & Woods, R. E. (2008). *Digital Image Processing.* New Jersey: Pearson Education, Inc.

Herniter, M. E. (2001). *Programming in Matlab(R).* Pacific Grove: Brooks/Cole Thomson Learning.

ISO 4308-1. (2003). *Cranes and lifting appliances - selection of wire ropes.* Geneva: International Standards Orginisation.

ITU-R. (2002). *Recommendation ITU-R BT.709-5.* Geneva: International Telecommunication Union.

Kotz, J. C., & Treichel, P. M. (2003). *Chemistry and Chemical Reactivity, 5 Ed.* London: Thomson Learning.

Microscribe. (2014). *MX G2 Intro*. Retrieved June 01, 2014, from MicroScribe and HDI 3-D Digitizers: http://www.3d-microscribe.com/MSG2_0704_V1.pdf

Mining-Technology. (2014). *South Deep Gold Mine, South Africa*. Retrieved 06 01, 2014, from Mining-Technology: http://www.mining-technology.com/projects/-south-deep-gold-mine-south-africa/-south-deep-gold-mine-south-africa4.html

Muralikrishnan, B., Ren, W., Everett, D., Stanfield, E., & Doiron, T. (2011). Performance evaluation experiments on a laser spot triangulation probe. *Measurement* , 333-343.

Russel, S., & Norvig, P. (2010). *Artificial Intelligence - A Modern Approach, 3rd ed.* Upper Saddle River: Prentice Hall.

SANS 10294. (2000). *The performance, operation, testing and maintenance of drum winders relating to rope safety.* Pretoria: The South African Bureau of Standards.

SCAW Metals Group. (2006). *Haggie Steel Wire Ropes for Mining - Technical Training Manual.* ???: ???

SCAW Metals Group. (2010). Installation and Maintenance of Winder Ropes. In R. B. Media, *Engineers Technical Handbook* (pp. 409-416). Johannesburg: Red Bird Media.

Stirk, A. (2012, 09 27). Dragline General Engineering Superintendent - Anglo Coal Regional Engineering Services [0832314191]. (P. Steyn, Interviewer)

Taylor, B. N., & Kuyatt, C. E. (1994). *Guidelines for Evaluating and Expressingthe Uncertainty of NIST Measurement Results.* Washington: NIST.

Ultich, K. T., & Eppinger, S. D. (2008). *Product Design and Development.* Boston: McGraw Hill.

van der Walt, G. (2014, 03 15). Limitations of Condition Monitoring. (P. Steyn, Interviewer)

van der Walt, G. (2014, 05 07). Plaster Cast Procedures. (P. Steyn, Interviewer)

Verreet, R. (2011). What we can learn from wire rope failures: Predictable and unpredictable failures. *OIPEEC Conference Proceedings: Safe Use of Ropes.* College Station: OIPEEC, 2011.

Wire Rope Technical Board. (1993). *Wire Rope Users Manual, 3rd edition.* Woodstock: Wire Rope Technical Board.

Wirerope Works Inc. (2008). *Technical Bulletin 2 Sheaves and Drums.* Retrieved September 11, 2012, from Wireropeworks: http://www.wireropeworks.com/product_pdfs/MNL_TB_02.pdf

Wong, P. L., & Li, K. Y. (1999). In-process roughness measurement on moving surfaces. *Optics & Laser Technology*, 543-548.

Yang, D., Jackson, M. R., & Parkin, R. M. (2006). Inspection of wood surface waviness defects using the light sectioning method. *Journal of Systems and Control Engineering*, 617-626.

Zhang, Z. (2004). Camera Calibration. In G. Medioni, & S. Kang, *Emerging Topics in Computer Vision* (pp. 4-43). Upper Saddle River, NJ: Prentice Hall Professional Technical Reference.

APPENDICES

APPENDIX 1: DISCUSSION

A1.1. A discussion about references used

In Chapter 2, the author made use of several unconventional references. When considering the context of the chapter, it may make sense. The type of work that was being investigated is not of a strictly academic nature. The experts in this field are experts because of their experience in doing the work, not because of their lists of publications. They have knowledge based on informal training and experiential learning that has not been recorded anywhere but in their memories. This necessitated the use of several interviews to acquire the state of the art and the various discrepancies they had with different profilers.

It was also necessary to look at standards and OEM recommendations to get a guideline as to what portion of the sheave wheel needs to be inspected. This, again, is technically a grey area for an academic document like this, but the author deemed it acceptable due to the fact that the legislation and the OEM recommendations are the only concrete reference to this and also that it is the industry standard by which the new profiler's capability would be judged.

APPENDIX 2: UNCERTAINTY ANALYSIS

In every measurement that is made, irrespective of the accuracy of the measurement instrument, there exists a certain degree of doubt about the accuracy of the measurement. This is termed the uncertainty of the measurement. In order to make useful conclusions about a measurement, it is necessary to indicate the degree of certainty the measurer has in the measurement that has been made. This will provide the reader with a generalised idea of the trust that can be placed in the result and would allow for a quantitative comparison between different experimental results.

The uncertainty of measured results is so important that several entities have attempted to produce a standardised method for determining and interpreting uncertainty in measured results. These include ISO, NIST, NPL and BIPM. Based on the recommendations and interpretations of the ISO standards done by the National Physical Laboratory in the UK (Bell, 2001), the uncertainty of various components has been classified as follows:

- Type A: Uncertainty estimates from statistics (usually from repeated readings)
- Type B: Uncertainty estimates from other sources of information

Some of the uncertainty components considered in this document fall under Type A while others fall under Type B. For a Type A analysis, the following calculations must be done:

The estimated standard deviation of a set of *n* measurements is calculated by

$$s = \sqrt{\frac{\sum_{i=1}^{n}(x_i - \bar{x})^2}{(n-1)}},$$

where x_i is the result of the i^{th} measurement and $\bar{x}$ is the arithmetic mean of the *n* results considered.

The standard uncertainty of a result from a Type A analysis can then be calculated as follows:

$$u_A = \frac{s}{\sqrt{n}}$$

Where n is the number of measurements in the data set. According to NIST, the ideal is to have around 10 results to use this method, but anything from four would suffice.

For Type B uncertainties the uncertainty of the results can be calculated as follows:

$$u_B = \frac{a}{\sqrt{3}}$$

Where a is the semi-range between the upper and lower limits (i.e. half the resolution). The divisor ($\sqrt{3}$) is based on the assumption of a rectangular distribution. In cases where a normal distribution can be assumed (e.g. calibration data), the divisor is 2.

Considering the Law of Propagation of Uncertainty, the combined standard uncertainty is calculated by the method of summation in quadrature:

$$u_c = \sqrt{{u_1}^2 + {u_2}^2 + {u_3}^2 + \cdots + {u_n}^2}$$

This uncertainty value is based on the standard uncertainty which provides a default confidence interval of 68%. To increase the confidence interval, a coverage factor can be implemented as follows:

$$U = k \cdot u_c$$

- $k = 1, \quad for\ a\ confidence\ interval\ of\ 68\%$
- $k = 2, \quad for\ a\ confidence\ interval\ of\ 95\%$
- $k = 2.58, \quad for\ a\ confidence\ interval\ of\ 99\%$
- $k = 3, \quad for\ a\ confidence\ interval\ of\ 99.7\%$

According to NIST (Taylor & Kuyatt, 1994) the convention is to use k=2 which provides a 95% confidence interval.

Initially the experimental uncertainty of the two Known Sample Experiments will be determined based on the machining tolerance of the blocks. The rest of the uncertainties are shown in the uncertainty budgets which have been drawn up for each of the profiling methods. Wherever there has been referred to "data uncertainty" this should imply a Type A uncertainty which has been determined from the raw data and the number of samples.

V1 Block Experiment Uncertainty:

- Block manufacturing tolerance: 0.1 mm (BSi, 1999)
- Surface roughness: 0.0008 mm (BSi, 1999)
- Analysis: Type B (only one source of information)
- Convergence factor: k = 2 (95 % confidence interval)
- Distribution: Rectangular → divisor =$\sqrt{3}$ (random error assumed)

$$u_B = \frac{a}{\sqrt{3}}$$

Manufacturing tolerance: $u_1 = \frac{0.1}{\sqrt{3}} = \frac{0.1}{1.73} = 0.0578\ mm$

Surface roughness: $u_2 = \frac{0.0008}{\sqrt{3}} = \frac{0.0008}{1.73} = 0.00046\ mm$

Combined uncertainty: $u_c = \sqrt{{u_1}^2 + {u_2}^2}$

$$u_c = \sqrt{(0.0578)^2 + (0.00046)^2} = 0.0578\ mm$$

Expanded uncertainty: $U = k \cdot u_c = 2 \cdot (0.0578)$

$$U = 0.12\ mm\ with\ a\ 95\%\ confidence\ interval$$

PA Block Experiment Uncertainty:

- Block manufacturing tolerance: 0.15 mm (see Appendix 4.3 for drawing: TEST BLOCK 0101)
- Surface roughness: 0.0008 mm (see Appendix 4.3 for drawing: TEST BLOCK 0101)
- Analysis: Type B (only one source of information)
- Convergence factor: k = 2 (95 % confidence interval)
- Distribution: Rectangular → divisor = √3 (random error assumed)

$$u_B = \frac{a}{\sqrt{3}}$$

Manufacturing tolerance: $u_1 = \frac{0.15}{\sqrt{3}} = \frac{0.15}{1.73} = 0.087\ mm$

Surface roughness: $u_2 = \frac{0.008}{\sqrt{3}} = \frac{0.0008}{1.73} = 0.00046\ mm$

Combined uncertainty: $u_c = \sqrt{{u_1}^2 + {u_2}^2}$

$$u_c = \sqrt{(0.087)^2 + (0.00046)^2} = 0.087\ mm$$

Expanded uncertainty: $U = k \cdot u_c = 2 \cdot (0.087)$

$$U = 0.17\ mm\ with\ a\ 95\%\ confidence\ interval$$

A2.1. Uncertainty analysis for plaster cast experiments

Table 20: Uncertainty analysis for plaster cast experiments

Experiment	Measurement	Unit	Uncertainty Source	± value [mm]	Probability Distribution	Divisor	Standard Uncertainty	$(\mu_i)^2$
V1 Block	x- coordinate error	mm	V1 Block machining tolerance	0.12	Rectangular	$\sqrt{3}$	0.069282032	0.0048
		mm	Digital Calliper uncertainty	0.029	Normal	2	0.0145	0.00021025
		mm	Data uncertainty	-	Normal	$\sqrt{n}$	0.148	0.021904
		mm	Pencil thickness (bias)	0.5	Rectangular	$\sqrt{3}$	0.288675135	0.08333333
			[95% Confidence interval=> k=2] Combined Uncertainty:					0.66407103
	y- coordinate error	mm	V1 Block machining tolerance	0.12	Rectangular	$\sqrt{3}$	0.069282032	0.0048
		mm	Digital Calliper uncertainty	0.029	Normal	2	0.0145	0.00021025
		mm	Data uncertainty	-	Normal	$\sqrt{n}$	0.215	0.046225
		mm	Pencil thickness (bias)	0.5	Rectangular	$\sqrt{3}$	0.288675135	0.08333333
			[95% Confidence interval=> k=2] Combined Uncertainty:					0.73367182
PA Block	x- coordinate error	mm	PA Block machining tolerance	0.17	Rectangular	$\sqrt{3}$	0.098149546	0.00963333
		mm	Digital Calliper uncertainty	0.029	Normal	2	0.0145	0.00021025
		mm	Data uncertainty	-	Normal	$\sqrt{n}$	0.071	0.005041
		mm	Pencil thickness (bias)	0.5	Rectangular	$\sqrt{3}$	0.288675135	0.08333333
			[95% Confidence interval=> k=2] Combined Uncertainty:					0.62679476
	y- coordinate error	mm	PA Block machining tolerance	0.17	Rectangular	$\sqrt{3}$	0.098149546	0.00963333
		mm	Digital Calliper uncertainty	0.029	Normal	2	0.0145	0.00021025
		mm	Data uncertainty	-	Normal	$\sqrt{n}$	0.123	0.015129
		mm	Pencil thickness (bias)	0.5	Rectangular	$\sqrt{3}$	0.288675135	0.08333333
			[95% Confidence interval=> k=2] Combined Uncertainty:					0.65819729
Sheave Sample	Flare Angle [A]		Digital Calliper uncertainty	0.029	Normal	2	0.0145	0.00021025
			Data uncertainty	-	Normal	$\sqrt{n}$	0.08	0.0064
			Pencil thickness (bias)	0.5	Rectangular	$\sqrt{3}$	0.288675135	0.08333333
			[95% Confidence interval=> k=2] Combined Uncertainty:					0.59981191
	Root Radius [R]	mm	Digital Calliper uncertainty	0.029	Normal	2	0.0145	0.00021025
		mm	Data uncertainty	-	Normal	$\sqrt{n}$	0.57	0.3249
		mm	Pencil thickness (bias)	0.5	Rectangular	$\sqrt{3}$	0.288675135	0.08333333
			[95% Confidence interval=> k=2] Combined Uncertainty:					1.27819182
	Depth of Groove [H[	mm	Digital Calliper uncertainty	0.029	Normal	2	0.0145	0.00021025
		mm	Data uncertainty	-	Normal	$\sqrt{n}$	0.41	0.1681
		mm	Pencil thickness (bias)	0.5	Rectangular	$\sqrt{3}$	0.288675135	0.08333333
			[95% Confidence interval=> k=2] Combined Uncertainty:					1.00328178
	Web Thickness [W1]	mm	Digital Calliper uncertainty	0.029	Normal	2	0.0145	0.00021025
		mm	Data uncertainty	-	Normal	$\sqrt{n}$	0.14	0.0196
		mm	Pencil thickness (bias)	0.5	Rectangular	$\sqrt{3}$	0.288675135	0.08333333
			[95% Confidence interval=> k=2] Combined Uncertainty:					0.64231949
	Web Thickness [W2}	mm	Digital Calliper uncertainty	0.029	Normal	2	0.0145	0.00021025
		mm	Data uncertainty	-	Normal	$\sqrt{n}$	0.11	0.0121
		mm	Pencil thickness (bias)	0.5	Rectangular	$\sqrt{3}$	0.288675135	0.08333333
			[95% Confidence interval=> k=2] Combined Uncertainty:					0.61852594

A2.2. Uncertainty analysis for laser profiler experiments

Table 21: Uncertainty analysis for laser profiler experiments

Experiment	Measurement	Unit	Uncertainty Source	± value [mm]	Probability Distribution/typ	Divisor	Standard Uncertainty	$(\mu_i)^2$
V1 Block	x- coordinate error	mm	V1 Block machining tolerance	0.12	Rectangular	$\sqrt{3}$	0.069282032	0.0048
		mm	Data uncertainty	-	Normal	$\sqrt{n}$	0.431	0.185761
			[95% Confidence interval=> k=2] Combined Uncertainty:					0.87306586
	y- coordinate error	mm	V1 Block machining tolerance	0.12	Rectangular	$\sqrt{3}$	0.069282032	0.0048
		mm	Data uncertainty	-	Normal	$\sqrt{n}$	1.048	1.098304
			[95% Confidence interval=> k=2] Combined Uncertainty:					2.10057516
PA Block	x- coordinate error	mm	PA Block machining tolerance	0.17	Rectangular	$\sqrt{3}$	0.098149546	0.00963333
		mm	Data uncertainty	-	Normal	$\sqrt{n}$	0.277	0.076729
			[95% Confidence interval=> k=2] Combined Uncertainty:					0.58774938
	y- coordinate error	mm	PA Block machining tolerance	0.17	Rectangular	$\sqrt{3}$	0.098149546	0.00963333
		mm	Data uncertainty	-	Normal	$\sqrt{n}$	0.351	0.123201
			[95% Confidence interval=> k=2] Combined Uncertainty:					0.72892889
Sheave Sample	Flare Angle [A]		Data uncertainty	-	Normal	$\sqrt{n}$	0.21	0.0441
			[95% Confidence interval=> k=2] Combined Uncertainty:					0.42
	Root Radius [R]	mm	Data uncertainty	-	Normal	$\sqrt{n}$	0.44	0.1936
			[95% Confidence interval=> k=2] Combined Uncertainty:					0.88
	Depth of Groove [H]	mm	Data uncertainty	-	Normal	$\sqrt{n}$	0.28	0.0784
			[95% Confidence interval=> k=2] Combined Uncertainty:					0.56
	Web Thickness [W1]	mm	Data uncertainty	-	Normal	$\sqrt{n}$	0.47	0.2209
			[95% Confidence interval=> k=2] Combined Uncertainty:					0.94
	Web Thickness [W2}	mm	Data uncertainty	-	Normal	$\sqrt{n}$	0.26	0.0676
			[95% Confidence interval=> k=2] Combined Uncertainty:					0.52

A2.3. Uncertainty analysis for pantograph experiments

Table 22: Uncertainty analysis for pantograph experiments

Experiment	Measurement	Unit	Uncertainty Source	± value [mm]	Probability Distribution	Divisor	Standard Uncertainty	$(\mu_i)^2$
V1 Block	x- coordinate error	mm	V1 Block machining tolerance	0.12	Rectangular	$\sqrt{3}$	0.069282032	0.0048
		mm	Digital Calliper uncertainty	0.029	Normal	2	0.0145	0.00021025
		mm	Data uncertainty	-	Normal	$\sqrt{n}$	0.3	0.09
		mm	Pencil thickness (bias)	0.5	Rectangular	$\sqrt{3}$	0.288675135	0.08333333
			[95% Confidence interval=> k=2] Combined Uncertainty:					0.8446149
	y- coordinate error	mm	V1 Block machining tolerance	0.12	Rectangular	$\sqrt{3}$	0.069282032	0.0048
		mm	Digital Calliper uncertainty	0.029	Normal	2	0.0145	0.00021025
		mm	Data uncertainty	-	Normal	$\sqrt{n}$	0.344	0.118336
		mm	Pencil thickness (bias)	0.5	Rectangular	$\sqrt{3}$	0.288675135	0.08333333
			[95% Confidence interval=> k=2] Combined Uncertainty:					0.90924053
PA Block	x- coordinate error	mm	PA Block machining tolerance	0.17	Rectangular	$\sqrt{3}$	0.098149546	0.00963333
		mm	Digital Calliper uncertainty	0.029	Normal	2	0.0145	0.00021025
		mm	Data uncertainty	-	Normal	$\sqrt{n}$	0.624	0.389376
		mm	Pencil thickness (bias)	0.5	Rectangular	$\sqrt{3}$	0.288675135	0.08333333
			[95% Confidence interval=> k=2] Combined Uncertainty:					1.38932058
	y- coordinate error	mm	PA Block machining tolerance	0.17	Rectangular	$\sqrt{3}$	0.098149546	0.00963333
		mm	Digital Calliper uncertainty	0.029	Normal	2	0.0145	0.00021025
		mm	Data uncertainty	-	Normal	$\sqrt{n}$	0.488	0.238144
		mm	Pencil thickness (bias)	0.5	Rectangular	$\sqrt{3}$	0.288675135	0.08333333
			[95% Confidence interval=> k=2] Combined Uncertainty:					1.15120965
Sheave Sample	Flare Angle [A]		Digital Calliper uncertainty	0.029	Normal	2	0.0145	0.00021025
			Data uncertainty	-	Normal	$\sqrt{n}$	0.28	0.0784
			Pencil thickness (bias)	0.5	Rectangular	$\sqrt{3}$	0.288675135	0.08333333
			[95% Confidence interval=> k=2] Combined Uncertainty:					0.80484429
	Root Radius [R]	mm	Digital Calliper uncertainty	0.029	Normal	2	0.0145	0.00021025
		mm	Data uncertainty	-	Normal	$\sqrt{n}$	1.17	1.3689
		mm	Pencil thickness (bias)	0.5	Rectangular	$\sqrt{3}$	0.288675135	0.08333333
			[95% Confidence interval=> k=2] Combined Uncertainty:					2.41034735
	Depth of Groove [H[	mm	Digital Calliper uncertainty	0.029	Normal	2	0.0145	0.00021025
		mm	Data uncertainty	-	Normal	$\sqrt{n}$	0.18	0.0324
		mm	Pencil thickness (bias)	0.5	Rectangular	$\sqrt{3}$	0.288675135	0.08333333
			[95% Confidence interval=> k=2] Combined Uncertainty:					0.68100979
	Web Thickness [W1]	mm	Digital Calliper uncertainty	0.029	Normal	2	0.0145	0.00021025
		mm	Data uncertainty	-	Normal	$\sqrt{n}$	0.48	0.2304
		mm	Pencil thickness (bias)	0.5	Rectangular	$\sqrt{3}$	0.288675135	0.08333333
			[95% Confidence interval=> k=2] Combined Uncertainty:					1.12061337
	Web Thickness [W2}	mm	Digital Calliper uncertainty	0.029	Normal	2	0.0145	0.00021025
		mm	Data uncertainty	-	Normal	$\sqrt{n}$	0.53	0.2809
		mm	Pencil thickness (bias)	0.5	Rectangular	$\sqrt{3}$	0.288675135	0.08333333
			[95% Confidence interval=> k=2] Combined Uncertainty:					1.20738326

APPENDIX 3: SURVEY RESULTS

TABLE 23: SURVEY RESULT SUMMARY

Date	Name	Position and Company	Pantograph	Plaster Casts	Sheave Gauges	CMM	Laser Profiler	Other
9/7/2014	Gert van der Walt	Director NDT, Quest Technical Services					x	x
9/7/2014	Byron Blucher	NDT Technician, Quest Technical Services					x	
16/07/2014	Chris Els	Senior Machinery inspector, Anglo Technical Solutions	x		x	x	x	
16/07/2014	Jaco Venter	Senior Machinery inspector, Anglo Technical Solutions	x		x		x	
16/07/2014	Louwrens de wet	Manager Anglo American Field services	x				x	
16/07/2014	Evert Viljoen	Senior Machinery Inspector ,Anglo Field Services	x		x		x	
17/07/2014	Jean-Pierre	NDT Inspector	x		x		x	
21/07/2014	Marionè	Inspector/Technician	x		x		x	
29/07/2014	Prive Naidoo	Dragline Inspector, Anglo American Thermal Coal			x		x	
14/08/2014	Roland Verreet	Engineer, Wire Rope Technology, Aachen, Germany		x	x			
18/08/2014	Chris Ebersöhn	General Engineering Supervisor, Barberton Mines, Sheba Section	x		x		x	
21/08/2014	P. Pretorius	BH927066		x	x			
11/9/2014	Ian du Plessis	Technical sales engineer at Bridon, Senior Rope Inspector at Anglo Field Services			x			
		Number of times a method was mentioned	7	2	10	1	10	1
		Total Number of methods used:	31					
		Percentage	22.58%	6.45%	32.26%	3.23%	32.26%	3.23%

APPENDIX 4: SPECIFICATION SHEETS/CERTIFICATES

A4.1. Specifications of CMOS sensor

GALAXYCORE

Application

- Cellular Phone Cameras
- Notebook and desktop PC cameras
- PDAs
- Toys
- Digital still cameras and camcorders
- Video telephony and conferencing equipment
- Security systems

Product features

- Standard optical format of 1/6.5 inch
- Various output formats YCbCr4:2:2, RGB565 Raw Bayer
- Digital video port(DVP) parallel output interface
- Single power supply requirement (2.8v)
- Windowing support
- Horizontal /Vertical mirror
- Image processing module
- Package CSP

Product specifications

- Optical Format: 1/6.5 inch
- Pixel Size: 3.4um x 3.4um
- Active pixel array 648 x 488
- ADC resolution: 10 bit ADC
- Max Frame rate 30fps@24Mhz,VGA
- Power Supply 2.7 ~ 3.3V, typical 2.8V
- Power Consumption: 70mW@ 30fps VGA,
- <10uA @ standby
- SNR TBD
- Dark Current: TBD
- Sensitivity TBD
- Operating temperature: 20~70°C
- Stable Image temperature 0~60°C
- Optimal lens chief ray angle(CRA):27°(linear)
- Package type: CSP

A4.2. Calibration certificate for digital calliper

Linberts Calibration Services cc

SANAS ACCREDITED LABORATORY

ACCREDITATION NO.017

sanas Calibration Laboratory 017

CERTIFICATE OF CALIBRATION

CERTIFICATE NO. E 7742 PAGE 1 of 1

CALIBRATION DATE : 21-01-2014

DESCRIPTION	DIGITAL VERNIER CALIPER 0 - 300 mm	TRACEABLE EQUIPMENT / STANDARDS USED
CUSTOMER	[illegible] MACHINES (PTY) LTD	GAUGE BLOCKS SERIAL NO.5561
ADRESS	CNR SMUTS & BASSON STREETS	LENGTH BARS SERIAL NO.12870,2
ADRESS	ROCKY DRIFT, WHITE RIVER	
MANUFACTURER	TA	
SERIAL NO.	TA 01	EQUIPMENT TRACEABLE TO NATIONAL STANDARDS
TEMPERATURE °C	20°C ± 1°C	REFERENCE PUBLICATION : BS.887
HUMIDITY % RH	50% RH ± 10% RH	CALIBRATION PROCEDURE : 00125LM
NOTE : ALL RESULTS ARE STATED IN MILLIMETERS (mm)		PRE CALIBRATION : 0,001 / POST CALIBRATION : 0,000

MEASUREMENT UNCERTAINTY ± 0,029mm

FEATURE	SPEC. OR PERMISSIBLE ERROR	ACTUAL
Parallelism of external measuring faces	0,008	0,020*
Parallelism of internal measuring faces	0,010	0,005
Accuracy of reading	0,0	0,00
	30,1	30,10
	60,2	60,20
	90,3	90,30
	120,4	120,40
	150,5	150,40
	180,6	180,50
	210,7	210,60
	240,8	240,70
	270,9	270,80
	300,0	299,90
Maximum Permissible error	0,02	0,003
Depth rod		-0,08

Note : All measurements were taken at the back of the jaws.

: *Denotes out of specification.

Actom Electrical Machines (Factory), Cnr. Van Dyk & Aberdeen Rd's, Benoni Industrial, [illegible], Benoni, 1500

Tel : (011) 899-1073 Fax : (011) 899-1082 e-mail : [illegible]

Calibrated by : B.J Jacobs APPROVED BY : TECHNICAL SIGNATORY

A4.3. Calibration certificate and drawing for the PA calibration block

Phoenix Inspection Systems Limited
Dalton House
40 Hardwick Grange
Woolston
Warrington
WA1 4RF
UNITED KINGDOM
Tel +44 (0) 1925 826000
Fax +44 (0) 1925 838788
e-mail sales@phoenixisl.co.uk
Website www.phoenixisl.co.uk

PHOENIX

CERTIFICATE OF CONFORMITY

Customer Name and Address:

QUEST TECHNICAL SERVICES (PTY) LTD
18 NORITE ROAD
WILROPARK
ROODEPORT
JOHANNESBURG
SOUTH AFRICA 1724

In reference to your purchase number

ITEM:	**Phased Array Calibration Block**
SERIAL NUMBER/BATCH NUMBER:	**11/34/22**
MANUFACTURED SPECIFICATION:	**Has been manufactured to Phoenix Inspection Systems Ltd Drawing TEST BLOCK 0101,in Accordance with sections 2,3,4.1,4.3 & 6.b of EN12223.2000**
QUANTITY:	**ONE**
CONDITION OF MATERIAL:	The test block complies with the specification upon dispatch.

Certified that the supplies/services detailed hereon have been inspected and tested in accordance with the conditions and requirements of the contract or purchase order and unless otherwise noted below, confirm in all respects to the specification(s), drawings(s) relevant thereto.

Signed: J. Boughey .... Date 23/01/2012..........
Position: Assistant Manager (Probe Department)

Certificate Number : 13727

Company Registration No 1718157 DIRECTOR K P QUIRK B ENG & MAN (Managing Director)

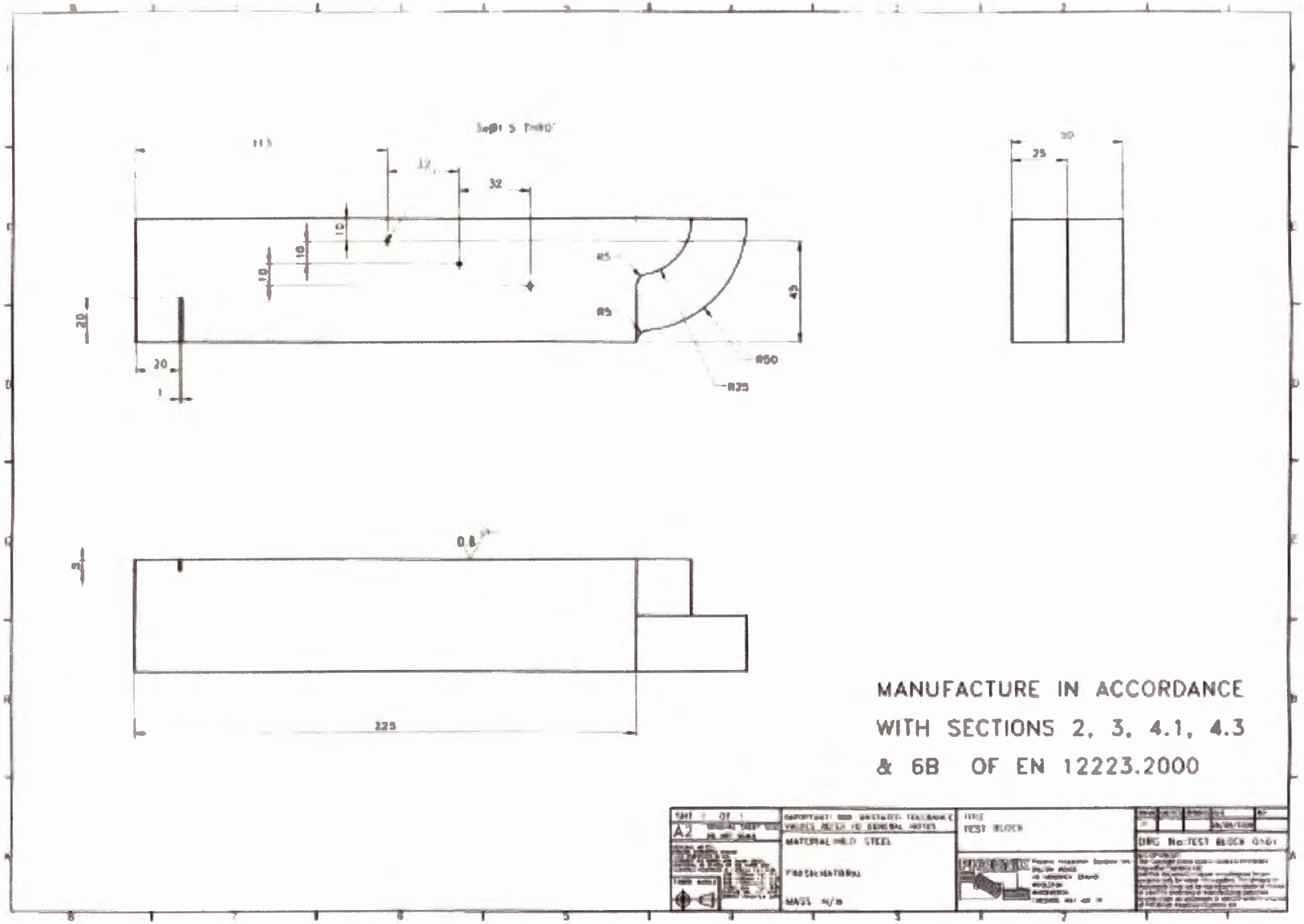
MANUFACTURE IN ACCORDANCE
WITH SECTIONS 2, 3, 4.1, 4.3
& 6B OF EN 12223.2000
MATERIAL MILD STEEL
TEST BLOCK
225
R50
R25
R5
45
50
25
32
20

"For instance, on the planet Earth, man had always assumed that he was more intelligent than dolphins because he had achieved so much – the wheel, New York, wars and so on- whilst all the dolphins had ever done was muck about in the water having a good time. But conversely, the dolphins had always believed that they were far more intelligent than man- precisely for the same reasons."

Douglas Adams